Slow dynamics of complex fluids

Balaji Yendeti

A Dissertation Submitted for the Degree award of

Doctor of Philosophy

in the School of Physics

University of Hyderabad, Gachibowli

Hyderabad, INDIA

Febrauary 2015

PUBLICATIONS

Publications in scientific journals

1) **Balaji Yendeti**, G. Thirupathi, Ashok Vudaygiri, and R. Singh, Eur. Phys. J. E **37**: 70, (2014).
2) S. Dhara, **Y. Balaji**, J. Ananthaiah, P. Sathyanarayana, V. Ashoka, A. Spadlo, and R. Dabrowski, Phys. Rev. E. **87**, 030501(R), (2013).

Manuscript under preparation

3) Balaji Yendeti and Ashok Vudaygiri, Memory effects in tumbling nematics of 8CB liquid crystals - Under preparation.
4) Balaji Yendeti and Ashok Vudaygiri, Microrheology in bent core liquid crystals - Under preparation.
5) Balaji Yendeti and Ashok Vudaygiri, Microrheology in tumbling nematics of 8CB liquid crystals - Under preparation.
6) Balaji Yendeti and Ashok Vudaygiri, Diffusing diffusivity in liquid crystals - Under preparation.

CERTIFICATE

This is to certify that the thesis entitled **"Slow Dynamics of Complex Fluids"** being submitted to the University of Hyderabad by **Yendeti Balaji** (Reg. No: 06PHPH08), for the award of the degree of **Doctor of Philosophy in Physics**, is a record of bonafide work carried out by him under my supervision and is free of plagiarism. The matter embodied in this report has not been submitted to any other university or institution for the award of any degree or diploma.

Dr. Ashok Vudayagiri
Thesis Supervisor,
School of Physics,
University of Hyderbad.

Dean,
School of Physics,
University of Hyderabad.

Date:-

DECLARATION

I, **Yendeti Balaji**, declare that the work presented in this thesis entitled **"Slow Dynamics of Complex fluids"** has been carried out by me under the supervision of Dr. Ashok Vudayagiri, Assistant Professor, School of Physics, University of Hyderabad, as per the Ph.D. ordinances of the university, which is also plagiarism free. I declare, to the best of my knowledge, that no part of this thesis has been submitted for the award of a research degree or diploma of any other university. I hereby agree that my thesis can be deposited in Shodhganga/ INFLIBNET.

Balaji Yendeti
o6PHPHo8

Date:-

Acknowledgments

In this note, I sincerely thank all those people who helped me through out my long journey of thesis work.

Firstly, deep regards to my thesis supervisor Dr. Ashok Vudayagiri, who guided me to attempt different research topics. He always have encouraged me to make things from scratch. I cannot forget those days which we both sincerely attempted to write labview software code for image processing of Brownian motion. Under his guidance, I have learnt how to cope with new fields of research work and understand the physics and think in my own way by comparing with very generalized phenomena.

I would like to take this opportunity to extend my gratitude to Prof. Surya P. Tiwari, who has provided "bread and butter" by giving fellowship. Also, the suggestions he gave during doctoral committee meetings have always helped me.

At times, I had come across many failures in obtaining results using optical tweezers. I thank Dr. S. Dhara, our collaborator who gave me opportunity to work in the liquid crystals group. I have learnt to work in a systematic way under his guidance. I also thank currently Dean, school of Physics, Prof. R. Singh, who had asked us to attempt Ferro fluids.

The important practical tips in building microscopes that i had from Prof. Nirmal Viswanathan have changed my way of attempting optics experiments. I am very thankful to him for important discussions I had with him.

The discussions in understanding different structures of bent core liquid crystals with Prof. V.S.S. Sastry and Prof. Claudio Zannoni (during his visit to university of Hyderabad) have helped me to understand our experimental results. I am greatful to them for providing their time for discussions despite their busy schedule.

When I observed some new experimental results, we have sought expert advice on those issues. Prof. K.P.N. Murthy had always encouraged us with his suggestions on crucial aspects. I am greatful to the kind support I had from him.

In my personality management skills, Prof. Anantha Lakshmi's help is endless. I am thankful to her efforts in helping me to improve

and sell my thesis topic. Also, I thank Prof. D. Narayana Rao, Prof. Suneel singh for their suggestions during doctoral committee meetings.

It has been great pleasure to work with students in liquid crystals lab. Dr. T. Arun Kumar, had taught me how to prepare a liquid crystal cell. Ananthaiah helped by cooperating with me through out my stay in that lab. P. Satyanaryana, Sai, Rasna, Zuhail, and Reshmita also have helped me at some or the other point. I would like to thank all these friends for their kind cooperation.

Thriupathi has really supported me by synthesizing ferrofluids, in beautifying the graphs for our published work on ferrofluids. I sincerely thank for the kind of support he has given me.

I thank my lab mates, B. Sita laksmi, Sachin, Ram soorath, Ajmathulla and Mahendar for their support. Though we all had different research problems, we have always worked together, helped each other to shine ourselves. Also, I thank my Ph.D. batch mates.

I thank all other optics teaching faculty, other faculty members of school of physics, ACRHEM faculty, for their cooperation.

I thank M.Sc. lab technicians Pentaiah, Mukund reddy, for their support in providing the equipments. I thank workshop technicians, for their support in making new equipment.

It is difficult to express the kind of cooperation I had from my family members. My parents (Swamy, Subbaratnam) has given all kinds of support necessary to never feel 'low' by me. My elder sister (Lakshmi Prasanna) always encouraged me to look high and go a step forward in life. My brother (Sudhakar) had always encouraged me with his advice to go ahead with new thoughts. My wife (Kavitha) had given whole and sole support to me. Without her support, I could not imagine completing my Ph.D work. My cute little daughters have supported me in their ways. All other family members had given their support in one or the other ways.

Lastly, I thank the almighty god "Lord Venkateswara" .

CONTENTS

1 INTRODUCTION 1
- 1.1 Complex fluids 1
- 1.2 Early efforts 2
- 1.3 Liquid Crystals 4
  - 1.3.1 Classification of thermotropic liquid crystals 5
  - 1.3.2 Isotropic 5
  - 1.3.3 Nematic 5
  - 1.3.4 Cholestric 6
  - 1.3.5 Smectic 7
- 1.4 Bent-core Liquid Crystals 10
- 1.5 Properties of nematic liquid crystals 10
  - 1.5.1 Orientational order parameter 10
  - 1.5.2 Elasticity 11
  - 1.5.3 Pretilt angle 11
  - 1.5.4 Anchoring energy 11
- 1.6 Defects in nematic liquid crystals 12
  - 1.6.1 Free energy density 12
- 1.7 Magnetic fluids 13
  - 1.7.1 The magnetoviscous effect 14
- 1.8 Salient features of the thesis 15
- 1.9 Out line of the thesis 15

2 BROWNIAN MOTION OF COLLOIDAL PARTICLE IN LIQUID CRYSTALS 21
- 2.1 Colloids in liquid crystals 21
  - 2.1.1 Topological defects with colloids in liquid crystals 22
- 2.2 Diffusion of colloidal particle in liquid crystals 24
- 2.3 Nematodynamics: Flow of nematic liquid crystals 27
- 2.4 The Experiment 33
  - 2.4.1 Sample preperation 33
  - 2.4.2 Sample cell preparation 34
  - 2.4.3 Particle tracking with inverted microscope 36

2.5 Experimental microrheology and analysis procedure 39
2.5.1 Relation between MSD and velocity auto correlation function(VACF) 40
2.5.2 Relation between MSD and elastic(G′), viscous(G″)moduli 41
2.5.3 Relation between viscosity(η) and probability distibution of diffusion 41
2.6 Conclusions 42

3 PASSIVE VISCOSITIES OF BENT-CORE NEMATIC LIQUID CRYSTALS 47
3.1 introduction 47
3.2 The Experiment 49
3.3 Results and discussion 50
3.4 Conclusions 54

4 MEMORY EFFECTS IN TUMBLING NEMATICS OF 8CB LIQUID CRYSTALS 59
4.1 introduction 59
4.2 The Experiment 63
4.3 Results and discussion 63
4.4 Conclusions 72

5 MICRORHEOLOGY IN TUMBLING NEMATICS OF 8CB LIQUID CRYSTALS 77
5.1 introduction 77
5.2 The Experiment 79
5.3 Results and discussion 80
5.4 Conclusions 91

6 MICRORHEOLOGICAL PROPERTIES OF BENT-CORE NEMATIC LIQUID CRYSTALS 95
6.1 Introduction 95
6.2 The Experiment 97
6.3 Results and discussion 97
6.3.1 Isotropic phase 100
6.3.2 Nematic phase 102
6.3.3 Proof of “spontaneous” biaxiality 112
6.3.4 Out of plane orientations 115
6.3.5 Surface anchoring effects 116

6.4 Viscous modulus(G″) 122
6.5 Conclusions 122

7 DIFFUSING DIFFUSIVITY IN LIQUID CRYSTALS 129
7.1 Introduction 129
7.2 Results and discussion 130
7.3 conclusions 140

8 FIELD DEPENDENT ANISOTROPIC MICRO RHEOLOGICAL AND MICROSTRUCTRUAL PROPERTIES OF FERROFLUIDS 143
8.1 introduction 143
8.2 The Experiment 144
8.3 Results and discussion 147
8.3.1 Magnetic properties 147
8.3.2 Micro-rheological properties 148
8.3.3 Micro-structural properties 154
8.4 Conclusion 157

9 CONCLUSIONS AND FUTURE DIRECTIONS 163
9.1 Conclusions 163
9.1.1 Dynamics of tumbling nematic director in liquid crystals 164
9.1.2 Consequences of irregular shape of molecules in liquid crystals 165
9.1.3 Inference on the diffusivity in liquid crystals 166
9.1.4 Field dependent diffusion in ferrofluids 167
9.2 Future directions 167

LIST OF FIGURES

Figure 1.1 Schematic representation of liquid crystals molecular alignment in the calamitic nematic phase 6

Figure 1.2 Schematic representation of liquid crystals molecular alignment in the Smectic A phase 7

Figure 1.3 Schematic representation of liquid crystals molecular alignment in the Smectic C phase. The lc molecules are tilted with respect to layer normal ($\hat{\mathbf{k}}$). 8

Figure 1.4 Schematic representation of liquid crystals (lc) molecular alignment in the Smectic C^* phase. The tilt direction rotates between successive layers 9

Figure 1.5 Uniaxiality(left) and biaxiality(right) in bent core liquid crystals 9

Figure 2.1 In the above figure left picture represents dipole defect with 0.98μ m colloidal particle picture on right is a chain of collodial particles with dipole defects. 23

Figure 2.2 Quadrupole defect with 0.98μ m colloidal particle. 24

Figure 2.3 a,b,c structures in nematic phase of liquid crystals represent vorticity(x), velocity(y), and velocity gradient(z) directions 28

Figure 2.4 Schematic diagram of liquid crystals sample cell 35

Figure 2.5 Photograph of Nikon *Eclipse* inverted microscope with sample cell in a heating stage. 37

Figure 2.6 Flowchart diagram of experimental and analysis procedure for passive microrheology. 40

Figure 3.1 Schematic representation of the three fundamental director orientations in the nematic phase. Miesowicz viscosities corresponding to each orientation are designated by η_1, η_2, η_3 respectively. 49

Figure 3.2 Histogram of particle displacements parallel(circles) and perpendicular(stars) to the director for τ = 1 S. The solid lines are Gaussian fits. 51

Figure 3.3 Diffusion ratio $D_{\parallel} > D_{\perp}$ for every $5 \circ C$ difference in temperature. Average of this ratio is at 1.6. 51

Figure 3.4 Variation of ηeff (stars), $\eta_{\parallel}$(squares), and $\eta_{\perp}$ as a function of shifted temperature. 52

Figure 3.5 Schematic molecular orientation around the microsphere with a dipolar defect configuration. It may be noted that, the clusters attached to the microsphere are permanent, whereas they are temporal in nature in the bulk. The small dot near the top indicates a hyperbolic hedgehog defect. 53

Figure 3.6 The two dimensional projection of trajectories of a microsphere closer to the N-I transition($T - T_{NI} = -7.6^{\circ}C$). 53

Figure 3.7 The two dimensional projection of trajectories of a microsphere closer to the N-I transition($T - T_{NI} = -47.6^{\circ}C$) 54

Figure 4.1 a,b,c structures in nematic phase of 8CB liquid crystals represent vorticity(x), velocity(y), and velocity gradient(z) directions 62

Figure 4.2 At $\Delta T_{N-I} = -0.5^{0}C$, VACF vs time in $b^{'}$ regime, $C_{v\parallel}$ is shown by open circles(blue color) and $C_{v\perp}$ is shown by star(blue color)and solid line(red color) is fit. 65

Figure 4.3 At $\Delta T_{N-I} = -2.5^{0}C$, VACF vs time in a_m regime, $C_{v\parallel}$ is shown by open circles(blue color) and $C_{v\perp}$ is shown by star(blue color)and solid line(red color) is fit. 66

Figure 4.4 At $\Delta T_{N-I} = -3.5^0C$, VACF vs time in a_s regime, $C_{v\parallel}$ is shown by open circles(blue color) and $C_{v\perp}$ is shown by star(blue color)and solid line(red color) is fit. 66

Figure 4.5 At $\Delta T_{N-I} = -4.5^0C$, VACF vs time in a_s regime, $C_{v\parallel}$ is shown by open circles(blue color) and $C_{v\perp}$ is shown by star(blue color) and solid line(red color) is fit. 67

Figure 4.6 At $\Delta T_{N-I} = -5.5^0C$, VACF vs time in $a(b)$ regime, $C_{v\parallel}$ is shown by open circles(blue color) and $C_{v\perp}$ is shown by star(blue color) and solid line(red color) is fit. 67

Figure 4.7 At $\Delta T_{N-I} = -6.5^0C$, VACF vs time in a_c regime, $C_{v\parallel}$ is shown by open circles(blue color) and $C_{v\perp}$ is shown by star(blue color) and solid line(red color) is fit. 68

Figure 4.8 angular frequency (ω) vs ΔT of precessional motion of $(\hat{\mathbf{n}})$ in different regimes of nematic phase of 8CB liquid crystals. $(\omega_{\parallel})$ is shown by open circles and $(\omega_{\perp})$ is shown by closed (red) circles. 71

Figure 4.9 Time of relaxation (τ) vs ΔT of $(\hat{\mathbf{n}})$ in different regimes of nematic phase of 8CB liquid crystals. $(\tau_{\parallel})$ is shown by open circles and $(\tau_{\perp})$ is shown by closed (red) circles. 71

Figure 4.10 Elastic constant (K) vs ΔT in different regimes of nematic phase of 8CB liquid crystals. $(K\|)$ is shown by open circles and $(K_{\perp})$ is shown by closed (red) circles. 73

Figure 4.11 Quality factor (Q) vs ΔT of precessional motion of $(\hat{\mathbf{n}})$ in different regimes of nematic phase of 8CB liquid crystals. $(Q_{\parallel})$ is shown by open circles and $(Q_{\perp})$ is shown by closed (red) circles. 73

Figure 5.1 MSD vs time for (a) Isotropic(solid square) ($\Delta T_{N-I} = +0.5^{\circ}C$) and nematic phase(closed and open circles for parallel and perpendicular MSD) ($\Delta T_{N-I} = -1.5^{\circ}C$) and (b) In case of tumbling nematic director(closed and open circles for parallel and perpendicular MSD) at ($\Delta T_{N-I} = -3.5^{\circ}C$) of 8CB liquid crystals. solid line(red colour) represents the power law fit. 81

Figure 5.2 In nematic phase of 8CB liquid crystals, at ($\Delta T_{N-I} = -0.5^{\circ}C$), $G_{\parallel}^{'}$ and $G_{\parallel}^{''}$ represent the parallel components of $G^{'}$ and $G^{''}$. Here, $G^{'}$ is solid square(black colour) and $G^{''}$ is star(blue colour).(b) $G_{\perp}^{'}$ and $G_{\perp}^{''}$ represents perpendicular components of $G^{'}$ and $G^{''}$. Thin line(red colour) with a small open circle shows fitting. 84

Figure 5.3 In nematic phase of 8CB liquid crystals, parallel components of elastic ($G_{\parallel}^{'}$) and viscous modulus ($G_{\parallel}^{''}$) vs frequency (ω) of different regimes($a_m, a_s, a(b), a_c$). Here, $G^{'}$ is represented by line with solid square(black colour) and $G^{''}$ is represented by line with star(blue colour). Thin line(red colour) with a small open circle shows fitting. 85

Figure 5.4 In nematic phase of 8CB liquid crystals, perpendicular components of elastic ($G_{\perp}^{'}$) and viscous modulus ($G_{\perp}^{''}$) vs frequency (ω) of different regimes($a_m, a_s, a(b), a_c$). Here, $G^{'}$ is represented by line with solid square(black colour) and $G^{''}$ is represented by line with star(blue colour). Thin line(red colour online) with a small open circle shows fitting. 86

Figure 5.5 Temperature dependent variation of dynamic viscosity($\eta^{''}$). $\eta_{\parallel}$ and $\eta_{\perp}$ are represented with open circles and closed circles(red colour). 91

Figure 6.1 Elastic modulus (G') in the parallel and perpendicular direction to the director $(\hat{\mathbf{n}})$ at ($\Delta T_{N-I} = 1.5^{\circ}C$, $\Delta T_{N-I} = 0.5^{\circ}C$). Scale is linear on Y-axis and logarithmic on X-axis. parallel and perpendicular components are represented with open and closed circles respectively. 101

Figure 6.2 Fig. (a) represents orthorhombic biaxial nematic phase with (D_{2h}) symmetry of bent core molecules. Fig (b) represents monoclinic biaxial nematic phase with (C_{2h}) symmetry. Fig.(c) represents "bow" shape of the bent core liquid crystal molecules and the corresponding two orientational axes of these molecules. 102

Figure 6.3 Elastic modulus (G') in the parallel and perpendicular direction to the director $(\hat{\mathbf{n}})$ at ($\Delta T_{N-I} = -1.5^{\circ}C$). Scale is linear on Y-axis and logarithamic on X-axis 103

Figure 6.4 Elastic modulus (G') in the parallel and perpendicular directions to the director $(\hat{\mathbf{n}})$ at ($\Delta T_{N-I} = -3.5^{\circ}C$). Scale is linear on Y-axis and logarithamic on X-axis 103

Figure 6.5 Elastic modulus (G') in the parallel and perpendicular directions to the director $(\hat{\mathbf{n}})$ at ($\Delta T_{N-I} = -5.5^{\circ}C$). Scale is linear on Y-axis and logarithamic on X-axis 104

Figure 6.6 Elastic modulus (G') in the parallel and perependicular directions to the director $(\hat{\mathbf{n}})$ at ($\Delta T_{N-I} = -8.5^{\circ}C$). Scale is linear on Y-axis and logarithamic on X-axis 104

Figure 6.7 Elastic modulus (G') in the parallel and perpendicular directions to the director $(\hat{\mathbf{n}})$ at ($\Delta T_{N-I} = -10.5^{\circ}C$). Scale is linear on Y-axis and logarithmic on X-axis 105

Figure 6.8 Elastic modulus (G') in the parallel direction to the director $(\hat{\mathbf{n}})$ at ($\Delta T_{N-I} = -13.5^{\circ}C$). Scale is linear on Y-axis and logarithamic on X-axis 105

Figure 6.9 Elastic modulus (G') in the parallel and perpendicular directions to the director ($\hat{\mathbf{n}}$) at ($\Delta T_{N-I} = -18.5^{\circ}C$). Scale is linear on Y-axis and logarithamic on X-axis 106

Figure 6.10 Elastic modulus (G') in the parallel and perpendicular directions to the director ($\hat{\mathbf{n}}$) at ($\Delta T_{N-I} = -23.5^{\circ}C$). Scale is linear on Y-axis and logarithamic on X-axis 106

Figure 6.11 cybotactic clusters 108

Figure 6.12 Elastic modulus (G') in the parallel direction to the director ($\hat{\mathbf{n}}$) at ($\Delta T_{N-I} = -28.5^{\circ}C$). Scale is linear on Y-axis and logarithamic on X-axis 115

Figure 6.13 Elastic modulus (G') in the parallel direction to the director ($\hat{\mathbf{n}}$) at ($\Delta T_{N-I} = -30.5^{\circ}C$). Scale is linear on Y-axis and logarithamic on X-axis 116

Figure 6.14 Elastic modulus (G') in the parallel and perpendicular directions to the director ($\hat{\mathbf{n}}$) at ($\Delta T_{N-I} = -33.5^{\circ}C$). Scale is linear on Y-axis and logarithmic on X-axis 117

Figure 6.15 Elastic modulus (G') in the parallel and perpendicular directions to the director ($\hat{\mathbf{n}}$) at ($\Delta T_{N-I} = -35.5^{\circ}C$). Scale is linear on Y-axis and logarithmic on X-axis 117

Figure 6.16 Elastic modulus (G') in the parallel and perpendicular direction to the director ($\hat{\mathbf{n}}$) at ($\Delta T_{N-I} = -38.5^{\circ}C$). Scale is linear on Y-axis and logarithmic on X-axis 118

Figure 6.17 Elastic modulus (G') in the parallel and perpendicular directions to the director ($\hat{\mathbf{n}}$) at ($\Delta T_{N-I} = -40.5^{\circ}C$). Scale is linear on Y-axis and logarithamic on X-axis 118

Figure 6.18 Elastic modulus (G') in the parallel and perpendicular directions to the director ($\hat{\mathbf{n}}$) at ($\Delta T_{N-I} = -43.5^{\circ}C$). Scale is linear on Y-axis and logarithamic on X-axis 119

Figure 6.19 Elastic modulus (G') in the parallel and perpendicular directions to the director $(\hat{\mathbf{n}})$ at $(\Delta T_{N-I} = -45.5^{\circ}C)$. Scale is linear on Y-axis and logarithamic on X-axis 119

Figure 6.20 Elastic modulus (G') in the parallel and perpendicular directions to the director $(\hat{\mathbf{n}})$ at $(\Delta T_{N-I} = -48.5^{\circ}C)$. Scale is linear on Y-axis and logarithamic on X-axis 120

Figure 6.21 Elastic modulus (G'') in the parallel and perpendicular directions to the director $(\hat{\mathbf{n}})$ for temperatures from 180◦ C to 125 ◦ C at $(\Delta T_{N-I} = -48.5^{\circ}C)$. 121

Figure 7.1 colloidal particle in liquid crystals 130

Figure 7.2 MSD $< x^2 >$ Vs Time in the parallel and perpendicular direction to the director $(\hat{\mathbf{n}})$ for temperatures from $(\Delta T_{N-I} = -1.5^{\circ}C)$ to $\Delta T_{N-I} = -6.5^{\circ}C$. Scale is logarithamic on X and Y-axis. 132

Figure 7.3 VACF(C_v) Vs Time in the parallel and perpendicular direction to the director $(\hat{\mathbf{n}})$ from temperatures at $(\Delta T_{N-I} = -2.5^{\circ}C)$ to $(\Delta T_{N-I} = -6.5^{\circ}C)$. Scale is linear both on X and Y-axis. parallel components are represented with solid lines and perpendicular components are represented with short dots respectively. 133

Figure 7.4 MSD $< x^2 >$ Vs Time in the parallel and perpendicular direction to the director $(\hat{\mathbf{n}})$ for temperatures at $\Delta T_{N-I} = -3.5^{\circ}C$. Scale is linear on X and Y-axis. 135

Figure 7.5 VACF (C_v) Vs Time in the parallel and perpendicular direction to the director $(\hat{\mathbf{n}})$ at $\Delta T_{N-I} = -3.5^{\circ}C$. 135

Figure 7.6 Probability distribution of displacements Vs positions of the particle in the parallel and perpendicular direction to the director $(\hat{\mathbf{n}})$ for temperatures at $\Delta T_{N-I} = -47.6^{\circ}C$. Scale is linear on X and Y-axis. 137

Figure 7.7 Probability distribution Vs positions of the particle in the parallel and perpendicular direction to the director ($\hat{\mathbf{n}}$) for temperatures from ($\Delta T_{N-I} = -3.5^{\circ}C$). Scale is logarithmic on Y-axis and linear on X axis. 138

Figure 8.1 TEM images of nanoparticle. Inset shows histogram for particle size distribution 145

Figure 8.2 M-H curve for the sample at room temperature, showing superparamagnetic nature with zero coercivity 145

Figure 8.3 Home built microscope with sample cell in magnetic filed with helmholtz coil 147

Figure 8.4 Mean square displacements of probe particle in magneto rheological fluid for different external magnetic field strengths. Parallel to the external field (empty) and perpendicular to external field (filled) components are plotted as a function of deformation frequency ω. Nanoparticles form chains along the magnetic field direction. Suggested slope for the curves are represented as m=1 (zero field) and m=0 (high field) 149

Figure 8.5 (Histogram of particle displacements parallel (open circles) and perpendicular (closed circles) to the magnetic field for τ = 1 s. The solid lines are Gaussian fits. Top figure is for low magnetic field (60 mT). Bottom one is for is for high field (240 mT). Anisotropy between parallel and perpendicular behaviour is clearly visible for high field case. 150

Figure 8.6 Field dependent variation of $\eta_{\parallel,\perp}$ with varying concentration of superparamagnetic particles. Concentrations are for 16%, 14%, 10% and 8% by weight, respectively for (a), (b), (c), (d) 151

Figure 8.7 A representative rendering of chain formation by magnetic nanoparticles (irregular particles) and the position of silica beads (regular spheres) in relationship to them. Cases mentioned in text as (i), (ii), (iii) and (iv) are clearly seen in figure 153
Figure 8.8 (color online) All values of storage (G′) and loss (G″) moduli for different magnetic fields, as a function of time, plotted together for comparison. Empty symbols represent parallel components and filled ones are are corresponding perpendicular components. 154
Figure 8.9 Storage (G′) (left) and loss (G″) (right), moduli for different magnetic fields as a function of deformation frequency. It can be noticed that G″ dominates G′ at lower fields. At intermediate fields, their values are closer to each other. At much higher fields G′ becomes significantly higher than G″. Furthermore, at these higher fields, both components become almost constant across deformation frequency ω, indicating a solid like behaviour, due to strong chain formation 155
Figure 8.10 Relaxation time scale τ as a function of field (above) and for different concentrations (below). Perpendicular components are indicated by filled symbols and parallel are by open symbols. 159
Figure 8.11 Field dependent variation of α 160

1

INTRODUCTION

1.1 COMPLEX FLUIDS

A material composed of a liquid base within which supra molecular structures such as polymers, droplets, particles whose physical attributes are between solids and liquids [1] can be described as complex fluids. These materials are neither purely elastic nor purely viscous but viscoelastic. In such materials, energy is stored and dissipated in a frequency dependent way in a way are similar to deformable solids. We come across several examples of complex fluids in everyday life, such as polymer materials, living biological cells, Micells, cytoplasm, corn starch, liquid crystals, ferro fluids etc.,. Among complex fluids, materials like liquid crystals exhibit local spatial homogeneity but also have a preferred orienteation, and leads to anisotropic diffusivity; these are anisotropic complex fluids. But, materials like cytoplasm, micells are inhomogeneous and do not have preferred direction in the alignment.

The peculiarities of the complex fluids stem from their complex structures and dynamics with their dynamical variations at micro and nano length scales and possesing slow dynamical variations on small time scales. Important technological applications like fast switching operations in LCD (liquid crystal displays), medical applications like drug deliveries, paints, food, cosmetics industry, coolants, oil recovery, processing of plastics are few examples that shows the necessity of understanding of dynamics of complex fluids.

In this thesis, anisotropic complex fluids that possess a particular alignment of particulate and the concerned dynamics are of criteria to study . In particular, slow diffusion dynamics of 8CB (4-cyano $4^{'}$ Octyl biphenyl) liquid crystals with phase transition temperatures as : Crystalline 21.5°C Smectic A 33.5°C Nematic 40.5°C Isotropic. A131 bent core liquid crystals (BCN) with phase transition temperatures as : 82.5°CCrystalline 93.5°C Smectic Y 104.3°C Smectic X 118.5°C biaxial nematic N_b 149°C uniaxial nematic N_u 176.5°C Isotropic and

$Mn_{0.75}Zn_{0.25}Fe_2O_4$ super paramagnetic fluids are studied. Normally, in liquid crystals, molecules are aligned in a particular direction called nematic director ($\hat{\mathbf{n}}$) [2]. In this thesis, we present our study of three specific complex fluids and their dynamical behavior. Two types of liquid crystals, viz., 8CB liquid crstals, and bent core A131 and a ferrofluid composed of $Mn_{0.75}Zn_{0.25}Fe_2O_4$ are the fluids chosen for our study. All the three exhibit a preferred orientational direction, which can be obtained either by chemical coating on to the surfaces of the sample cell as in case of liquid crystals, or by application of external magnetic field as in case of ferro fluids. All the three materials show very interesting dynamics, by virtue of the fact that they are complex fluids. In addition, each of these have a unique behavior which arises from their microstructural properties. For instance, 8CB liquid crystals show collective molecular orientations which tumble along different axis with change in temperature. In bent core liquid crystals, bent shape of the moleculues leads to spontaneous biaxiality. There is some ambiguity in earlier research work with respect to the experimental evidence of this biaxiality. Both 8CB and BCN show presence of different structural formations. As temperature varies, each of these structures show its own unique signature of dynamics. Ferrofluids, on the other hand, are suspensions of magnetic nano particles in a fluid media. These nano particles tend to form long chains. The elastic and diffusion properties of these chains are additionally affected by the external magnetic field.

1.2 EARLY EFFORTS

Experimental investigations to understand the structures and aspects of tumbling nemato dynamics of 8CB liquid crystals, has been undertaken using several different experimental techniques. X-ray scattering studies [3], shear rheology [4, 5], etc., are few techniques that were used in earlier work. Similarly, bent core liquid crystals, were studied using X-ray scattering[6], NMR[7], dynamic light scattering[8] , Raman scattering[9]. But, yet discriminating orientational director fluctuations and tumbling orientations in bent core liquid crystals is still difficult. Also, there are still ambiguities present in the proof of spontaneous biaxiality. To understand the flow properties of ferrofluids, experimental

techniques like, bulk rheology [10, 11] were used and the theoretical understanding of flow properties of these ferrofluids are understood using magneto hydrodynamics. Different experiments need to be performed to measure different flow properties of ferrofluids.

Isolated particle tracking method to determine the Brownian motion is a simple method to setup, learn and understand these complex fluids. In complex fluids, structural properties, mesophases formed, equilibrium and non-equilibrium dynamics of complex fluids, rheological properties are coupled with one another. Micro rheology is a way to study the flow characteristics, deformation of of small volumes of materials, typically involving the thermal motion of the colloidal probe in small volumes of complex fluids.

In microrheology, a passive tracer bead probes the evolution of a material with minimal perturbation and also gives information about the local material heterogenities. During evolution process, materials generally gets deformed and energy is dissipated. This dissipated energy need not be in the thermal form. It can also be in mechanical forms (translational or rotational). Which leads to biased Brownian motion of the tracer particle. Hence anomalies in the diffusive motion of the probing colloidal particle. The major advantage of single particle tracking experiment lies in its requirement for small volumes (10 to 50 μl) of sample. as opposed to large volumes of sample (about 1ml) in shear rheology. This proposes additional difficulty, because the synthesis of such materials are difficult. Bulk rheology also requires that different frequency components have to be separately measured. Whereas in microrheology, data can be Fourier transformed to obtain results for a wide range of frequencies. In bulk rheology measurements each frequency is measured seperately. Also, local material heterogeneties can be probed by the colloidal particle motion, which is inaccessible to bulk rheology measurements. Further, the the single particle tracking experiment requires standard laboratory equipment and thus experiment is relatively simple.

In this thesis, single particle tracking experiment is used to measure the microrheological, microstructural and micromechanical properties of typical complex fluids viz., 8CB, bent core liquid crystals and $Mn_{0.75}Zn_{0.25}Fe_2O_4$ ferrofluids. Specifically, this experimental technique is useful to apply for zero shear conditions and incase of the collective molecular orientations that vary slowly in time can be probed,

hence understand the structures formed in the complex fluids. The basic advantage of single particle tracking technique in addressing the material heterogeneties is used in case of bent core liquid crystals. In bent core liquid crystals, orientational director fluctuations and tumbling molecular orientations were discriminated by measuring them along parallel and perpendicular directions to the nematic director. Also, microrheological measurements that shows the dissipation of energy during the rotational motion of clusters of the bent core molecules have been useful to identify the symmetry and physical properties of the bent core liquid crystals. Also, the consequences of spontaneous biaxiality are verified using this expeimental technique. The simple measurements of viscosity of ferrofluid using single particle tracking experiment, have led to compute the flow properties of the ferrofluids. Magneto viscous effect, phase transition from fluid to viscoelastic to solid behavior were also observed as the results of usin this experimental technique.

This experimental data is analyzed by using Stokes-Einstein equation, of course, is useful to measure, only two distinct diffusivities along parallel and perpendicular directions to the nematic director and the measured viscosities are the effective averages of the five distinct viscosities, four elastic constants that are expected from using Ericksen-Leslie equations.

In measuring the Brownian motion of collodial particle in liquid crystals, a commercial inverted microscope with built in particle tracking programmes is used. But, a home-built microscope set up with a homogeneous magnetic field is used in particle tracking measurements for ferrofluids.

1.3 LIQUID CRYSTALS

A state of matter intermediate between that of a crystalline solid and isotropic liquid are called Liquid crystals (LCs). These organic compounds exhibits many of mechanical properties which are liquid like such as viscosity, surface tension, inability to support shear(shear thinning). Anisotropy in optical, electrical and magnectic properties are similar to crystals [12, 13]. Frederich Reinitzer first discovered this

state of matter in 1888, Lehmann in 1889 characterized and suggested the name 'liquid crystal'.

There exist two types of liquid crystals:

- thermotropic (liquid crystalline phase is manifested by virtue of temperature)
- lyotropic (liquid crystalline phase is manifested by virtue of concentration)

In this thesis we study the dynamically varying micro structural and micro mechanical properties of thermotropic liquid crystals.

1.3.1 *Classification of thermotropic liquid crystals*

These elongated moleculear shape leads to shape anisotropy. Classification of thermotropic liquid crystals is dependent on the shape of the constituent molecules.

1. Calamitic liquid crystals : made of rod shape molecules
2. Discotic liquid crystals : made of disc shape molecules
3. Bent-core liquid crystals : made of bent shape molecules

In this thesis, physical properties of calamitic LCs (8cb liquid crystals) and bent-core LCs are discussed.

Thermotropic liquid crystalline phases:

1.3.2 *Isotropic*

Molecules are randomly oriented in this phase. Ordinary viscous behavior is assimilated. No correlations would exist between molecules.

1.3.3 *Nematic*

Liquid crystal molecules in nematic phase have long range orientational order. In nematic phase of calamitic liquid crystals, the long axes of the molecules tend to align along a preferred direction. But, the locally preferred direction may vary through out the liquid crystal

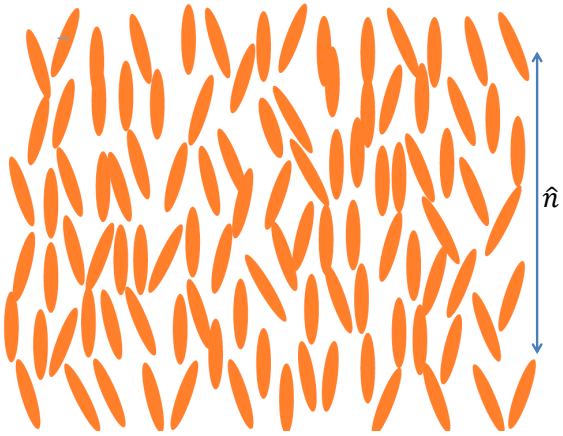

Figure 1.1: Schematic representation of liquid crystals molecular alignment in the calamitic nematic phase

medium. Many interesting phenomenon of LCS depends on dynamics and geometry of the preferred axis. It is useful to define a vector field that defines these local orientation of LCs. The direction of this vector field is represented by a dimensionless unit vector called director $(\hat{\mathbf{n}})$. Though there is long range orientational order, but there is no long-range order in the positions of centers of mass of the molecules. These molecules rotate about their long axes but with no preferential arrangement of two ends of the molecules. So, the director $(\hat{\mathbf{n}})$ is apolar. That means, $(\hat{\mathbf{n}})$ and -$(\hat{\mathbf{n}})$ cannot be distinguished. Thus, optically a calamitic nematic behaves as a uniaxial material with a center of symmetry. In nematic phase, molecules are arranged in groups. In these groups, centers of mass of the molecules in each group lies in one plane. That means, there exists short-range order of the smectic clusters (Details of smectic phase liquid crystals are discussed later in this section).

1.3.4 *Cholestric*

In cholestric phase, the director $(\hat{\mathbf{n}})$ rotates continuously in space along the Z-direction with a spatial period of π/p. Here p defines the pitch of the helix of cholestric phase which can be righ or left handed. The chirality of this system leads to a helical distortion. The configuration

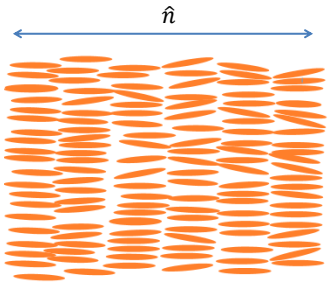

Figure 1.2: Schematic representation of liquid crystals molecular alignment in the Smectic A phase

of nematic which is initially aligned along the y axis, if twisted about the x axis visualizes the cholestric phase.

1.3.5 *Smectic*

In smectic phase of liquid crystals, molecules are arranged in layers and there exists positional correlation and orientational ordering in these molecules. There exist many types of smectic liquid crystals depending on the molecular arrangement within the layer. In view of thesis contents, here we discuss about smectic A, smectic C, and smectic C^* phases.

Smectic A

In smectic A phase, the centers of the molecules in each layer are randomly arranged, but the average orientation of the long axes of the molecules is along the layer normal as shown in fig. 1.2. That means, the molecules are aligned perpendicular to the layers with no long range crystalline order. But, the layers can freely slide one over the other. So, this phase is considered as a one-dimensional crystal and two-dimensional liquid.

Figure 1.3: Schematic representation of liquid crystals molecular alignment in the Smectic C phase. The lc molecules are tilted with respect to layer normal $(\hat{\mathbf{k}})$.

Smectic C

In smectic C phase, the preferred axis is not perpendicular to the layers. But, the molecules are tilted with respect to the layer normal as shown in fig.1.3. So, this phase shows biaxial symmetry (N_b). In contrary to uniaxial symmetry (N_u), where the molecules are oriented along the director $(\hat{\mathbf{n}})$, in the N_b phase, there exists additional orientational ordering along a second axis or secondary director $(\hat{\mathbf{m}})$. So, in the (N_b) phase the physical properties in the plane perpendicular to $(\hat{\mathbf{n}})$ are anisotropic.

*Smectic C**

Smectic C^*, gets manifested by the smectic C phase composed of chiral molecules with chiral interactions that lead to the formation of helical structure as shown in fig.1.4

In general nematic N and smectic A liquid crystals are uniaxial. Because, these molecules although they are not cylindrically symmetric, they freely rotate about the long molecular axis.

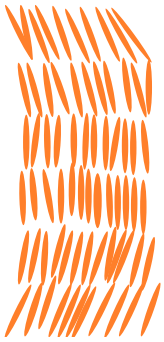

Figure 1.4: Schematic representation of liquid crystals (lc) molecular alignment in the Smectic C^* phase. The tilt direction rotates between successive layers

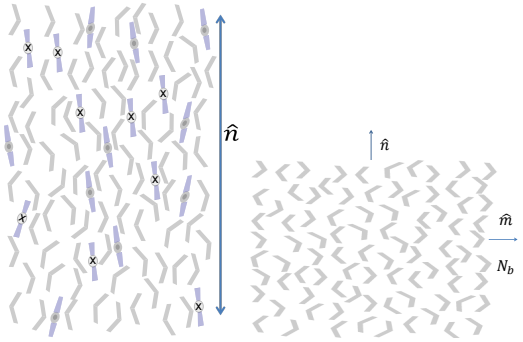

Figure 1.5: Uniaxiality(left) and biaxiality(right) in bent core liquid crystals

1.4 BENT-CORE LIQUID CRYSTALS

The bent-core liquid crystals, because of their bent shape with a bent angle of $\sim 120^{\circ}$ possess some new liquid crystalline phases along with phases observable in the calamitic liquid crystals [12, 13]. The bent core shape of these molecules can be compared with a bow, the molecule's long axis with the string (wingspan), and the apex of the core which shows the direction of the "bend" with respect to the direction of arrow. The long axes of these molecules with 'in plane' and 'out of plane' orientations lie along one direction which is primary director of the bent core liquid crystals showing uniaxiality . The left figure in This "bow" shape of these molecules naturally prefers a secondary direction for orientational ordering, which is orthogonal to uniaxial director $(\hat{\mathbf{n}})$. In brief, these bent core molecules are polar, biaxial in shape and deviate from cylindrical symmetry 1.5.

1.5 PROPERTIES OF NEMATIC LIQUID CRYSTALS

1.5.1 *Orientational order parameter*

In different phases of liquid crystals, a measure of order defines the order parameter. The orientational order parameter (S) describes the average orientation of the long axes of the molecules along $(\hat{\mathbf{n}})$. S in nematics is described by a second rank symmetric traceless tensor. The degree of order is specified by order parameter S represented by the average of the second Legendre polynomial

$$S = \langle 3cos^2\theta - 1 \rangle /2 \tag{1.1}$$

the angle between the molecular long axis (θ) and the director n, and the brackets indicate an average over all the molecules in the liquid crystal. The liquid crystal order parameter for nematic phase is a scalar varying in the interval $(0 < S < 1)$ where as for isotropic phase S=0 and for perfectly ordered states S=1.

1.5.2 *Elasticity*

In nematic liquid crystals varying director orientations in space causes deformations. These deformations brings differences in elastic energy densities among the molecular clusters or layers. This causes elastic distortions, which are combinations of three types of basic curvature elastic deformations. They are called splay, twist and bend elastic deformations. The free energy density deformations (F_d) is

$$F_d = \frac{1}{2}K_{11}(\nabla.\hat{\mathbf{n}})^2 + \frac{1}{2}K_{22}(\hat{\mathbf{n}}.\nabla \times \hat{\mathbf{n}})^2 + \frac{1}{2}K_{33}(\hat{\mathbf{n}} \times \nabla \times \hat{\mathbf{n}})^2 \qquad (1.2)$$

here K_{11}, K_{22} and K_{33} are the splay, twist and bend elastic constants respectively. These elastic constants are of the order of k_BT/a, here k_B is the Boltzmann constant and a is diameter of the molecule. Typically magnitude of these constants are $\sim 10^{-11}$ N/m. Generally, in nematic phase of liquid crystals, $K_{33} > K_{11} > K_{22}$ [14].

1.5.3 *Pretilt angle*

In a planar cell, the director $\hat{\mathbf{n}}$ is uniformly oriented along the easy axis which makes an angle θ with respect to the cell alignment direction. This angle θ defines the minimum of the surface anchoring potential and is called pretilt angle.

1.5.4 *Anchoring energy*

The planar alignment surface generally imposes some preferred orientational directions, anchoring directions(easy direction). The orientation of the director $\hat{\mathbf{n}}$ at the interface of a surface depends on a polar surface angle (ψ_s), and of an azimuthal angle, ϕ_s. The energy required to rotate the director from easy axis is called anchoring energy. The surface free energy per unit area is

$$F_s = \frac{1}{2}Asin^2\psi_s \qquad (1.3)$$

here ψ_s is the tilt angle of the director $\hat{\mathbf{n}}$ with respect to the surface and A is anchoring energy per unit area [15]. If the anchoring to

a surface is strong, $\hat{\mathbf{n}}$ makes a well-defined angle with the surface, irrespective of the resultant elastic distortions [16]. Where as, in the limit of weak anchoring, the competition between anchoring energy and elastic distortions may lead to different orientations of the director at the interface, which leads to more complex behavior [17].

1.6 DEFECTS IN NEMATIC LIQUID CRYSTALS

Liquid crystals in confined untreates substrates will have director varying slowly in space and schlieren textures can be observed between crossed polarizers. These textures exhibit sets of curved dark brushes. These dark brushes correspond to the extinction of the nematic director field $\hat{\mathbf{n}}$ coinciding with the direction of either polarizer or analyzer. These brushes come together to form a singular point or vortex. These singularities are notified as disinclinations with defect strength (s). These brushes are commonly two or fourfold type. The sense of rotation of brushes with respect to polarizer's rotation defines the sign of the defect. If dark brushes rotate in the same direction as that of optic axis of polarizer's, then it is called a plus (+) defect, otherwise it is minus (-) defect. Any liquid crystals sample will have equal number of defects and anti defects. Defects of same strength but opposite sign attract and annihilate.

1.6.1 *Free energy density*

In a planar structure, the director is confined to the xy plane. So, the components of the director $n_x = \cos\phi$, $n_y = \sin\phi$, and $n_z = 0$. Considering the liquid crystals medium being elastically isotropic, with one-constant approximation($K_{11} = K_{22} = K_{33} = K$) with static deformation, the free (elastic) energy density is

$$F_d = K(\nabla\phi)^2/2 \tag{1.4}$$

minimizing the free energy density by ,

$$\nabla^2\phi = 0 \tag{1.5}$$

the solutions of equation 1.4 are $\phi = 0$ and $\phi = s\theta + c$. Here

$$\theta = tan^{-1}(y/x) \tag{1.6}$$

The director configuration around a disclination line can be described by this equation.

1.7 MAGNETIC FLUIDS

Ferromagnetic

A material that holds magnetic ordering in the absence of external magnetic field are termed ferromagnetic.

Ferrofluids

These are suspensions of nano meter or sub micrometer sized magnetic particles in solvents like water or organic solvents(kerosene etc.,) and are coated with a surfactant to keep them dispersed [18].

The suspensions of magnetic nano particles in appropriate carrier liquid with a combination of physical properties like normal liquid behavior with the possibility to control their flow properties, changes its physical propeties with the application of magnetic field. Due to their small size ($\sim$ 10 nm in diameter), they neither sediment nor agglomerate in the carrier liquids. Generally, these carrier liquids are water, kerosene, and various oils that do not evaporate easily. By coating these nano particles with a long chain organic molecules (eg.DMOAP), a stable suspension can be achieved. These organic molecules generate a repulsive force which prevents the particles to form aggregates or to get destabilized.

Super paramagnetic

Ferrofluids behaves as super paramagnetic because, although these nano particles are ferromagnetic, once after removing the field, the induced magnetic ordering disappears over volumes containing many particles. In ferrofluids, because of thermal disorder of particle orientation and also tendency for magnetic particles in suspension to arrange in groups cancels out the net field produced.

If the applied field is zero, the magnetization of super paramagnetic particles becomes zero. As the field is applied, particles acquire a magnetic dipole. If the field is high, magnetization saturates and hence these fluids are called super paramagnetic [19].

1.7.1 *The magnetoviscous effect*

The peculiarity of ferrofluids is combination of normal liquid behvior with a magnetic control of their physical flow properties. The origin of these physical properties can be interpreted by considering each magnetic nano particle as a thermally agitated single domain particle in the carrier liquid. Each particle in the ferrofluid carries magnetic moment of about $10^4 \mu B$. Here B is the applied magnetic field strength. The changes in fluid properties with change in magnetic field strength can be interpreted by considering an isolated, non interacting magnetic dipole, but with a magnetic moment fixed in the particle. Thermal motion of the carrier liquid will generate translational and rotational motion of the magnetic nano particles and thus the translational and rotational motion of the magnetic moment. The axis of rotation of the nano particle is aligned with the vorticity of the flow. The application of external magnetic field will tend to align the magnetic moments of the particles with the magnetic field direction. The assumption of fixing the moment in side the particle, will bring a dis- alignment of magnetic moment with the magnetic field. Here, the translational and rotational motion caused by the viscous friction will lead to disalignment of the magnetic moment. This disalignment gives rise to magnetic torque which counteracts the mechanical torque due to the translational flow due to thermal or Brownian motion. Thus, thermal motion and free rotation of the magnetic nano particle will be hindered leads to an increase of viscosity [10].

Magnetic relaxation process

The contribution of magnetic moment of each particle to the magneto viscous effect depends mainly on the magnetic relaxation behavior of the particles. These nano particles with fixed magnetic moment can align with the field by a rotation of the whole particle, process called 'Brownian relaxation' or by a change of the direction of magnetic moment inside the particle, called N*é*el relaxation process. Brownian relaxation process is characterized by volume of the particles $\tilde{V}$ and the viscosity of the fluid. Brownian relaxation time is

$$\tau_B = 3\tilde{V}\eta / k_B T \tag{1.7}$$

Neel relaxation time depends on the volume of the magnetic core V and the anisotropy constant K_a of the particles and is given by

$$\tau_N = f_0^{-1} exp\,(K_a V / k_B T) \tag{1.8}$$

where f_0 is the Larmour frequency of the magnetic moment in the anisotropy field of the particle.

1.8 SALIENT FEATURES OF THE THESIS

1. The rheological parameters of the liquid crystals are obtained in two distinct orthogonal directions - parallel and perpendicular to the nematic director and in case of ferrofluids, these are obtained parallel and perpendicular to the applied external field.
2. Subsequent parameters such as elastic(G') and viscous modulus(G''), the velocity auto correlation function, relaxation time etc., were also obtained in both parallel and perpendicular directions.
3. Distinct signature of the tumbling of nematic director of 8CB liquid crystals was observed from our results. Consequences of various structural formations in the nematic phase of 8CB was also observed.
4. Structural biaxiality despite an optical isotropy was observed in the isotropic phase of bent core liquid crystals. Also, we could propose an unambiguous signature of spontaneous biaxiality as a positive proof.
5. In case of ferrofluids, a transition from liquid to viscoelastic and to solid behavior was seen with the increase in magnetic field. Flow parameters and microstructural properties of ferrofluids are computed by applying the measured viscosity values in magneto hydrodynamics equations. This has been a new and simple approach to measure these parameters.

1.9 OUT LINE OF THE THESIS

In **chapter 1**, introduction about complex fluids, liquid crystals, types of liquid crystals, various phases, sub phases of liquid crystals and

brief description about the physical properties of liquid crystals is presented. Also, ferrofluids, super paramagnetic fluids, the physics behind the physical properties of ferrofluids are reported.

In **chapter 2**, how the presence of colloidal particle perturbs the nematic director and consequences as defects around the colloidal probes are discussed. Diffusion of colloidal particle using stokes drag equations, fundamentals of microrheology, advantages and disadvantages of stokes drag method over using Ericksen-Leslie equations are presented. Also, nemato dynamics and theory from literature on perturbed nematic director by the motion of the colloidal particle is discussed. Further, surface treatment for collodial probe (silica bead), liquid crystal sample cell preparation, single particle tracking experiment details for colloidal particle motion in liquid crystals are presented.

In **chapter 3**, results of diffusion dynamics of a 0.98 μm silica sphere is used in determining precessional motion of director in various nematic phase of 8CB liquid crystals, as it probes those oriented structures which are of the same wavelength as of the sphere size. Velocity auto correlation(VACF) is used in determining those structures in both parallel and perpendicular orientations to the neamatic director. Further, a generic approach by considering the time dependent harmonic oscillator motions is used to understand the VACF distribution function. This approach leads to observe a transition in the structures of nematic phase are comparable to transformations from underdamped harmonic oscillator motion to critically damped motion. We also have measured the microstructural properties and calculated micromechanical properties.

In **chapter 4**, results of this chapter on microrheological properties of 8CB liquid crystals is in continuation with chapter 3. In nematic (orientationally order fluid) phase of 8CB liquid crystals, $(\hat{\mathbf{n}})$ tumbles between flow axis(parallel to $(\hat{\mathbf{n}})$) and flow gradient axis (perpendicular to $(\hat{\mathbf{n}})$). This tumbling director leads to different structural regimes in nematic phase of 8CB liquid crystals. Tracking the Brownian motion of a microsphere elastic($G^{'}$) and viscous modulus($G^{''}$) are computed. The frequency dependence of ($G^{'}$) in different regimes, resulted in addressing the tumbling of behavior of $(\hat{\mathbf{n}})$ by comparing with motion of a coupled harmonic oscillator. This is a generic approach and can be followed in understanding the anomalous behavior of complex fluids.

We also have measured the dynamic viscosity from viscous modulus (G'').

In **chapter 5**, the measurements of viscosities of bent-core nematic liquid crystals is reported. From the thermal motion of the colloidal sphere, the self diffusion coefficients are measured in a planar aligned sample. passive viscosities are measured by measuring self diffusion coefficients of a microsphere of 0.98 μm diameter. The temperature dependence of passive viscosities is stronger than that of active viscosities. The effect of presmectic fluctuations are profound at much higher temperatures than the N-Sm-C transition temperature than commonly seen in calamitic liquid crystals. The study of Brownian motion is useful to understand the smectic fluctuations in bent-core nematic liquid crystals.

Microrheology experiment is a sensitive technique to measure the mechanical response of complex fluids to weak forces applied by the colloidal particle motion. This mechanical response is generally frequency dependent and viscoelastic. This response of the material are described by elastic and viscous moduli of the material. In **chapter 6**, microrheology experiment is used to probe the structure and dynamics of bent core liquid crystals in both isotropic and nematic phases. orientational director fluctuations and tumbling molecular orientations were discriminated by measuring them along parallel and perpendicular directions to the nematic director. The inhomogeneity, physical rigidity of nano particulate kind of suspension in the isotropic phase is reported. The uniaxiality, uniaxial to biaxial properties during the slow motion and complete rotation of the bent core molecule clusters are addressed in terms of the dissipation of energy during their motion. Also, orthogonal biaxiality and monoclinc biaxiality are differentiated in terms of the frequency response of the materials by reporting the presence of nematic and smectic clusters in the perpendicular direction to the nematic director. Also, a sudden jump in the dissipation of energy are observed and reported as consequences of total flip or out of plane motion of the molecular clusters. Further, close to smectic phase, the decrease in the values of dissipation of energy are observed which is a consequence of surface anchoring effects.

chapter 7 is meant for the inference on the diffusion of colloidal particle in liquid crystals and the best approach to be followed in such complex fluids. The diffusivity memory but no direction memory in

the particle trajectory of complex fluids leads to both linear ity in mean square displacement and a non-Gaussian at short times. A recently proposed theoretical model to understand the diffusivity undergoing biased random walk which was termed as "diffusing diffusivity" is applied to the diffusion of colloidal particle in 8CB liquid crystals. It is observed that, this concept of "diffusing diffusivity" well suits for the addressing the sub diffusive motion of colloidal particles in 8CB liquid crystals. Also, it was realized that, in addressing the diffusion of colloidal particle in complex fluids, the best practice is to understand the correlation between molecules which describes the structures formed during the dynamics of complex fluids along with anomalies in diffusion of Brownian motion.

chapter 8 consists of microrheological and micro-structural properties of a super paramagnetic ferrofluid made of $Mn_{0.75}Zn_{0.25}Fe_2O_4$ nanoparticles measured using a home built inverted microscope. Thermal motion of a probe microscphere was measured for different values of an applied magnetic field and analyzed. The analysis shows anisotropy in the magneto viscous effect[20]. Additional microrheological properties, such as storage modulus, loss modulus and their transition is observed. Following theory of magneto hydrodynamics [21], [22], we obtained the micro structural properties such as elongational flow coefficient λ_2, relaxation time constant (τ), coefficient of dissipative magnetization α. From the measured viscosity data, all the above parameters could be obtained. Our values for the above parameters are in agreement with the earlier theoretical and shear rheology experiments.

In **chapter 9**, finally, in this chapter, conclusions and future scope of the work are presented.

BIBLIOGRAPHY

[1] Todd M. Squires and Thomas G. Mason, Annu. Rev. Fluid Mech. **42**, 413 (2010).

[2] J. C. Loudet, P. Hanusse, P. Poulin, Science, **306**, 1525 (2004).

[3] C. R. Safinya, E. B. Sirota, and R. J. Piano, Phys. Rev.Lett., **66**, 15, (1991).

[4] D.F. Gu and A.M. Jamieson, J.Rheol. **38**, 3 (1994).

[5] K. Negita, J. Chem. Phys. **105**, 7837 (1996).

[6] Bharat R. Acharya, Andrew Primak, and Satyendra Kumar, Phys.Rev.Lett. **92**, 14, (2004).

[7] Valentina Domenici, Diego Frezzato, and Carlo Alberto Veracini, J.Phys. Chem. B **110**, 24884 (2006) and Valentina Domenici, Soft Matter, **7**, 1589 (2011).

[8] D. Wiant, S.Stojadinovic, K. Neupane, S. Sharma, K.Fodorcsorba, A.Jakli, J.T. Gleeson and S. Sprunt, Phys. Rev. E **73**, 030703 (2006).

[9] M.S.Park, B.J.Yoon, J.O.Park, Veena Prasad, S.Kumar, M.Srinivasarao, Phys.Rev. Lett. **105**, 027801 (2010).

[10] S. Odenbach, J. Phys. Cond. Matt. **23**, 346002 (2011).

[11] Hamid Shahnazian and Stefan Odenbach, J. Phys.: Condens. Matter, **20**, 204137 (2008).

[12] P.G. de Gennes, "The Physics of Liquid crystals", 2nd ed.(Oxford university Press,Oxford), (1993).

[13] S.Chandrasekhar, Liquid crystals, 2nd ed.(Cambridge University Press), (1992).

[14] T. Arun Kumar, "Study of perfluoro polymer as an alignment layer for nematic liquid crystals", University of Hyderabad, Ph.D. Thesis - Unpublished (2012).

[15] A. Rapini, M. Papoular, J. Phys. Colloq. France **30**, C4-54 (1969).

[16] P. Poulin and D. A. Weitz, Phys. Rev. E., **57**, 1 (1998).

[17] O. V. Kusenok, R. W. Ruhwandl, S. V. Shiyanovskiin, and E. M. Terentjev, Phys. Rev. E, **54**, 5198 (1996).

[18] Noel A. Clark, Nature **504**, 229, (2013) and references therein.

[19] Jordi Faraudo, Jordi S. Andreu and Juan Camacho, Soft Matter, **9**, 6654 (2013).

[20] Stefan Odenbach, and Hanns Walter Mller, Phys. Rev.Lett., **89**, 3 (2002).

[21] Oliver Muller, Dorothea Hahn and Mario Liu, J. Phys.Condens. Matter **18**, S2623 (2006) and references therein.

[22] S. Mahle, P. Ilg, M. Liu, Phys.Rev. E. **77**, 016305 (2008) and references therein.

2

BROWNIAN MOTION OF COLLOIDAL PARTICLE IN LIQUID CRYSTALS

2.1 COLLOIDS IN LIQUID CRYSTALS

In nematic liquid crystals(NLC), liquid crystal molecules are orientationally ordered complex fluids. These molecules are aligned spontaneously along the nematic director $\hat{\mathbf{n}}$ [1],[2]. Oriented molecules in certain direction leads to anisotropy. This orientation of NLC can be manipulated by anisotropic surfaces, electric and magnetic fields. A colloidal particle introduced into NLC disturbs the local orientation of nematic molecules [3]. Because, these NLC molecules interacts with the surfaces of colloidal particle. This disturbance can be considered as an elastic deformation of the NLC and it spreads on a micrometer scale. This deformation depends on the confinement, size of colloidal particles, strength of anchoring at the surfaces[4].

In this thesis, colloids dispersed in liquid crystals were treated with DMOAP (Sigma-Aldrich) to induce perpendicular surface orientation (homeotropic alignment) of the liquid crystal molecules. But, the surfaces of the cell that confines the liquid crystal were chemically treated with polymide AL 1254 to induce parallel orientation (planar alignment). This kind of alignment on colloidal sphere and on surfaces of cell results in elastic distortions. This leads to repulsive interaction between the colloids and the walls of the cell. Hence, this configuration of alignment leads to elastically stabilizing the colloids in the middle of the NLC layer. Also, this anisotropy in energies of interaction leads to anisotropy in the mobility properties. In general, the parallel and perpendicular direction mobilities of liquid crystal molecules are different from each other. Which induces the relative diffusion of the colloidal particle with respect to $\hat{\mathbf{n}}$ [5].

2.1.1 *Topological defects with colloids in liquid crystals*

An ordered medium is generally free of defects. Defects in liquid crystals can be simply defined as localized spots with *ill defined* order parameter and hence the director orientation is also not defined (singular point or disordered spot) [6]. These defects alters the physical properties of NLC locally and increases the overall free energy. However, the influence of surfaces, lowering of the symmetry during phase transitions, external field applications can spontaneously or controllably generate and stabilize topological defects. The director lines meet at a central point with radial symmetry in the far field, resulting in the topological defect. Simply, topological defects abound systems with broken symmetries. Colloidal particle with homeotropic anchoring is a source to a topological defect called as radial hedgehog. Hedgehogs are point defects in which the director $\hat{\mathbf{n}}$ sweeps out all directions on a unit sphere an integer number of times on a spherical surface enclosing the defect. Characterization of these defects is generally done by topological charge.

Topological charge

The integer specifying the number of times the unit sphere is wrapped by the director $\hat{\mathbf{n}}$ [7]. The defect line is along z axis and the director orientation starting from one point on this path, the director vector $\vec{\mathbf{n}}$ makes an angle of $\theta = 2\pi s$ over one complete angular trip. Here, s is the topological 'rank' of the defects. If the medium is apolar, then $s = \pm 1/2, \pm 1, \pm 3/2...$, where as for polar medium $s = \pm 1, \pm 2, \pm 3.....$ Depending on the sense of rotation of the director θ can be positive or negative, which determines the topological 'charge' of the defects. Topological charges always occurs in pairs with opposite signs. Hence, the net topological charge of a system remains conserved. Hedgehogs with positive and negative charges are indistinguishable. Because, in liquid crystals, **n** is equivalent to **-n**. Hence, in liquid crystals, hedgehog defects are characterized with positive charges only. Two hedgehogs with different charges s_1 and s_2 respectively, can combine to form hedgehog with charge $s_1 + s_2$ or $s_1 - s_2$. The boundary conditions and the geometry of NLC impose topological constraints. To conserve energy, these boundary conditions of the topological constraints must

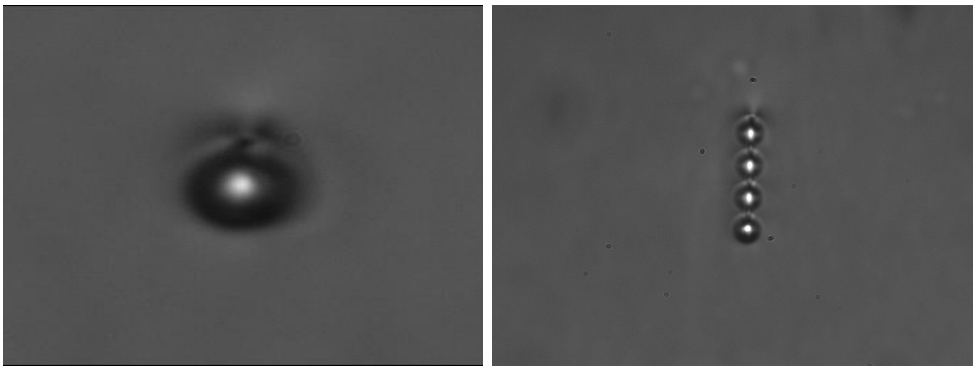

Figure 2.1: In the above figure left picture represents dipole defect with 0.98μ m colloidal particle picture on right is a chain of collodial particles with dipole defects.

be satisfied by the director field of the NLC. These topological defects play an important role in determining the elastic interactions between colloidal particles suspended in a liquid crystal medium. When the boundary conditions are not satisfied, the energy scale of elastic distortion around a colloidal particle is indeed driven by anchoring effects of the NLC molecules and this elastic distortion is of the order of Ka, where K is a elastic constant of the NLC ($K \sim 10^{-11}N$) and a is the radius of the colloidal particle ($a = 1\mu m$). Thus, energy scale of distortion, $Ka \simeq 1000k_BT$ where k_B is the Boltzmann constant and T is the temperature. Hence, the elastic interactions of NLC dominate the entropic free energy of the colloidal particle.

In case of homeotropic anchoring for a spherical colloidal particle embedded in a nematic cell, this particle imposes the director at its surface and this tends to align the director field with the normal of the bead. Here, the bead is a source of singularity for the director field. Because of the uniform far-field director in the cell and the conservation of the topological charge, a topological defect appears in the close vicinity of the director field [8]. colloidal particles with homeotropic anchoring possess two types of topological defects as shown in figures 2.1, 2.2. A homeotropic anchoring on the colloidal particle induces distortion in the director field close to its surface resulting in the generation of topological point defects. For strong homeotropic anchoring, the topological defect is a hyperbolic hedge-

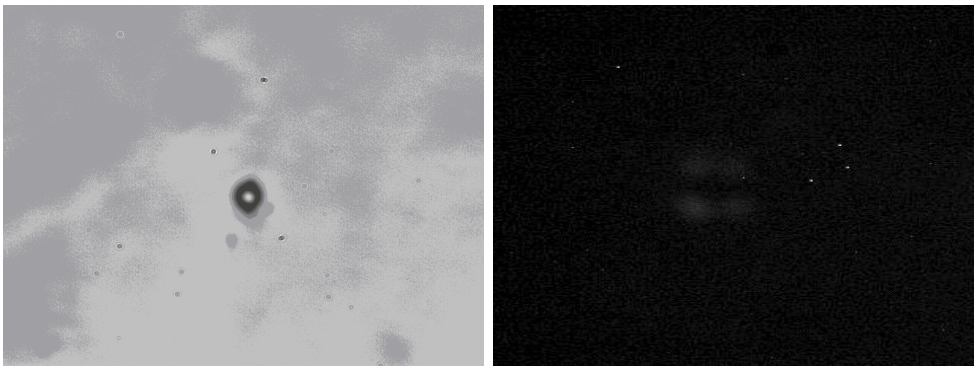

Figure 2.2: Quadrupole defect with 0.98μ m colloidal particle.

hog point defect, which forms an elastic dipole with the colloidal particle. In this case, both colloid and hedgehog are oriented along the rubbing direction. Thus forming an analog of the electric dipole [9]. These dipoles spontaneously assemble into dipolar chains oriented along the rubbing direction of the director. The dipole comprising the point like defect is known as "hyperbolic hedgehog" defect and if the colloidal particle itself behaves as a source of orientational field is known as "radial hedgehog" defect. Topological charges of hyperbolic and hedgehog defects corresponds to -1 and $+1$ respectively. Whereas, for weak anchoring strength, the defect adopts the shape of a thin disclination line encircling the particle. The director field exhibits a quadrupolar symmetry in this case. This symmetry is also obtained with the planar or homogeneous anchoring of the colloidal particle.

2.2 DIFFUSION OF COLLOIDAL PARTICLE IN LIQUID CRYSTALS

Microrheology is the study of flow and deformation of very small volumes of materials, typically involving thermal motion of a probe bead [10]. If softmaterials gets strained, their microstructures both store and dissipate the deformation energy in the frequency dependent manner, reflecting viscoelasticity. The linear mechanical response of soft materials to weak forces is generally frequency dependent and viscoelastic, and can be described by a complex shear modulus $G(\omega) = G'(\omega) + G''(\omega)$, which gives information about the equi-

librium micro structure and dynamics of the material. In passive microrheology, the linear response properties of the materials are extracted from the motion of a thermally fluctuating colloidal probe. Passive microrheology uses micro meter sized polystyrene beads or silica beads as probes embedded within materials to measure local rheological properties such as $G(\omega)$. These probe beads enable measurements to be made with minimal perturbation during the evolution of the soft materials. Also, local material heterogeneities can be probed which is inaccessible in bulk rheology. In passive microrheology, the quantity measured will be the mobility of the probe bead with in the material, from which the passive microrheological parameters are extracted using Generalized Stokes-Einstein relation(GSER). The Stokes component of the GSER relates the measured mobility of the probe bead to the complex shear modulus of the material. But, to validate the Stokes component, the material needs to be homogenous, isotropic, quasi-steady, incompressible continuum. Significantly, the failure of the Stokes component does not render microrheology worthless[11]. Instead, its proper interpretation can provide additional material information that would otherwise inaccessible to bulk rheology. For example, there are reports wherein the mean square displacement of a bead in Phospholipid fluid tubules is Fickian, that is, MSD is proportional to time, but, yet the probability distribution is non-Gaussian that shows the anomalous diffusion behavior [12]. Calculating the Stokes drag in anisotropic media requires Ericksen-Leslie(E-L) description of hydrodynamics. The major difference between the Stokes drag and E-L description is, E-L equations couple the fluid motion to the director motion and therefore requires a solution for the fluid motion and director motion. These equations are complex and only few examples with analytical solutions are available. Some of the problems that can be solved exactly involves shearing the softmatter to find the Miesowicz shear viscosities.

Using generalized Stokes-Einstein's theory of Brownian motion describes that in isotropic fluids, random displacements of a colloidal probe is proportional to the dissipation of kinetic energy which is directly related to the temperature of the medium. Though, the mean displacement is zero but, the averaged one-dimensional mean squared displacement of the Brownian motion of a colloidal sphere grows linearly with time i.e., MSD $\langle r^2(\tau)\rangle = 2D\tau$ Where D is the translational

diffusion coefficient. But, in anisotropic fluids like liquid crystals, because of the orientally ordered structure in the nematic phase, the Brownian motion of the colloidal probe diffuses to longer distances along the nematic director, MSD values will be larger along this direction of nematic director. The mean square displacement(MSD) of μm diameter sized bead is computed from the Brownian motion of colloidal particle using video microscopy. These mean square displacements undergo several dynamical transitions with the change in temperature in liquid crystals. These dynamical transitions are related to the short time and long time dynamics of the relaxation time scales of liquid crystal nematic director surrounding the probing micro sphere. The nematic director deformations and fluctuations in the liquid crystals would lead to anomalous behavior in the Brownian motion of the silica micro sphere. This would lead to power law behavior of the MSD in the liquid crystals as in complex fluids[13, 14] i.e., MSD $\langle r^2(\tau)\rangle = \tau^{\alpha}$. If the exponent value of $\alpha < 1$ then it is subdiffusion, and if it is > 1 then it is super diffusion. Earlier in the literature[15, 16, 17, 18], these complex fluid behaviors are unnoticed at relatively longer time(τ) lags. But,this behvior in nematic liquid crystal was noticed by T.Turiv et.al.,[19] recently. In this paper, they have shown how the the nematic orientational order and its fluctuations results in anisotropic and anomalous diffusion of colloidal particle in liquid crystals The subdiffusive motion for a sphere in liquid crystals is illustrated in that paper as the difference in the elastic energies that arises because of the thermal motion of the bead, generates an opposite restoring elastic force, $\mathbf{F}_{sub} = -K\Delta\mathbf{x}/d$ that slows down the diffusive motion, Here $\Delta\mathbf{x}$ is the distance moved by the colloidal sphere, because of the thermal fluctuations by liquid crystal molecules and d is the diameter of the colloidal sphere, K is elastic constant. Similarly, for the super diffusive motion of a normally anchored sphere, the particle experiences an attractive or repulsive force towards the splay, $\mathbf{F}_{super} = -\nabla U$ where $U = -4\pi K \int \mathbf{P.n}(\nabla.\mathbf{n})dV$ and P is the elastic dipole of the sphere $P \propto d^2$[20].

2.3 NEMATODYNAMICS: FLOW OF NEMATIC LIQUID CRYSTALS

The orientational and positional ordering of the liquid crystal molecules determine the various phases present in it [1, 2]. Dispersion of colloids in nematic liquid crystals(NLC)imposes an orientation on the liquid crystal molecules that locally breaks the uniform nematic alignment and gives rise to elastic interactions. This leads to topological defects that determine the long-range deformation field and govern colloidal pattern formation. The thermal motion of this colloidal particle drags a nematic deformation along its random trajectory. Diffusion of this colloidal particle behaves as a sensitive probe to the local order parameter and surface anchoring. The microrheological properties of liquid crystals strongly depends on the microscopic structure of the constituent molecules and the mesophases. In isotropic liquids, viscosity tensor is symmetric and hence can be approximated by a scalar quantity. Whereas, in nematic liquid crystals, viscosity is a tensor quantity and the nematic director (the average alignment direction along the long axes of the molecules) and velocity fields exert forces on each other. Hence, the viscous stress of a diffusing particle on the surrounding liquid crystal molecules is not the same for motion in parallel and perpendicular directions to the nematic director which results in two different diffusion coefficients, this leads to anisotropy in the microrheological properties of the liquid crystals. There are several theoretical and experimental studies of the low molecular weight liquid crystals, where the molecules have mostly cylindrical symmetry [1].

A schematic view of a director orientation in a calamatic(rod like) nematic liquid crystal with respect to the shear and showing a colloidal particle in liquid crystal(Fig.2.3 crystals picture). The particle moves along the Y-axis. The shear in the plane y=0 is indicated by the decay of the fluid velocity field. It is known that the nematic N phase has three principal viscosities called Miesowicz viscosities, namely η_1, η_2 and η_3 depending on the direction of shear and the orientation of the liquid crystal director. These viscosities can be expressed in terms of Leslie coefficients $\alpha_1 - \alpha_6$, which are used to define nematic stress tensor. In NLC, both α_2 and α_3 are negative close to the nematic-isotropic(N-I) transition and the director is aligned along the flow direction with an angle $\theta = \tan^{-1}\left(\sqrt{\alpha_2/\alpha_3}\right)$. If the liquid crystal compound contains

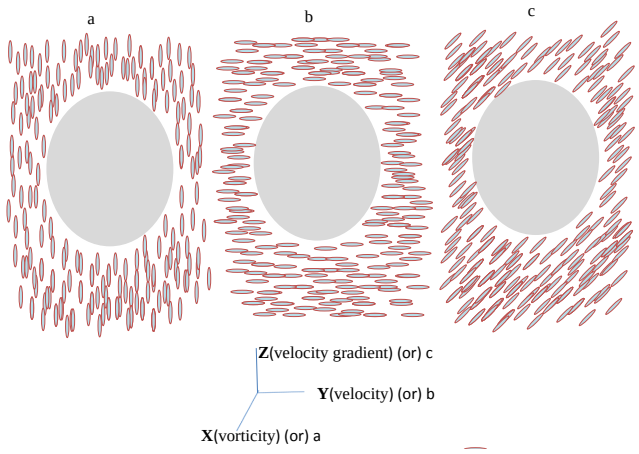

Figure 2.3: a,b,c structures in nematic phase of liquid crystals represent vorticity(x), velocity(y), and velocity gradient(z) directions

smectic-A(Sm-A) phase below the nematic phase, α_3 is renormalized. That means renormalized α_3 value is a positive value with a few degrees below the N-I transistion temperature. As a result, the ratio α_2/α_3 becomes negative and hence the director changes its orientation to the neutral direction(X-axis). As the temperature is further reduced, it has been shown that, $\dot{\gamma}\tau \to 1$ where $\dot{\gamma}$ and τ are the shear rate and relaxation time of the critical fluctuations and consequently, α_3^R tend to diverge a few degrees above the N-Sm-A transition[21]. As a result, the director undergoes precessional motion with an angular frequency $\omega_0 = \left[\gamma^2\left(-\alpha_2\alpha_3^R\right)/\gamma_1^2\right]^{1/2}$ along the neutral direction X. Here $\dot{\gamma}$ is shear rate and α_3^R is the renormalized viscosity coefficient of α_3 including the effect of the Sm-A fluctuations and $\gamma_1 = \alpha_3 - \alpha_2$. This ω_0 can be described by the equation of an ellipse $n_y^2(t)/n_{y0}^2 + n_z^2(t)/n_{z0}^2 = 1$, Where $n_y(t) = n_{y0}\cos(\omega_0 t)$ and $n_z(t) = n_{z0}\sin(\omega_0 t)$ are components of the director $n(t) = \left[n_x(t), n_y(t), n_z(t)\right]$ [22, 23].

The first calculations on diffusion of colloids in nematic solvents are by Ruhwandl and Terentjev [24] who concentrated on the Saturn ring configuration. Later, Stark and Ventzki concentrated on the dipole configuration, who treated the dynamics explicitly by relaxing the constraint of a fixed director field. The novelties of the diffusion of a

colloid in a nematic solvent are three fold: i) It is an isotropic, which offers the possibility of lift forces. ii) Coupling between translational and rotational motion are possible iii) The Stokes-drag is highly non-linear. As it was explained in the earlier paragraph, calculating the Stokes drag in anisotropic media requires Ericksen-Leslie(E-L) description of hydrodynamics. So, Stokes drag by a colloid in nematic liquid crystals is with the description of general Stokes drag in an isotropic fluid followed by an explanation of the Ericksen-Leslie equations which describes the dynamics of nematic liquid crystals [25].

A colloidal particle moving in an isotropic medium with velocity v_0 experiences Stokes-drag force, $F_S = 6\pi\eta r v_0$ or $F = \gamma v_0$ where r is the radius of the colloidal particle and $\gamma = 6\pi\eta r$ is the Stokes friction coefficient. An incompressible fluid flowing around a particle at rest with a velocity v_∞ at infinity and the non-slip boundary condition$(v = 0)$ at the particle surface. The velocity(v) and pressure(p) fields follow from the incompressibility condition and the momentum balance:

$$\text{div } v = 0, -\nabla p + div\sigma^{visc} = 0 \tag{2.1}$$

where $\sigma_{ij}^{visc} = 2\eta A_{ij} = \eta(\nabla_i v_j + \nabla_j v_i)$ is the viscous stress tensor in an isotropic fluid, and the ratio of inertial forces to viscous forces which is known as Reynolds number is chosen to be small enough that the convective term $v.\nabla v$ can be neglected. Integrating the total stress tensor including the pressure over the particle surface results in the Stokes friction coefficient γ. To calculate the Stokes drag in a nematic liquid crystal, Erickson Leslie equations are to be solved. Even in this case, the momentum balance equation is valid, whereas the viscous stress tensor has to be replaced by:

$$\sigma^{visc} \rightarrow \sigma^{el} + \sigma^{visc}, \tag{2.2}$$

where

$$\sigma_{ij}^{el} = -\partial f_n / \partial \nabla_j n_k \tag{2.3}$$

and

$$\sigma_{ij^{visc}} = \alpha_4 A_{ij} + \alpha_1 n_i n_j n_k n_l A_{kl} + \alpha_5 n_j n_k A_{ik} + \alpha_6 n_i n_k A_{jk} + \alpha_2 n_j N_i + \alpha_3 n_i N_j \tag{2.4}$$

An elastic contribution σ^{el} to the stress tensor is due to elastic disortions of the nematic director and is described by the Frank free

energy, $f_n = K(\nabla_i n_j)^2/2$, Where K is the Frank elastic constant in the one-constant approximation. The viscous stress tensor σ^{visc} with the Leslie viscosities α_i contains of course the isotropic term but, in addition, the strain rate A also couples to the nematic director due to the local uniaxial symmetry of a nematic. According to these terms, several Miesowicz shear viscosities exist depending on the shear geometry. Further, the viscous stress contains the rate of change of the director relative to a fluid vortex:

$$N = \partial n/\partial t + v.\nabla n - curl v \times n/2 \tag{2.5}$$

also contains another dynamic equation, which governs the temporal evolution of the director field n(r,t), the balance with in elastic and viscous torques is: $n \times h^{el} = n \times h^{visc}$, where

$$h_i^{el} = \nabla_j \partial f_n/\partial \nabla_j n_i - \partial f_n/\partial n_i \tag{2.6}$$

$$h_i^{visc} = \gamma_1 N_i + \gamma_2 A_{ij} n_j \tag{2.7}$$

In the static case, the director field is determined by $n \times h^{el} = 0$. In h^{visc}, the coefficient γ_1 represents rotational viscosity of the director motion. This γ_1 contributes to the viscous torque even in the stationary case, whenever $\nabla n \neq 0$. Onsager relations require a connection to the Leslie viscosity coefficients: $\gamma 1 = \alpha 3 - \alpha 2$ and $\gamma 2 = \alpha 2 + \alpha 3 = \alpha 6 - \alpha 5$[[1, 2]. These relations reduces the viscosity tensor to five independent Leslie coefficients α_i. Finally, the Stokes drag on the colloidal particle is calculated by integrating the complete stress tensor over the surface of the colloidal particle : $F_S = \int_S (-p\mathbf{1} + \sigma^{el} + \sigma^{visc})dS$, Where dS is a vector directed towards the fluid. The solutions of the Ericksen-Leslie equations are non-trivial. By introducing the Ericksen number E_r, which gives an estimate for the ratio of frictional forces to elastic forces in nematic liquid crystals, $E_r = \alpha_4 v_\infty a/2K$ Where v_∞ and a denote a characteristic velocity and length scale of the system. At low Ericksen numbers ($E_r \ll 1$) we can neglect the response of the director field to the flow field and just use the static director field $v = 0$, with this, the elastic stress tensor σ_{el} of 2.3 renormalizes the pressure, so only the viscous stress tensor σ^{visc} of equation 2.2 has to be considered. Since the Ericksen number $E_r \ll 1$, the momentum balance is linear in the velocity field and the director field does not

contribute to the dynamics. This leads to a linear relation between the Stokes force and the velocity v_∞. Whether the configuration is dipole or Saturn-ring or just a uniform director field, liquid crystals exhibit an overall uniaxial symmetry say along Y-axis. Then, Stokes force will not point along v_∞; Then, friction tensor γ is introduced to give

$$F_S = \gamma v_\infty \tag{2.8}$$

with

$$\gamma = \gamma_\perp \mathbf{1} + (\gamma_\parallel - \gamma_\perp)\hat{y}\otimes\hat{y}$$

Where $\hat{y}$ is unit vector along the Y-axis. $\gamma_\parallel, \gamma_\perp$ denote, respectively, the friction coefficient along parallel and perpendicular directions to $\hat{y}$. Such a friction tensor allows drift or lift forces along and perpendicular to v_∞.

An alternative calculation of the Stokes drag using dissipation function was also described [15]. The fluctuation-dissipation theorem relates the friction coefficient to the velocity $u = F/6\pi\eta r$ of a spherical particle driven by an external force F. The Rayleigh function $\Psi = Fu$ gives an effective viscosity in the form $\Psi = 3\pi\eta r u^2$ with two values $\eta_\parallel$ and $\eta_\perp$ for motion parallel and perpendicular to the nematic director. The friction coefficients of nemato hydrodynamics for $n = 1$ and for an incompressible fluid, are calculated from the Lesslie-Ericksen equations . Energy dissipation occurs through two channels

$$\Psi = \int dV\psi, \psi = \sigma \cdot \mathbf{A} + \mathbf{h}.\mathbf{N}, \tag{2.9}$$

Where A and N are thermodynamic fluxes, and σ and $\mathbf{h}$ are the corresponding forces. The rate of strain tensor (A_{ij}) is as mentioned in equation(2.1). The vector quantity $\mathbf{N}$ is given by equation(2.5). The conjugate forces, the viscous stress tensor σ in equation(2.2 and the molecular field $\mathbf{h}$ in equation (2.7), are linear functions of the components of $\mathbf{A}$ and $\mathbf{N}$. Inserting these expressions in equation(2.9) gives

$$\psi = \alpha_1(\mathbf{n}.\mathbf{A}.\mathbf{n})^2 + (\alpha_3 - \alpha_2)\mathbf{N}^2 + (\alpha_3 + \alpha_2 + \alpha_6 - \alpha_5)$$

$$\mathbf{n}.\mathbf{A}.\mathbf{N} + \alpha_4\mathbf{A} : \mathbf{A} + (\alpha_5 + \alpha_6)\mathbf{n}.\mathbf{A}.\mathbf{A}.\mathbf{n} \tag{2.10}$$

Parodi's relation $\alpha 2 + \alpha 3 = \alpha 6 - \alpha 5$[[1, 2] reduces the viscosity tensor to five independent Leslie coefficients α_i. The results of the scalar products are an intricate dependence on the relative orientation of the macroscopic director n_0 and the particle velocity v_0. If $\mathbf{n} = 0$, that is in the absence of nematic ordering, the power density reduces to $\psi = \alpha_4\Sigma_{ij}\mathbf{A}_{ij}^2$. The tensor (A_{ij}) is readily calculated from the velocity field of a spherical particle moving in an isotropic liquid,

$$V = \left(\frac{3a}{4s}(1 + \hat{\mathbf{s}}\hat{\mathbf{s}}) + \frac{a^3}{4r^3}(1 - 3\hat{\mathbf{s}}\hat{\mathbf{s}})\right).v_0 \tag{2.11}$$

Where $\hat{\mathbf{s}} = \mathbf{s}s$. Then Rayleigh function

$$\Psi_0 = \frac{3}{2}\pi r\alpha_4 u^2 \tag{2.12}$$

which defines the isotropic viscosity $\eta_0 = \frac{1}{2}\alpha_4$. Actually, Ψ is a complicated function of the Leslie coefficients in NLC, because the velocity and director field depend on each other through the equations for σ and $\mathbf{h}$. Also it is not possible to single out the dissipation term. It was mentioned by F. Mondiot et.al.,[15], that, though the problem can be solved with considerable numerical effort [1, 2, 15],the resulting numbers for the effective viscosities give no physical insight in the underlying mechanism. To further solve these equations, approximations such as, solving the equations of rate of strain tensor$\mathbf{A}_{ij}$ and rate of change of director relative to a fluid vortex $\mathbf{N}$ with the velocity field V in an isotropic liquid were considered. This leads to linearize ψ with α_i another approximation is the director **n(r)** is independent of the velocity field and which depends on the particle size, that means, the director has no intrinsic length. Hence, for now, there is no choice apart from considering the Stokes drag equation to measure the diffusion properties of colloidal particles in liquid crystals with out using solutions of Ericksen-Leslie equations.

2.4 THE EXPERIMENT

2.4.1 *Sample preperation*

Liquid crystal molecules align on the surface of the treated colloidal spheres by the physico chemical processes and anisotropic forces generated from functionalized surface coupling agent. Silica microspheres of $0.98\mu m$(Bangs laboratories) are treated with Octadecyldimethyl(3-trimethoxysilylpropyl) ammonium chloride (DMOAP) for the alignment of liquid crystal molecules on it. The surface generated orienting forces acting on the liquid crystal molecules may generate from the hydrogen bonding, Van der waal's, mechanical interactions and dipolar interactions as a result of the liquid crystals anisotropic elasticity. The difference in the surface tensions of liquid crystals and surface of the bead $\gamma_L - \gamma_c$ is a measure of the free energy favoring liquid crystal molecular orientation, where γ_L is the surface tension of the liquid crystals and γ_c is the surface tension of the surface of the bead. The liquid crystal molecules orientation will be determined by the balance of all the above mentioned forces, also by the chemical composition of both the surface and liquid crystals and by the surface topology. Homeotropically treated surfaces mainly contains long chains of Octadecyl(propyl) hydrocarbon chains lying normal to the surface of the silica bead. These propyl chains are randomly aligned on the surface of the silica bead and they do not have any axis of symmetry. The oriented liquid crystal molecules, will tend to have its long molecular axis parallel to the substrate plane with random azimuth.

Surface Treatment for silica beads using DMOAP

Untreated silica beads are mixed with 1 ml of water and about $20\mu l$ of DMOAP solution and this solution is mixed using vibronic mixer for 10 minutes. This mix forms uniform alignment of Octadecyl chains on the surface of silica. When we centrifuge the mixture, a foam layer can be observed on the surface of this solution. Then, excess solution is removed. Again washed with distilled water. Further the whole process is repeated one more time . Then the remained silica beads are to be heated in a oven to 120^0C and dry the silica particles for 30

minutes. These treated silica beads can be dispersed in nematic liquid crystals [26].

These DMOAP coated beads promotes homeotropic alignment of the liquid crystal molecules. In the case of anisotropic liquid crystal molecules on a homeotropically aligning surface, an orientation of the molecules perpendicular to the surface is sterically favored [18].

2.4.2 *Sample cell preparation*

:

The quantitative measurements of phyiscal properties of liquid crystals depends on two types of alignment layers namely: planar(homogeneous) and vertical(homeotropic). If the nematic director of the liquid crystals is parallel to the substrate, it is planar alignment. Whereas in homeotropic alignment, the director is perpendicular to the substrate. It is easy to align the uniaxial nematic liquid crystals, with rod like molecules(calamatic) both in planar and homeotropic cell alignment. By the texture observation of the compounds, we can determine how the unconventional nematic liquid crystals show planar alignment and are independent of the sign of the dielectric anisotropy. From previous reports[[27], [28]], conventional alignment layers for homeotropic alignment of unconventional liquid crystals like bent core liquid crystals is not possible. The bent-core nematic liquid crystals with negative dielectric anisotropy in general cannot be aligned in homeotropic cells. The orientation of the liquid crystal molecules on the substrate surface depends on the interaction forces such as steric interaction, short range dipolar and long range van der Waals interations. Steric interaction prefers planar alignment of the director [[29], [30]]. Because, steric forces, according to Pauli's exclusion principle, prevent different molecules from penetrating each other. Long range Vander Waals interaction prefers the large polarisability direction and is parallel to the substrate surface [[31], [32]]. Since most of the bent-core liquid crystals possess several phenyl rings, the polarisability is large and hence van der Waals interaction dominates. So, in bent-core nematic liquid crystals, both steric and van der Waals interactions prefers planar alignment. Further, if we consider short range dipolar interactions, which make the dipoles normal to the interface to maximize their

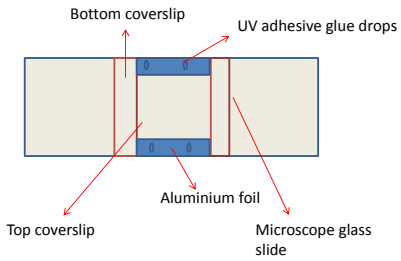

Figure 2.4: Schematic diagram of liquid crystals sample cell

interaction with the charges at the surface and have opposite alignment effect depending on the strength and orientation of the resultant dipole moment with respect to the long molecular axis. This short range dipolar interaction, aligns the long molecular axis(P) perpendicular to the surface, when the direction of the resultant dipole moment is parallel to P. otherwise, it orients the bow axis(P) parallel to the substrate, when the direction of dipolemoment(D) is perpendicular to P [33]. In bent-core liquid crystals with with $\Delta\epsilon < 0$ [1], D is almost perpendicular to P and is parallel to arrow axis and both D and P have similar alignment effect and hence it leads to planar alignment of the molecules and they do not exhibit homeotropic alignment. On the other hand, for compounds with $\Delta\epsilon > 0$, D is parallel to P and it leads to opposite alignment effect.

For planar alignment AL-1254 was used as alignment layer. For the preparation of the cells, cover slips of 130-170 μm were well cleaned by a standard cleaning procedure to remove the possible contamination which may cause non uniform alignment layer. Spin coating technique is used to deposit AL-1254 alignment layer with controlled speed revolution of the spinner. After drying and curing at 180^0C for about

[1] Dielectric constant is a measure of response of the material to an applied electric field.

90 minutes. Planar alignment can be achieved by rubbing coverslips in antiparallel way. This rubbing process causes local heating and stretching of the alignment layer, which causes the alignment of the main chain of the polymide as well as it generates grooves in the rubbing direction. To minimize the surface free energy, the liquid crystal molecules and the nematic director prefers to lie parallel to the rubbing direction. Thin Aluminum foil strips of thickness $25\mu m$ are used as spacers and drops of UV curable adhesive is put on to these strips and two cover slips are stuck to form the cell as shown in figure 2.4 . Edges of this cell is stuck using on to a thick microscope glass slide using scotch tape.

2.4.3 *Particle tracking with inverted microscope*

This sample cell is placed into a heating source hot stage (HCS402, Instec) and stuck the edges of the glass slide to the plates of heat source with a scotch tape. This heating source has to be heated to just above the known nematic isotropic transition temperature. Then, liquid crystal samples in the isotropic phase can be filled into the sample cells and cooled slowly to reach the nematic phase. The variation in set temperature and the actual temperature of the heating source is only $\pm 0.01^0 C$ and the temperature of the heating source can be set accurately by using a temperature controller (Instec, mk 1000). Also, phase transitions with decrease in temperatures of the liquid crystal compound have been verified by observing in a Olympus microscope with 20X microscope objective with a well controlled variation in temperature. Again, the liquid crystal sample cell with DMOAP coated silica micro spheres dispersed in the liquid crystals has to be verified with 40X microscope objective to observe the uniform dispersion of the colloids and with less chain formation by the colloids. UV sonication of the sample for 20 minutes before filling the sample will avoid this chain formation. Observation of uniform dispersion of the silica micro spheres along with very small random movement is a green signal for measurements of Brownian motion .

Then, this heating source has to be placed in an inverted polarizing microscope (Nikon *Eclipse*, Ti-U) with Olympus microscope air objec-

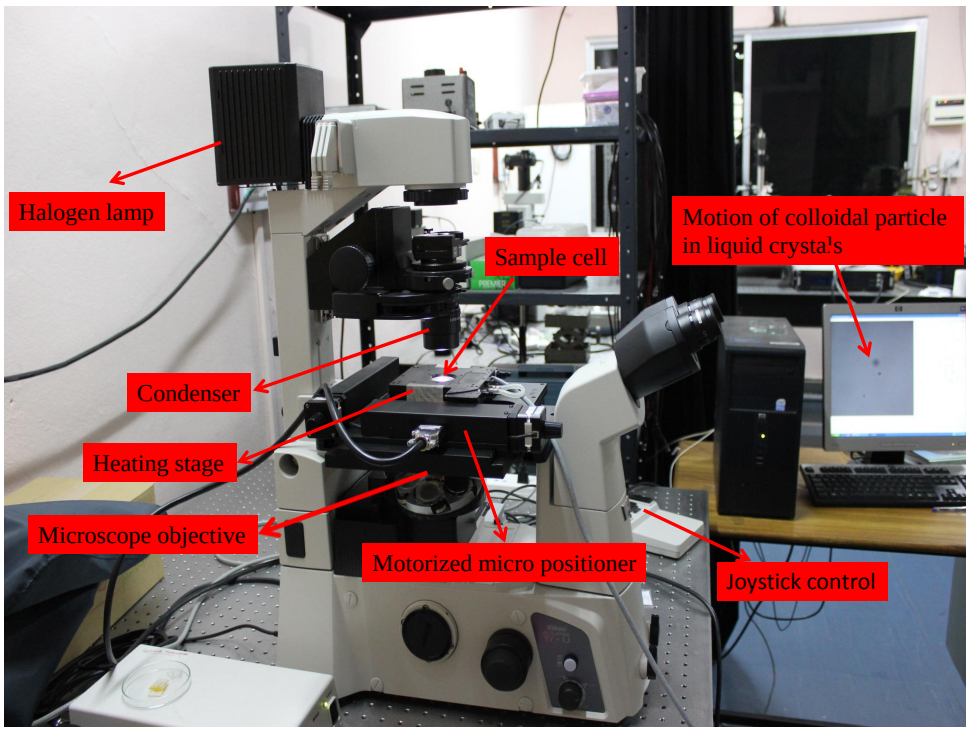

Figure 2.5: Photograph of Nikon *Eclipse* inverted microscope with sample cell in a heating stage.

tive lens of magnification 100X and Numerical Aperture 0.65 as shown in fig.2.5. A home made adpater ring is used to adjust the gap between the front face of the heating stage to the objective lens. Also, this is helpful in using Olympus microscope objectives in Nikon inverted polarizing microscope. Now, the heating source with heating plates both on top and bottom of the sample cell which is sealed completely with white sticky tape is placed onto a 3D motorized translation stage whose resolution in the stage movement is $10\mu m$ and this 3D stage can be controlled with a joystick controller for easy movement. A CCD camera attached in the right port of the polarizing microscope is used to record videos of the Brownian motion of the silica microspheres in the liquid crystals. These recorded videos were analyzed using a commercial particle tracking software. In this particle tracking software programme, a region of interest which comes as a square shape has to be chosen around an isolated silica micro sphere of diameter $0.98\mu m$. In these image processing software, with in the sphere's geometric center, the centroid of the brightest/darkest pixel has to be tracked in all the frames acquired per second. Then, for the real values of the bead motion, pixel calibration has been done. For this purpose, a stuck bead has to be brought to the center of the screen, measure the pixel value of the geometric center of the sphere and moved from the center of the screen to a known displacement and measure the pixel value of the geometric center. Then, measure difference in the pixel values to know the real world value of each pixel. This way, the measured pixel value is $1\mu m$. This implies an estimation of sensitivity to be $\pm$100nm which is $1/10^{th}$ of a pixel value. An amplitude of Brownian motion greater than 100nm can be tracked using this image processing software. To make uncorrelated measurements of fluctuating particle locations using video images, requires the shutter interval. This shutter interval depends on the number of frames acquired per second. About 22 frames per second with a time resolution between each step being 45 mSec was recorded. In our images acquisition system, shutter interval automatically adjusts itself to have good amount of exposure time. 3000 frames for 5 minutes of video recording of Brownian motion of an isolated bead motion was recorded and analyzed.

2.5 EXPERIMENTAL MICRORHEOLOGY AND ANALYSIS PROCEDURE

The thermal motion of colloidal particle in complex fluids is acquired and image processing is done to measure the real time values of motion of the colloidal particle. Generally in the image processing, region of interest around the colloidal particle of interest is chosen, also shape of the colloidal particle will also recognized by the image processing software. The centroid of the maximum or minimum intensity of the chosen shape is tracked in each of the frames recorded to obtain the trajectory of the colloidal particle. Noise filtering algorithms are used to have smooth and continuous trajectory. Measurements of position of the particle in each frame of the trajectory are recorded.

In this thesis, from the measured Brownian motion data, the physical, structural properties of the complex fluids are reported. Since Albert Einstein's prediction of theory of Brownian motion in 1905, there has been tremendous interest to the scientific commmunity in this concept [34]. In thermal equilibrium, collisions of the colloidal particle with the molecules in the fluid gives rise to the Brownian motion of a colloidal particle is due to the in a Newtonian fluid. The random displacements of the colloidal probe is proportional to the dissipation of kinetic energy which is directly related to the temperature of the medium. This Brownian motion can be quantified by the probe particle's mean square displacement (MSD)

$$\langle \Delta x^2(\tau) \rangle = \langle [x(t+\tau) - x(t)]^2 \rangle \tag{2.13}$$

Here $x(t)$ is the position of the particle at time t, τ is the time lag, it represents the speed of acquisition or time difference between two acquired frames of recorded video. $\langle\rangle$ represents time averaging over all initial times. Slope of MSD Vs τ represents the physical rigidity of the materials. If the slope is zero then the materials is rigid and is a solid material. If the slope lies between '0' and '1' , then its a visco elastic material and the slope being equal to '1' represents the isotropic fluid.

Brownian motion in liquid crystals..

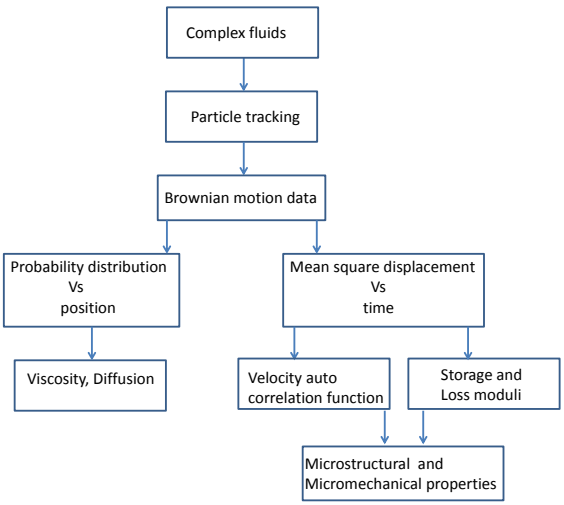

Figure 2.6: Flowchart diagram of experimental and analysis procedure for passive microrheology.

2.5.1 *Relation between MSD and velocity auto correlation function(VACF)*

Further the anomalies in diffusion of colloidal particle in liquid crystals are characterized by the velocity auto correlation function vs time. After computing the MSD from the Brownian motion, MSD in one dimensional motion along X-axis is related to the velocity auto correlation function (C_v) as :

$$\langle x^2(t)\rangle = 2\int_0^t dt' \int_0^{t'} C_{v_x}(t'')dt'' \tag{2.14}$$

Hence, $C_{v_x}(t) = \frac{1}{2}\frac{d^2\langle x^2(t)\rangle}{dt^2}$. This equation represents, in as in isotropic fluids, if $\langle x^2(t)\rangle \propto t$, then $C_{v_x}(t) = 0$. Other cases are, if MSD grows slower than time t, then $C_{v_x}(t) < 0$ represents subdiffusion and if MSD grows faster than t, then $C_{v_x}(t) > 0$ and represents super diffusion. This similar procedure is followed for calculating the VACF through out this thesis.

2.5.2 *Relation between MSD and elastic(G'), viscous(G")moduli*

From the measured thermal motion of the silica beads, elastic or storage modulus(G') and viscous or loss modulus (G'') can be computed using generalised Stokes-Einstein equation. G′ and G″ represent the fraction of energy induced by the deformation imposed on the material. This fraction of energy is lost by the viscous dissipation in case of loss modulus(G″), and, is stored elastically in case of storage modulus(G′). G′ and G″ as a function of rate of deformation ω were computed using the equations given in Ref.[35].

By expanding the equation of motion of mean square displacement around $t = 1/\omega$, the translational parameter β is defined as

$$\beta(\omega) = \left.\frac{\langle d \ln \Delta r^2(t)\rangle}{d \ln t}\right|_{t=\frac{1}{\omega}} \tag{2.15}$$

and the Fourier transform of this MSD equation would lead to give $G'(\omega)$ and $G''(\omega)$ as

$$\begin{aligned} G'(\omega) &= |G^*(\omega)| \cos\left(\frac{\pi\beta(\omega)}{2}\right) \\ G''(\omega) &= |G^*(\omega)| \sin\left(\frac{\pi\beta(\omega)}{2}\right) \end{aligned} \tag{2.16}$$

Where $|G^*(\omega)| = k_B T/\pi a\langle\Delta r^2(\frac{1}{\omega})\rangle\Gamma[1+\beta(\omega]$, and '$a$' the radius of the probing bead.

2.5.3 *Relation between viscosity(η) and probability distibution of diffusion*

The histogram of the microsphere displacements were fitted to Gaussian profile with a probability P that the particle would diffuse to a distance δ in the time interval τ is $P = P_0 \exp(-\delta^2/\Delta^2(t))$, Where $\Delta(\tau)$ is the width of the distribution and $P_0(\tau)$ is the normalization constant. The self diffusion coefficients of the micro sphere parallel($D_\parallel$) and perpendicular($D_\perp$) to the director are obtained by using the relation $D_{\parallel,\perp} = \Delta^2_{\parallel,\perp}/4\tau$. The corresponding viscosities are estimated by using the Stokes-Einstein relation $\eta_{\parallel,\perp} = k_B T/6\pi r D_{\parallel,\perp}$, where r is the radius of the micro sphere. From the time dependence of distribution

functions, the long-time self diffusion coefficients (D) can be from the distribution functions width through, $\Delta^2(\tau) = 2dD\tau + \Delta_0^2$, Where Δ_0^2 is the rapid short-time diffusion and in part from measurement errors which contribute $2d\Delta_\epsilon^2$. The error in centroid location estimated should be in consistency with the sensitivity of the image processing system. Hence, this error is significant at lower lag times.

2.6 CONCLUSIONS

This chapter is mainly aimed to report three important topics: 1) To understand the consequences of topological defects, deformation induced by the diffusion and how this deformations leads to anomalies in the diffusion of colloidal particle in liquid crystals. 2) Experimental procedures followed in homeotropic surface coating of colloidal particle, surface treatment for the planar alignment of liquid crystals, single particle tracking with inverted microscope. 3) Analysis procedures to relate the MSD with VACF, MSD with G′ and G″ and viscosity with particle diffusion.

Since, experiment procedure for the collodial particle motion in liquid crystals is described with details in this chapter, in rest of the chapters about this same topic, experimental details are not given. But, for single particle tracking experiment in ferrofluids chapter, a different experiment and procedures were used which are mentioned in that chapter.

BIBLIOGRAPHY

[1] P.G.de Gennes, "The Physics of Liquid crystals", 2nd ed., (Oxford university Press), Oxford (1993).

[2] S.Chandrasekhar, "Liquid crystals", 2nd ed., (Cambridge University Press), (1992).

[3] Igor Muševič, Miha Škarabot, U.Tkalec, Miha Ravnik, Slobodan Žumer, Science, **313**, 954 (2006).

[4] Bohdan Senyuk and Ivan I. Smalyukh, Soft Matter, **8**, 8729 (2012).

[5] J. A. Moreno-Razo, E. J. Sambriski, G. M. Koenig, E. Díaz-Herrera, N. L. Abbotta and J. J. de Pablo, Soft Matter, **7**, 6828 (2011).

[6] Anupam Sengupta, "Nematic liquid crystals and nematic colloids in microfluidic environment", Ph.D. thesis submitted to Georg-August University School of Science, (2013). - unpublished.

[7] P.Poulin and D. A. Weitz, Phys. Rev. E., **57** , 1 (1998).

[8] Christophe Blanca, Delphine Coursaultc, and Emmanuelle Lacazec, Liquid Crystals Reviews, **1(2)**, 83 (2013).

[9] O. D. Lavrentovich, Liquid Crystals, **24**, 117 (1998).

[10] Todd M. Squires and Thomas G. Mason, Annu. Rev. Fluid Mech., **42**, 413 2010.

[11] Denis Wirtz, Annu. Rev. Biophys. **38** 301, (2009).

[12] Bo Wang, Nat.Mat., **11**, 481 (2012).

[13] Thomas G. Mason, Rheol. Acta **39**, 371 (2000).

[14] Jingyuan Xu, Virgile Viasnoff, Denis Wirtz, Rheol Acta **37**, 387 (1998).

[15] F. Mondiot, J.C.Loudet, Olivier Mondain-Monval, Patrick Snaber, Alexandre Vilquin and Alois W., Phys. Rev. E., **86**, 010401(R) (2012).

[16] J. C. Loudet, Liquid Crystals Today, **14**,1 (2005).

[17] Daniel Abras, Gaurav Pranami and Nicholas L. Abbott, SoftMatter, **8**, 2026 (2012).

[18] Igor Muševič, Miha Škarabot, Soft Matter **6**, 5476 (2010).

[19] T. Turiv, I. Lazo, A. Brodin, B. I. Lev, V. Reiffenrath,V. G. Nazarenko, O. D. Lavrentovich, Science, **342**, 1315 (2013).

[20] T. C. Lubensky, David Pettey, and Nathan Currier and H.Stark,Phys. Rev.E., **57**, 610 (1998).

[21] D.J.Ternet, R.G.Larson, L.Gary Leal, Rheol Acta **38**, 183 (1999).

[22] C. R. Safinya, E. B. Sirota, and R. J. Plano, Phys. Rev. Lett. **66**, 15 (1991).

[23] K.Negita, M. Inoue, and S. Kondo Phys. Rev. E. **74**, 051708 (2006).

[24] Ruhwandl R W and Terentjev E M Phys. Rev. E., **54**, 5204 (1996).

[25] Stark H and Ventzki D Phys. Rev. E., **64**, 031711 (2001).

[26] V.S.R.Jampani, "Surface coupling agent (DMOAP) for colloidal liquid crystals".(online material)

[27] L. A. Madsen, T. J. Dingemans, M. Nakata and E. T. Samulski, Phys. Rev. Lett. **92**, 145505 (2004).

[28] J. Matraszek, J. Mieczkowski, J. Szydlowska and E. Gorecka, Liq. Cryst., **27**, 429 (2000).

[29] H. Kimura, J.Phys.Soc.Jpn., **62**, 2725 (1993).

[30] E. D. Violette and P.G. de Gennes, J.de Phys.Lett., **36**, L255 (1975).

[31] E. D. Violette and P.G. de Gennes, Colloid. Interface Sci, **57**, 403 (1976).

[32] C. Chen, P. J. Bos and J. E. Anderson, Liq. Cryst., **35(4)**, 465 (2008).

[33] T. Arun Kumar, K. V. Le, J. K. Kim, H. Takezoe and Surajit Dhara, Liq. Cryst. **38**, 917 (2011).

[34] Albert Einstein, "Investigations on the theory of the Brownian movement", Dove publications, (1956).

[35] T. G. Mason, T. Gisler, K. Kroy, E. Frey, D. A. Weitz, J. Rheol. **44**, 917 (2000).

Brownian motion in liquid crystals..

3

PASSIVE VISCOSITIES OF BENT-CORE NEMATIC LIQUID CRYSTALS

3.1 INTRODUCTION

The viscosity of liquid crystals strongly depends on the microscopic structures of the constituent molecules and the mesophases. There are several theoretical and experimental studies of the low molecular weight liquid crystals where the molecules have mostly cylindrical symmetry[[1],[2],[3]]. The nematic(N) phase of liquid crystals has three principal viscosities called Miesowicz viscosities, namely η_1, η_2, and η_3, depending on the direction of the shear and the orientation of the liquid crystal director(The average alignment direction of the long axes of the molecules). A schematic representation of the director orientation in a calamatic (rodlike) nematic liquid crystals is represented as shown in fig.1. These viscosities can be expressed in terms of Lesslie coefficients $\alpha_1 - \alpha_6$, which are used to define the nematic stress tensor. In nematic liquid crystals, both α_2 and α_3 are negative close to the nematic-isotropic (N-I) transition and the director is aligned along the flow direction with an angle, $Tan\theta = \sqrt{\alpha_2/\alpha_3}$[[4],[5]]. However, if the compounds also have a smectic-A (Sm-A) phase below the N phase, α_3 is renormalized (i.e., $\alpha_3^R > 0$)) a few degrees below the N-I transition temperature. As a result, the ratio $\frac{\alpha_2}{\alpha_3}$ becomes negative and the director changes its orientation to the neutral direction (x axis). As the temperature is further reduced, $\alpha_3^R > 0$) is tend to diverge a few degrees above the N-Sm-A transition[6]. As a result, the director undergoes precessional moiton with an angular frequency ω_0 along the neutral direction that can be described by the equation of an ellipse

$$\frac{n_y(t)^2}{n_{y0}^2} + \frac{n_z(t)^2}{n_{z0}^2} = 1 \tag{3.1}$$

where

passive viscosities..

$n_y(t) = n_{y0}\cos(\omega_0 t)$ and $n_z(t) = n_{z0}\sin(\omega_0 t)$ are components of the director $n(t) = (n_x(t), n_y(t), n_z(t))$ precessing around the x-axis with an angular frequency of

$$\omega_0 = \left[\frac{\dot{\gamma}^2(-\alpha_2\alpha_3^R)}{\gamma_1^2}\right]^{\frac{1}{2}} \tag{3.2}$$

Where $\dot{\gamma}$ is the shear rate, α_3^R is the renormalized viscosity coefficient of α_3 including the effect of the S_A fluctuations, and $\gamma_1 = \alpha_3 - \alpha_2$. Depending on the relative strength of the director components, steady structures that are observed: 1) a_m strucure: anisotropic precession with larger amplitude in the y-direction with $(n_{y0} > n_{z0})$. 2) a_s structure: isotropic precession with equal amplitude in the y and z direction $(n_{y0} = n_{z0})$. 3) $a(b)$ structure: anisotropic precession with larger amplitude in the z direction $(n_{y0} < n_{z0})$. 4) a_c structure: anisotropic precession with its larger amplitude of motion deflected along the z-axis $(n_{y0} << n_{z0})$. The above structural features are also reflected in the static dielectric measurements on a few calamitic compounds exhibiting a N-Sm-A phase transition[[7],[8]]. Liquid crystal molecules have created immense interests [[9],[10],[11],]. Usually, these molecules have a strong tendency to form smectic phases. However, they occasionally exhibit a nematic phase in which the physical properties are reported to be significantly different from conventional calamitic nematic liquid crystals [11]. The presence of temporarily fluctuating smectic clusters is also evident in many experiments. In this context, the measurements of flow in the bent-core liquid crystals is very rare. The major problem in shear rheology experiments is the requirement of a large sample, which in general is not easy to get. In this chapter, we report on the measurements of micro viscosities of a bent-core liquid crystal. Also, we show that the temperature dependent behaviors of the active viscosities and passive viscosities are noticeably different and the study of the self-diffusion of a microsphere is a sensitive technique to investigate the presmectic fluctuations in bent-core nematic liquid crystals.

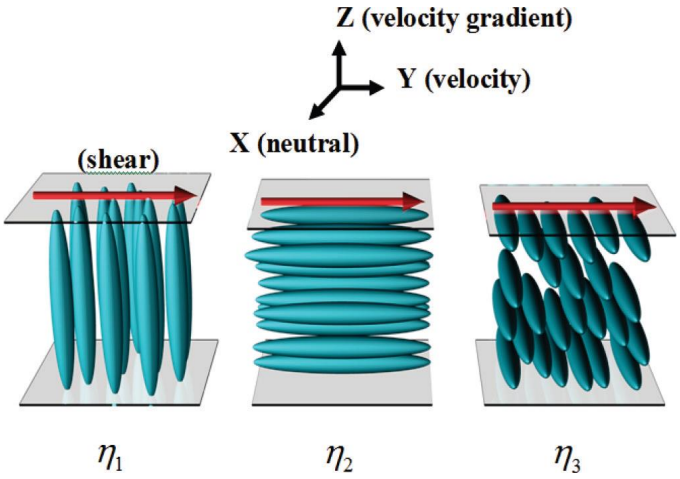

Figure 3.1: Schematic representation of the three fundamental director orientations in the nematic phase. Miesowicz viscosities corresponding to each orientation are designated by η_1, η_2, η_3 respectively.

3.2 THE EXPERIMENT

The chemical structure and the phase transition temperatures of the bent-core nematic (BCN) are shown in figure, which exhibits the following phase transitions (cooling): I at 178.5°Cto N at 120°C to Sm-C at 101.3°C to Sm-X at 90.4°C to Sm-Y at 60.2°C in cr. The purity of the compound was confirmed by the high-performance chromatography and other techniques. The single particle tracking technique using video microscopy is used to measure the self diffusion coefficients of a tiny silcia microsphere (with a diameter of 0.98μm and hence the passive viscosities of the sample parallel and perpendicular to the director. To promote a specific alignment on the surface, the silica microspheres were coated with octadecyldimethyl (3-trimethoxysilylpropyl) ammonium chloride (DMOAP) before mixing with the liquid crystal [12]. Details of the coating of the DMOAP alignment layer is done is chapter 2. The Brownian fluctuations of an isolated microsphere in a planar cell (d = 23 μm) was recorded and the position was determined with the help of a commercial software programme. The histogram of the microsphere displacements were fitted to Gaussian with a probability

passive viscosities..

P that the particle would diffuse a certain distance δ in the time interval τ is $P(\delta/\tau) = P_0(\tau)exp(-\delta^2/\Delta^2(\tau))$, where $\Delta(\tau)$ is the width of the distribution and $P_0(\tau)$ is the normalization constant. The self-diffusion coefficients of the microsphere parallel $(D_\parallel)$ and $(D_\perp)$ to the director are obtained by using the relation $D_{\parallel,\perp} = \Delta^2_{\parallel,\perp}/4\tau$. The corresponding viscosities are estimated by using the Stokes-Einstein relation $\eta_{\parallel,\perp} = k_B T/6\pi r D_{\parallel,\perp}$ where r is the radius of the microsphere[12].

3.3 RESULTS AND DISCUSSION

The study of Brownian fluctuations helps us understand the effect of smectic fluctuations on the passive viscosity of BCNs. The histograms of the particle displacement $\delta|r(t+\tau) - r(t)|$ in both $x(\parallel \mathbf{n})$ and $y(\perp n)$ are shown in Figure 3.2 . It is evident that $\Delta_\parallel > \Delta_\perp$, implying $D_\parallel > D_\perp$, as expected. The ratio $D_\parallel > D_\perp$ varies with temperature and changes from 1.4 to 1.7, which is close to the number (1.6) as shown in figure 3.4. These values are similar to those reported in calamitic liquid crystal, e.g, $4^{'}$ phenyl-4-cyanobiphenyl with dipole defects [13].

In fig.5 we show the temperature variation of $\eta_\parallel$ and $\eta_\perp$ of the BCN liquid crystal as determined from $D_\parallel$ and using $D_\perp$ using Stokes -Einstein relation. We note that in the isotropic phase $\eta_\parallel$ = $\eta_\perp$ and is comparable to η_{eff} measured in the rheometer. Just below the N-I transition the director is aligned along the flow direction and $\eta_\parallel$ is nearly equal to the Miesowicz Viscocity, i.e.,$\eta_\parallel \cong \eta_2 = (\alpha_3 + \alpha_4 + \alpha_6)/2$.

In the nematic phase $\eta_\parallel < \eta_\perp (\cong \eta_3 = \alpha_4/2)$ and both increases as the temperature is reduced η_{eff} also increases with temperature, but the relative rate of increase of the former two is larger. Two consideration can be made to understand their temperature dependence. First, apart from the temperature effect, the viscosity can also increase a the smectic phase is approached due to the occurrence of temporary smectic clusters in the bulk. Second, the colloids are coated with DMOAP, which promotes homeotropic alignment of the bent-core molecules. On the surface of the microsphere the free rotation of the molecules along the long axis is restricted due to steric hindrance;

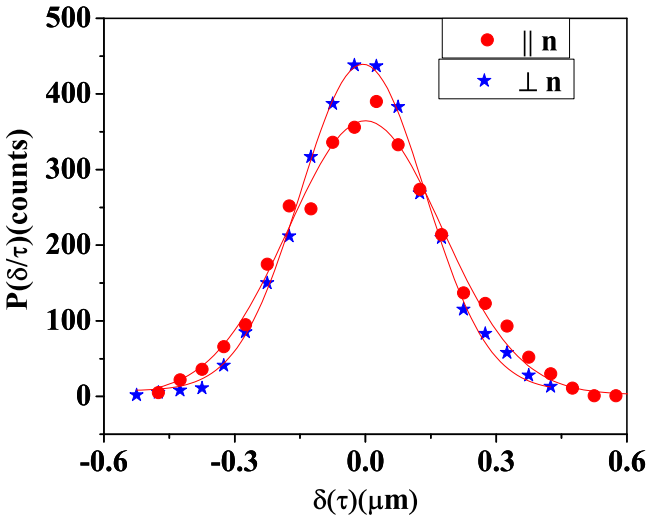

Figure 3.2: Histogram of particle displacements parallel(circles) and perpendicular(stars) to the director for τ = 1 S. The solid lines are Gaussian fits.

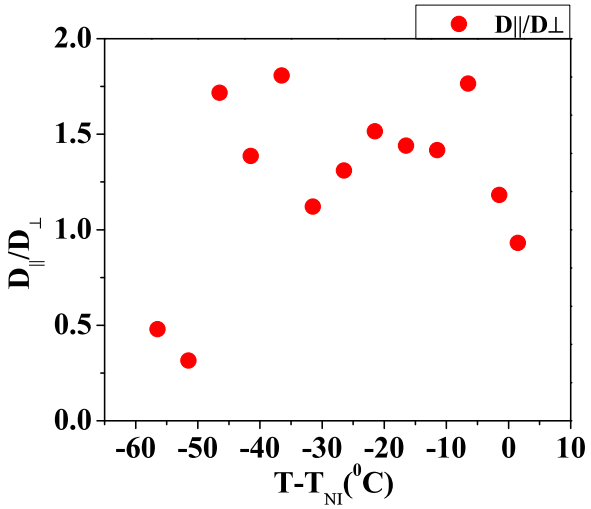

Figure 3.3: Diffusion ratio $D_{\parallel} > D_{\perp}$ for every 5$\circ$C difference in temperature. Average of this ratio is at 1.6.

passive viscosities..

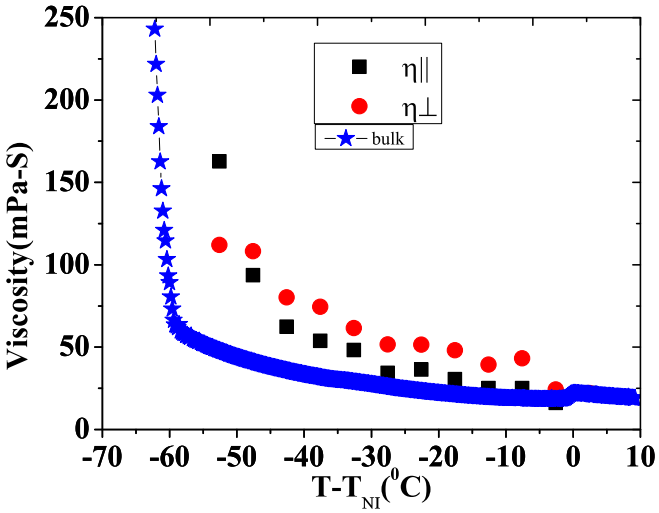

Figure 3.4: Variation of ηeff (stars), $\eta_{||}$(squares), and $\eta_{\perp}$ as a function of shifted temperature.

as a result they are pinned in a facilitating formation of permanent smectic clusters or layers around the microspheres. As a result, the hydrodynamic radius of the microsphere could be significantly larger than the actual radius due to the large cloud of the distorted nematic around the microsphere. Assuming $\eta_{||} = \eta_{eff}$ = 21.6 mPa s near the N-I transition $(T - T_{N-I} = -18^0C)$, the estimated hydrodynamics radius of the microsphere is 0.68μm, which is about 0.2 μm larger than actual radius. A schematic molecular orientation of bent - core molecules and some clusters around the microsphere with a dipolar defect is shown in figure3.5. In fact, it was shown that both diffusion coefficients $D_{||}$ and $D_{\perp} \propto 1/\eta$ decreases when the size of the microsphere is greater than 0.5 μm, which is attributed to the effective size of the microsphere, which is bigger than the geometric size[12]. In addition, the smectic layering effect can increase with decreasing temperature due to a kind of condensation of the clusters around the microsphere effectively increasing the diameter of the microsphere with decreasing temperature. As the temperature is further reduced and we approach the Sm-C phase, interestingly we notice that $\eta_{||}$ tends to diverge around 24°C above N-Sm-C transition.

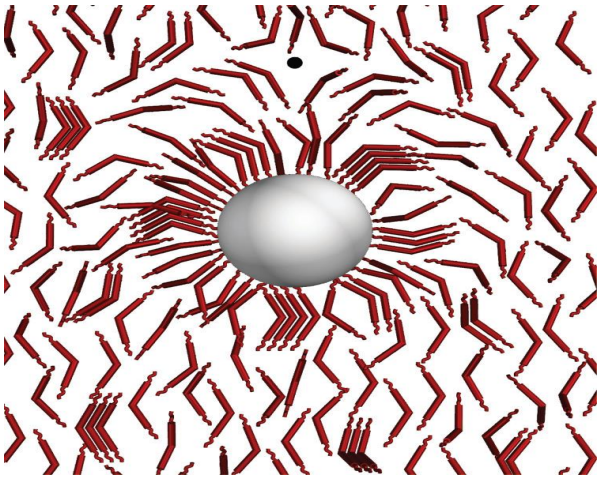

Figure 3.5: Schematic molecular orientation around the microsphere with a dipolar defect configuration. It may be noted that, the clusters attached to the microsphere are permanent, whereas they are temporal in nature in the bulk. The small dot near the top indicates a hyperbolic hedgehog defect.

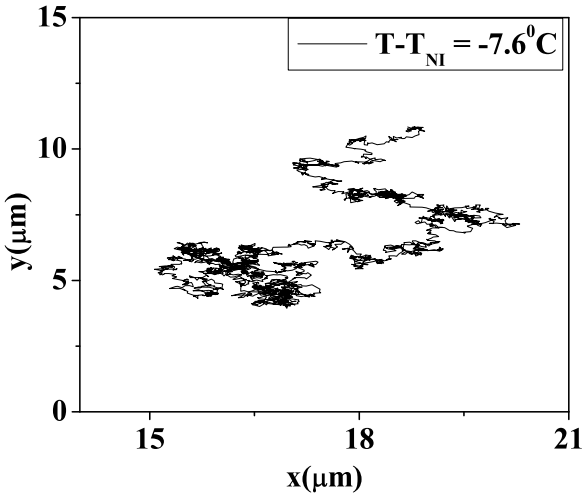

Figure 3.6: The two dimensional projection of trajectories of a microsphere closer to the N-I transition($T - T_{NI} = -7.6^{\circ}$C).

passive viscosities..

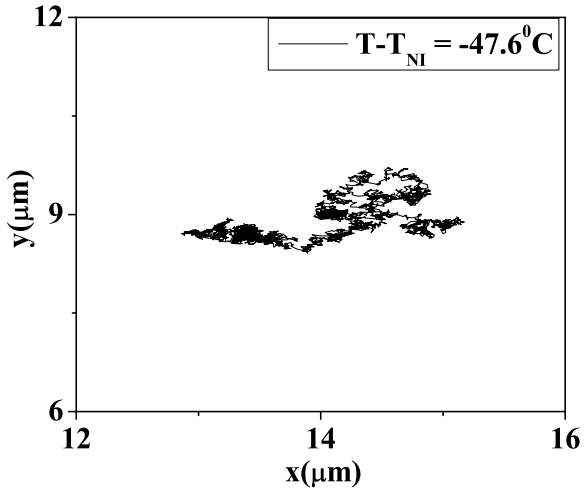

Figure 3.7: The two dimensional projection of trajectories of a microsphere closer to the N-I transition($T - T_{NI} = -47.6^{\circ}C$)

To understand this we look at the Brownian trajectory of a microsphere. The two dimensional projection of the trajectories of a microsphere near N-I ($T - T_{N-I} = -7.6^0C$) and N-Sm-C ($T - T_{N-I} = -47.6^0C$) transitions are shown in the figures 3.6 and 3.7. We notice that the fluctuations are highly restricted near the N-Sm-C transition compared to the N-I transition. Since the cell is rubbed, it is expected that the smectic layer planes in the rubbing direction. In this case the fluctuating clusters are large enough and the self diffusion of the microparticle in the direction perpendicular to the layer plane is expected to be lower than that in parallel direction and as result $\eta_{\|}$ can diverge.

3.4 CONCLUSIONS

We report the measurents of passive viscosities of a bent-core nematic liquid crystals. In this single particle tracking experiment, passive viscosities are measured by meausring the self-diffusion coefficient of a microsphere in the aligned sample. The anisotropy in the self-diffusion is observed. The temperature dependence of passive viscosities is stronger than that of active(bulk rhelogy measurement) viscosity. The

effect of presmectic fluctuations are observed much higher than the N-Sm-C transition temperature than commonly seen in calamitic liquid crystals. The study of Brownian motion is useful to understand the smectic fluctuations in bent-core nematic liquid crystals.

passive viscosities..

BIBLIOGRAPHY

[1] P.G. de Gennes, "The physics of Liquid crystals", 2nd ed. , Oxford University Press, Oxford, (1993).

[2] S. Chandrasekhar, "Liquid Crystals", 2nd ed., Cambridge University Press, Cambridge, (1992).

[3] V.V. Belyaev, Viscosity of Nematic Liquid Crystals, 1st ed. , Cambridge International Science, Cambridge, (2011).

[4] E.M. Leslie, J.Mech. Appl.Math. **19**,357 (1966).

[5] T. Carlsson and K. Skarp, Mol. Cryst. Liq. Cryst. **104**, 307 (1984).

[6] C. R. Safinya, E. B. Sirota, and R. J. Piano, Phys. Rev. Lett. **66**, 1986 (1991).

[7] K. Negita, M. Inoue, and S. Kondo, Phys.Rev. E **74**, 051708 (2006).

[8] J. Ananthaiah, M. Rajeswari, V.S.S. Sastry, R. Dabrowski and S. Dhara, Eur.Phys.J.E **34**, 74 (2011).

[9] S. Dhara, Y. Balaji, J. Ananthaiah, P. Sathyanarayana, V. Ashoka, A. Spadlo, and R. Dabrowski, Phys. Rev. E **87**, 030501(R) (2013).

[10] H. Takezoe-6 and Y. Takanishi, Jpn. J. Appl.Phys. **45**, 597 (2006).

[11] R.A. Reddy and C. Tschierske, J. Mater. Chem. **16**, 907 (2006).

[12] Miha Škarabot, Igor Muševič, Soft Matter **6**, 5476 (2010).

[13] J.C. Loudet, Liq, Cryst. Today **14**, 1 (2005).

passive viscosities..

4

MEMORY EFFECTS IN TUMBLING NEMATICS OF 8CB LIQUID CRYSTALS

4.1 INTRODUCTION

In nature, many of the things we observe are either time dependent or frequency dependent[1]. Dynamic correlations are described by time-dependent generalizations of correlation functions which contain information about the nature of dynamical modes. The dynamical properties of condensed matter systems are mostly dominated by harmonic oscillator-like modes. Correlation functions contain information about the frequency and damping of these modes. Velocity auto correlation function(VACF) can be used for the quantitative description of dynamics of molecular motion in fluids. The VACF denoted by $C_v(t)$ is the average of the initial velocity $V(0)$ of a particle multipled with its velocity $V(t)$ at a later time t, $C_v(t) = \langle V(t)V(0)\rangle$ [2]. Physically, it represents, temporal correlations between the random walkers and the background in a disordered medium. Any energy in the harmonic oscillator will tend to flow irreversibly into many modes of the fluid. This irreversible flow of energy into incoherent degrees of freedom, which is called as dissipation, is reflected in the sign of the viscous force which leads to the decay of $x(t)$ with time. $C_v(t)$ is a fundamental function, which is useful to obtain the systems physical properties like diffusion constant(D) from Kubo's relations as[3],[4]

$$D = \lim_{t\to\infty} \frac{1}{2t}\langle x^2(t)\rangle = \int_0^\infty C_v(t)dt \tag{4.1}$$

In nematic liquid crystals, the average orientation of molecules is determined by the nematic director $\hat{n}(r,t)$. The orientational order in a nematic liquid crystal effects the Brownian motion of spherical particles of micro meter size which leads to anisotropic diffusion[5]. In standard liquid crystals, like 5CB, The director field $\hat{n}\,(r,t)$ is coupled to the velocity field V(r,t) of the nematic. This coupling of the nematic director with its fluctuations and velocity field are perturbed by the

spherical particle in particle tracking experiments. Hence, the time averaged distribution of $\hat{n}(r,t)$ under flow can be characterized by *in situ* measurements of tracking Brownian motin of colloidal particle.

It is well known that [6], [7], [8], [9], in 8CB liquid crystals, along with phase transitions, there exists several regimes in nematic phase. Basically, the orientation or the isotropic and anisotropic precessional motions of the director around the velocity(V) or the flow gradient directions(ΔV) determines the structures in the nematic regime. From Ericksen-Leslie-Parodi(ELP) theory and critical nemato dynamics, it has been shown that, $\dot{\gamma}\tau \to 1$, where $\dot{\gamma}$ is shear rate and τ is relaxation time of the fluctuations of the director $(\hat{\mathbf{n}})$ and from experimental measurements, [10],[11],[12] it is known that, in apparent viscosity with shear rate, characteristics of tumbling amplitudes of motion of the director with oscillation periodicity were observed in 8CB liquid crystals. This tumbling motion in the nematic phase of 8CB liquid crystals was explained more precisely by K. Negita et.al.,[9]following, C.R.Safinya et.al.,[6]. Various structures in different regimes are mentioned with different notations. Here in this paper, we follow the same notations as prescribed by K. Negita et.al.,[9] in representing the regimes and those structures. Which were explained as: In nematic phase, there are mainly three different director orientations with respect to the velocity(flow) direction, namely a,b,c. The corresponding Miesowicz viscosities are η_3, η_2 and η_1 respectively. In nematic phase of all liquid crystals, a steady shear flow induces an alignment of the director $(\hat{\mathbf{n}})$, which has been understood in terms of the Leslie coefficients (α_i) where i varies from 1 to 6. These (α_i) defines the nematic stress tensor. In the temperature region just below the N-I transition point in $b^{'}$ regime, both α_2 and α_3 are negative. Hence, a flow alignment of the director occurs with its direction near the flow direction(y-axis). The $a-b$ structure is composed of coexistent a and b structures. Below this temperature, if the liquid crystals also have Sm-A phase below the nematic phase, α_3^R ((α_3) is renormalized and $(\alpha_3^R) > 0$) and the director changes its direction to the neutral or vortex direction(X). So, $\frac{\alpha_2}{\alpha_3}$ becomes negative to make the flow alignment of the director impossible, leading to $a-b, a_m, a_s, a(b)$ and a_c structures succesively with their stable regions depending on the temperature and shear rate. In these regions, tumbling motion of the director $(\hat{\mathbf{n}})$ is expected to occur[10],[11],[12]. As the director precesses about neutral

or vortex direction with angular frequency ω_0, the equation of motion is described by

$$\frac{n_y(t)^2}{n_{y0}^2} + \frac{n_z(t)^2}{n_{z0}^2} = 1 \tag{4.2}$$

is an equation of ellipse. Here $n_y(t) = n_{y0}\cos(\omega_0 t)$ and $n_z(t) = n_{z0}\sin(\omega_0 t)$ are components of the director $n(t) = (n_x(t), n_y(t), n_z(t))$ precessing around the x-axis with an angular frequency of

$$\omega_0 = \left[\frac{\dot{\gamma}^2(-\alpha_2\alpha_3^R)}{\gamma_1^2}\right]^{\frac{1}{2}} \tag{4.3}$$

Where $\dot{\gamma}$ is the shear rate, α_3^R is the renormalized viscosity coefficient of α_3 including the effect of the S_A fluctuations, and $\gamma_1 = \alpha_3 - \alpha_2$. Depending on the relative strength of the director components, steady structures that are observed:

- a_m structure: anisotropic precession with larger amplitude in the y-direction with $(n_{y0} > n_{z0})$.
- a_s structure: isotropic precession with equal amplitude in the y and z direction $(n_{y0} = n_{z0})$.
- $a(b)$ structure: anisotropic precession with larger amplitude in the z direction $(n_{y0} < n_{z0})$.
- a_c structure: anisotropic precession with its larger amplitude of motion deflected along the z-axis $(n_{y0} << n_{z0})$.

and in the S_A phase, the formation of the layer structure makes the precessional motion impossible.

X-ray scattering studies [6] in the nematic phase of 8CB liquid crystals discovered that, the time averaged distribution of $(\hat{\mathbf{n}})$ under flow reveal a sequence of regimes whose occurrence results from the interplay between the viscous frictional and flow induced fluctuation forces. This is an *in situ* X-ray diffraction measurement. Recently, anomalous diffusion, sub and super diffusive regimes and director$(\hat{n})$ deformations around a sphere in standard liquid crystals like 5CB were described by analyzing the C_v from thermal motion of colloidal particle [13]. In this paper, we rediscovered the non-equilibrium flow

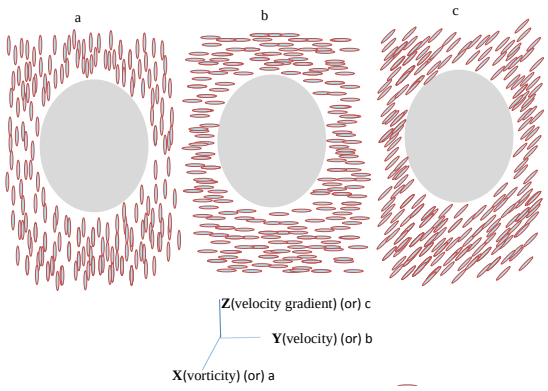

Figure 4.1: a,b,c structures in nematic phase of 8CB liquid crystals represent vorticity(x), velocity(y), and velocity gradient(z) directions

conditions of the nematic(N) to smectic A$(Sm-A)$ transition in 8CB liquid crystals by analyzing the Brownian motion of colloidal particle. VACF (C_v), is the rate of change in diffusion that represents the amplitude $r(t)$ of the deformed structures when diameter of the probing particle is nearly equal to the wavelength of the deformed structures. So, C_v is used in determining the time averaged distribution of the director $(\hat{\mathbf{n}})$ under flow to reveal a sequence of structures in both parallel and perpendicular directions to the director $(\hat{\mathbf{n}})$ orientations. These amplitudes and periodicity of the structures are compared with measurements usig X-ray diffraction, using shear rheology experiments. Further, a generic approach by fitting the (C_v) with time dependent harmonic oscillations under different conditions is followed. This approach reveals the kind of structural transitions, micro structural properties(relaxation time (τ), frequency of oscillations of the directorω) and micro mechanical properties like elastic constant (K)). Also, we measure the quality factor (Q) of precessional motion of $(\hat{\mathbf{n}})$, which represents the stability of fluctuations. Since, these precessional motions $(\hat{\mathbf{n}})$ are known to be anisotropic, in nematic phase of 8CB liquid crystals, it is important to study microstructural and micromechanical properties in both parallel and perpendicular directions to the director orientation.

4.2 THE EXPERIMENT

8CB(4,4$'$-n-Octylcyanobiphenyl) purchased from Sigma aldrich. Phase sequence is: Cr 21.5◦C Sm-A 34.5◦C N 40.5◦C I. Experiments were carried out in the temperature range from Sm-A 33.5◦C N 41.5◦C I. For a specific molecular alignment in the 8CB liquid crystals, the colloidal silica spheres of $0.98\mu m$ in size are coated with a monolayer of Octadecyldimethy(3-trimethoxysilylpropyl)ammonium chloride(DMOAP, Sigma aldrich) [14]. This monolayer ensures the strong perpendicular surface anchoring of the nematic liquid crystals with DMOAP coated surfaces[15]. These coated silica spheres are added to the 8CB liquid crystals and sonicated for the dispersion of these beads into liquid crystals. The uniform dispersion of micro spheres in a planar cell which is coated with AL-1254 on the glass walls and rubbed in one direction, are temperature controlled with a temperature controller(INSTEC) whose resolution is upto $\pm 0.01^{\circ}C$. This sample was observed under an inverted polarizing microscope (Nikon Eclipse,Ti - U) with a microscope objective lens of 100X magnification. Video microscopy is used in the single particle tracking of an isolated colloidal micro sphere to measure its Brownian motion. The position and Brownian motion of the colloidal particle is measured with the help of an appropriate computer program. The total experimental instruments used here are very similar to those mentioned in our previous chapter 2. The Brownian motion of an isolated micro sphere is video recorded for about 5 minutes and analyzed. Measurements are repeated with in the same and different cells.

4.3 RESULTS AND DISCUSSION

In previous experimental measurements, where the structural regimes are analyzed using ELP theory and critical nematodynamics. In those measurements, shear stress is applied on the material to understand the dissipative nature in various structural regimes and hence the precessional motions of $(\hat{\mathbf{n}})$. But, under zero shear conditions, considering either ELP theory is not a right approach, even as very low shear rate conditions. For example, in determining the angular frequency of precessional motion of $(\hat{\mathbf{n}})$, equation 4.3 contains shear rate

$\dot{\gamma}^2$, so, under zero shear conditions, structures in 8CB liquid crystals were not analyzed. In any disordered or complex medium, when the colloidal probe is of the same diameter as of the wavelength of disordered structures, colloidal particle gets navigated through disordered structures. Hence, single particle tracking technique is used in determining the precessional motion of $(\hat{\mathbf{n}})$ and is a correct and simple approach under zero shear limits. In 8CB liquid crystals, as the temperature is reduced, for transitions from N to $Sm-A$, the interplay between the viscous frictional forces and the flow induced fluctuation forces on the nematic director leads to a series of regimes [6]. In the isotropic regime, VACF of 8CB liquid crystals have shown normal diffusive behavior and when the temperature is reduced to just below N-I, at $\Delta T_{N-I} = -0.2^0 C$, these structures are flow aligning nematogens, similar to nematic regime of 5CB liquid crystals. In such a case, the coupling of the sphere's displacements to the director field and its fluctuations leads to anomalous subdiffusion. This subdiffusion is defined as fluctuative displacement of the sphere, that temporarily increases elastic energy density say, on to the left side to its motion and decreases it on the right side. This difference in elastic energy density creates a restoring elastic force $\mathbf{F}_{sub}$ which slows down the diffusion.

$$\mathbf{F}_{sub} \approx -K\frac{\Delta \mathbf{x}}{d} \tag{4.4}$$

where $\Delta \mathbf{x}$ is the change in displacement from left side to right side. As shown in figure 4.2, values of C_v are negative representing sub diffusive nature [13]. But, curve fitting for these VACF gave positive values for the amplitudes in both parallel and perpendicular directions to the director. This represents, the direction of the flow alignment of the director being with its direction near the flow direction(y-axis). From, $b^{'}$ to $a-b$ transition point, the amplitude of the VACF curves have changed from positive to negative value. VACF for structures below $a-b$ regime, were presented as shown in figure. These figures indicate the tumbling nematic director behavior in the apparent viscosity vs shear strain of shear rheology experiments [10]. From Kubo's relation 4.1, both memory function C_v and viscosity are related. Bulk rheology measurements show that, divergence of α_3 is accompanied by rapid increase in amplitude of oscillation with decrease in temperature[10]. But, near T_{Sm-A} regime, the damping of oscillation amplitude occurs

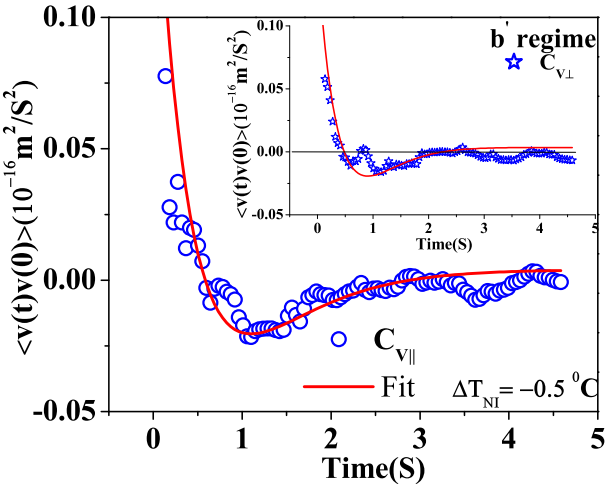

Figure 4.2: At $\Delta T_{N-I} = -0.5^0C$, VACF vs time in $b^{'}$ regime, $C_{v\parallel}$ is shown by open circles(blue color) and $C_{v\perp}$ is shown by star(blue color)and solid line(red color) is fit.

rapidly. Similar characteristics were observed for $C_{v\parallel}$. Where as, $C_{v\perp}$ decreases continuously in the values of oscillation amplitudes. This damping in oscillation amplitude may be due to several factors like out of plane motion of the director, the suppressive effect of the increasing elastic torque, and the appearance of a poly domain structure. But, clearly the faster decay in oscillation amplitudes near T_{SmA-N} can be attributed to the out of plane motion of the director[10].

Both $(C_{v\parallel})$ and $(C_{v\perp})$ have similarities with the periodicity in the apparent viscosity vs shear strain[10]. The periodicity of this oscillation cycle corresponds to a director rotation angle of π at low shear limits[16].

The VACF of these structures in all the regimes of nematic phase can be understood in the context of descriptions of C.R. Safinya [6] and K. Negita et.al.,[8]. From figure4.3, in a_m regime, at $\Delta T_{N-I} = -2.5^0C$, the characteristics of precessional motion starts dominating and periodic structures are very clear in this regime. In a_m regime, amplitude of first harmonic of $C_{v\perp} > C_{v\parallel}$. That is, there exists anisotropic precession with larger amplitude in the y-direction. From figure4.4, in a_s regime,

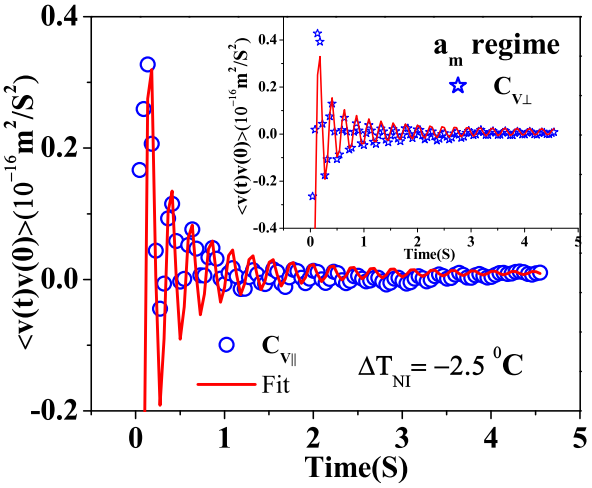

Figure 4.3: At $\Delta T_{N-I} = -2.5^0C$, VACF vs time in a_m regime, $C_{v\parallel}$ is shown by open circles(blue color) and $C_{v\perp}$ is shown by star(blue color)and solid line(red color) is fit.

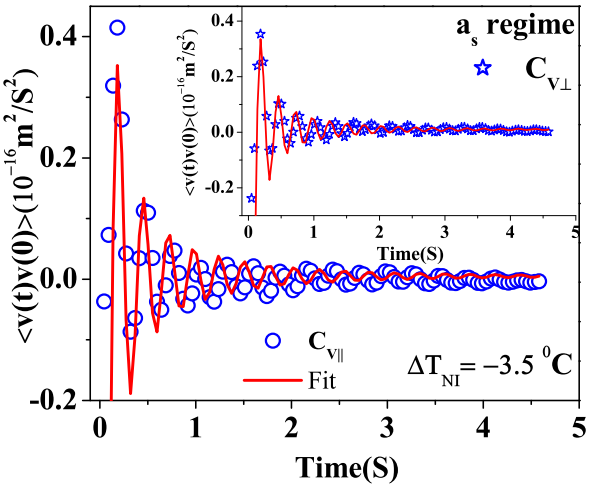

Figure 4.4: At $\Delta T_{N-I} = -3.5^0C$, VACF vs time in a_s regime, $C_{v\parallel}$ is shown by open circles(blue color) and $C_{v\perp}$ is shown by star(blue color)and solid line(red color) is fit.

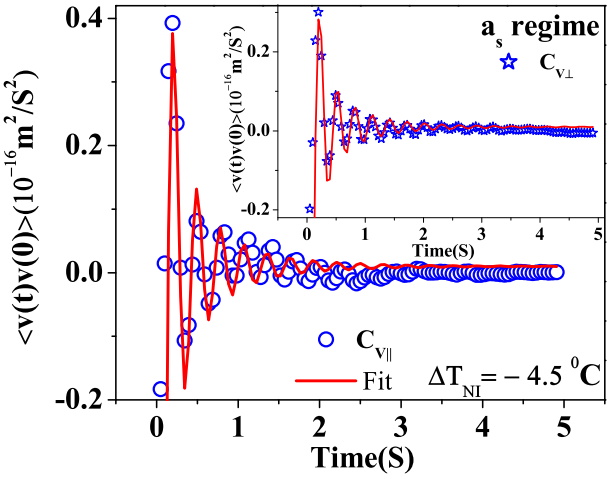

Figure 4.5: At $\Delta T_{N-I} = -4.5^0C$, VACF vs time in a_s regime, $C_{v||}$ is shown by open circles(blue color) and $C_{v\perp}$ is shown by star(blue color) and solid line(red color) is fit.

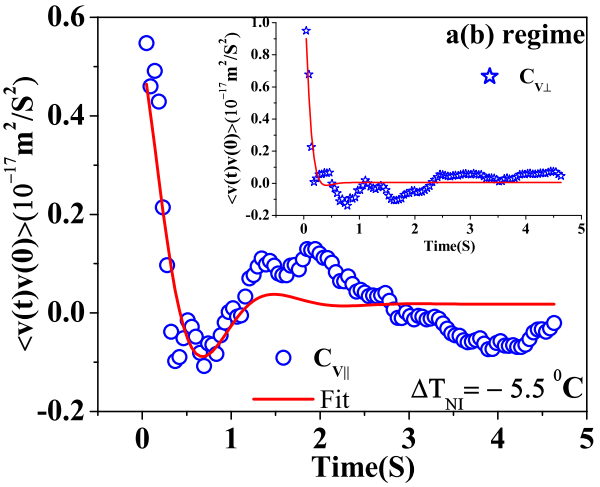

Figure 4.6: At $\Delta T_{N-I} = -5.5^0C$, VACF vs time in $a(b)$ regime, $C_{v||}$ is shown by open circles(blue color) and $C_{v\perp}$ is shown by star(blue color) and solid line(red color) is fit.

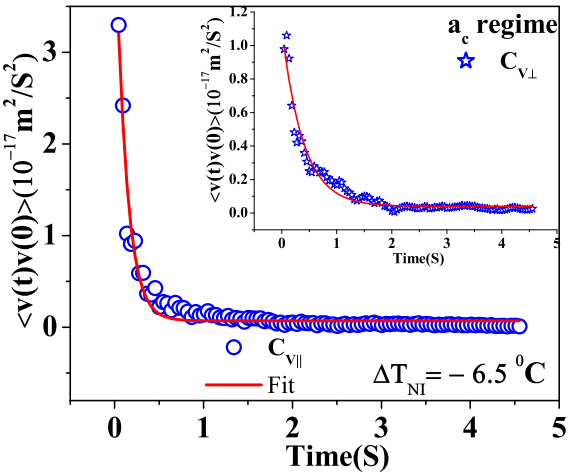

Figure 4.7: At $\Delta T_{N-I} = -6.5^0 C$, VACF vs time in a_c regime, $C_{v\parallel}$ is shown by open circles(blue color) and $C_{v\perp}$ is shown by star(blue color) and solid line(red color) is fit.

the amplitude of first harmonic of $C_{v\parallel} \simeq C_{v\perp}$. That is, a_s structure has isotropic precession with equal amplitude in the y and z- directions. From figure4.5, the amplitude of first harmonic of $C_{v\parallel} > C_{v\perp}$. This represents a change in the direction of precessional motion from y to z direction.That is, there exists anisotropic precession with larger amplitude in the z-direction. From figure 4.7, the amplitude of first harmonic of $C_{v\parallel} \ll C_{v\perp}$. This is because, the amplitude of the motion largely gets deflected along the z-axis, which becomes more an out of planed motion of the director, and hence the amplitude of oscillations decreases rapidly.

Further, in order to characterize these structures, here we present a more qualitative approach by fitting these VACF with solutions of time dependent harmonic oscillations.

Structures	$C_{v\parallel}$	$C_{v\perp}$
a_m	0.32	0.42
a_s	0.41	0.35
a(b)	0.0054	0.0095
a_c	0.032	0.01

Table 1: Amplitudes of first harmonics of $C_{v\parallel}$ and $C_{v\perp}$ are multiples of $10^{-15}m^2/S^2$

1. $b^{'}$ regime: At $\Delta T_{N-I} = -0.5^{\circ}C$, both $C_{v\parallel}$ and $C_{v\perp}$ fits with solutions of equation of motion(EOM) of under damped harmonic oscillations. Hence,

$$C_{v\parallel,\perp} = C_0 e^{\frac{-t}{2\tau_p}} \left(\cos\omega t + \frac{\sin\omega t}{2\omega\tau_p}\right) \tag{4.5}$$

2. a_m regime: At $\Delta T_{N-I} = -2.5^{\circ}C$, $Cv \parallel$ fits with solutions of EOM of coupled harmonic oscillations. Hence,

$$C_{v_\parallel} = C_0 \frac{\omega}{2\pi\tau_p} \left(\frac{\sin(\omega t)}{\omega t}\right) \tag{4.6}$$

   In this case, $C_{v\perp}$ fits with solutions of decaying coupled harmonic oscillations.

$$C_{v\perp} = C_0 \frac{\omega}{2\pi\tau_p} e^{\frac{-t}{2\tau_p}} \left(\frac{\sin(\omega t)}{\omega t}\right) \tag{4.7}$$

3. a_s regime: From $\Delta T_{N-I} = -3.5^{\circ}C$ to $\Delta T_{N-I} = -4.5^{\circ}C$, both $C_{v\parallel}$ and $C_{v\perp}$ fits with solutions of EOM of decaying coupled harmonic oscillations.

4. $a(b)$ regime: At $\Delta T_{N-I} = -5.5^{\circ}C$, both $C_{v\parallel}$ and $C_{v\perp}$ fits with solutions of equation of motion(EOM) of half critically damped harmonic oscillations.

$$C_{v\parallel,\perp} = C_0 e^{\frac{-t}{4\tau_p}} (\cos\omega t) \tag{4.8}$$

5. a_c regime: At $\Delta T_{N-I} = -6.5^{\circ}C$, both $C_{v\parallel}$ and $C_{v\perp}$ fits with solutions of equation of motion(EOM) of critically damped harmonic oscillations.

$$C_{v\parallel,\perp} = C_0 e^{\frac{-t}{4\tau_p}} \left[C_1 + (C_2 x)\right] \tag{4.9}$$

In these various forms of harmonic oscillator equations, C_0 is the normalized values of C_v, τ_p represents relaxation time of $(\hat{\mathbf{n}})$, ω is the frequency of oscillation of $(\hat{\mathbf{n}})$,and C_1, C_2 are constants. The orientational state of $(\hat{\mathbf{n}})$ can be determined by viscous and elastic torque forces acting on it. In $b^{'}$ regime, since $(\hat{\mathbf{n}})$ makes a small angle with $(\hat{\mathbf{V}})$ or $(\hat{\mathbf{b}})$ axis, so both $C_{v\parallel}$ and $C_{v\perp}$ are similar to those measured by T. Turiv et.al.,[13] for 5CB liquid crystals. Hence, they fit well with underdamped harmonic oscillator solutions. In a_m regime, there is no damping term in the equation 6.5 of $C_{v\parallel}$ which represents coupled harmonic oscillator motion. But, there is a damping term in the equation4.7 of $C_{v\perp}$. This represents beginning of formation of structures within this regime and is marginally stable [7]. From the synchrotron X-ray studies, a_s regime is known to be stable with undamped precessing motion [7]. But, from equation 4.7, which represents both $C_{v\parallel}$ and $C_{v\perp}$ have damping term. Though, damping term is present, but its value is relatively less in this regime. Because of anisotropic suppression of Sm-A fluctuations due to flow, $a(b)$ regime coexists with regions of the sample where $(\hat{\mathbf{n}})$ points along X-axis and regions where $(\hat{\mathbf{n}})$ points along Y-axis. Hence $C_{v\parallel}, C_{v\perp}$ fits with half critically damped oscillatory equations. In a_c regime, from [7], $(\hat{\mathbf{n}})$ points mostly along X-axis but, tumbles towards Z-axis. But, considering our sample plane, $(\hat{\mathbf{c}})$ is along Z-axis, hence we could not measure any precessional motion along this direction.

Also, microstructural properties like periodic oscillation frequency(ω), relaxation time(τ) of $(\hat{\mathbf{n}})$ are quantified by fitting $C_{v\parallel}$ and $C_{v\perp}$ with harmonic oscillator equations. From these properties, micro mechanical properties like elastic constant (K)(one elastic constant approximation), quality factor(Q) that describes stability of the precessional motion are calculated. These results predicts the similar nature to the precessional motion of $(\hat{\mathbf{n}})$ along different axes V , ΔV and neutral axis as mentioned in previous experimental results[6],[9] which are based on Ericksen-Leslie-Parodi(ELP) theory and critical nemato dynamics. In figure 4.8, for both $C_{v\parallel}$ and $C_{v\perp}$, precessional frequency increases

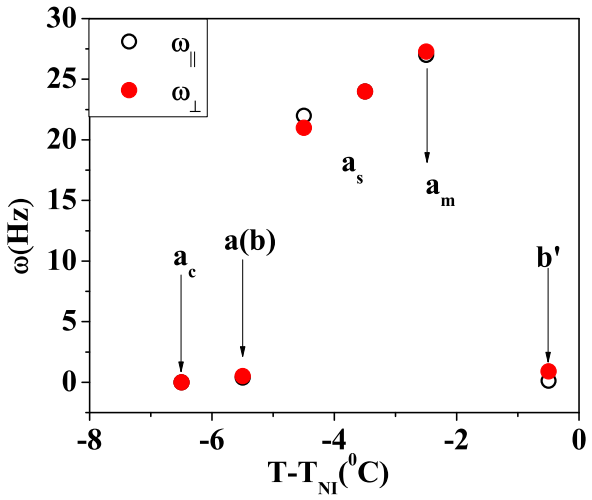

Figure 4.8: angular frequency (ω) vs ΔT of precessional motion of $(\hat{\mathbf{n}})$ in different regimes of nematic phase of 8CB liquid crystals. $(\omega_{\parallel})$ is shown by open circles and $(\omega_{\perp})$ is shown by closed (red) circles.

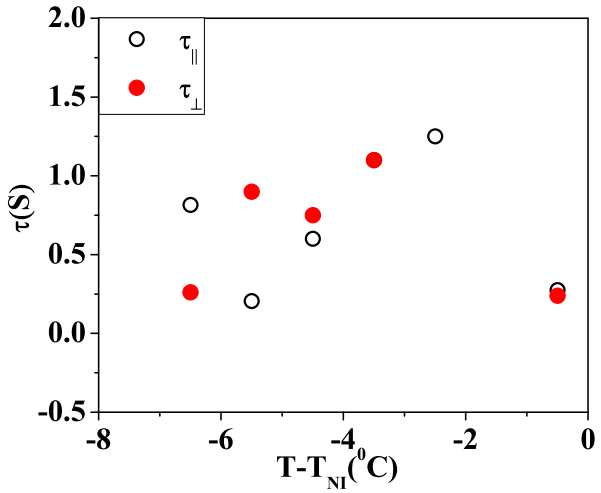

Figure 4.9: Time of relaxation (τ) vs ΔT of $(\hat{\mathbf{n}})$ in different regimes of nematic phase of 8CB liquid crystals. $(\tau_{\parallel})$ is shown by open circles and $(\tau_{\perp})$ is shown by closed (red) circles.

from regimes $b^{'}$ to a_m because of pretransitional Sm-A fluctuations and then it decreases rapidly as it reaches $a(b)$ regime and is zero in a_c regime, where, pretransitional Sm-A fluctuations is expected to give rise to flow induced fluctuation force similar to b' regime. Further, the measured values of τ represent the slow dynamics and are inversely proportional to viscosity($\sim \frac{1}{\gamma}$). In figure 4.9, from b' to a_m regime, τ increases, and it decreases almost steeply till $a(b)$. In a_m regime, at $\Delta T_{N-I} = -3.5^{\circ}C$, since $C_{v\perp}$ fits with coupled harmonic oscillator equation, with no damping term, the value of τ is not presented. This τ vs ΔT shows inversely proportionate behavior with η vs ΔT in shear rheology experimental results[9]. The decrease in the value of $\tau_{\parallel}$ at $\Delta T_{N-I} = -5.5^{\circ}C$, in $a(b)$ regime, can be attributed to the pre transitional Sm-A fluctuations which can be expected to give rise to a flow induced fluctuation force[6]. But,there is a crossover in $\tau_{\parallel}$ and $\tau_{\perp}$ values in a_c regime $\Delta T_{N-I} = -6.5^{\circ}C$. Here, the liquid crystal cell is rubbed, so the smectic layer planes in the temporarily fluctuating clusters, that are oriented perpendicular to the rubbing direction can be expected to have slow relaxation times[17]. Therefore, $\tau_{\perp}$ is lower than $\tau_{\parallel}$.

Negative values of auto correlations in C_v indicates a tendency to move back to earlier position. This antipersistant behavior is the characteristic of viscoelastic medium. From the measured values of ω, elastic constant (K) can be calculated $(K = m\omega^2)$. Obviously, the characteristics of K replicate the same characteristics of ω. In a_m, a_s regimes elastic nature is more dominant as shown in figure4.10. Further, in case of $\frac{1}{\tau} \ll \omega$, the quality factor$(Q)$ of harmonic oscillations is $Q = \omega\tau$. This Q represents the stability of the harmonic oscillations. From figure4.11, it is clear that, both a_m and a_s are more stable regimes.

4.4 CONCLUSIONS

For the first time, single particle tracking technique is used in determining the nature of the amplitudes of precessional motions of different structures in 8CB liquid crystals. Advantage of this technique is in tracking these precessional motions in parallel and perpendicular directions to the nematic director. The challenge of next step to identifying anomalous behavior lies in determining the underlying mechanism.

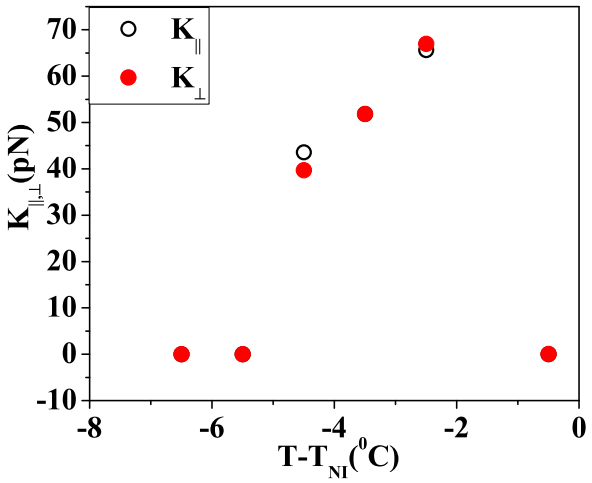

Figure 4.10: Elastic constant (K) vs ΔT in different regimes of nematic phase of 8CB liquid crystals. $(K\|)$ is shown by open circles and $(K_\perp)$ is shown by closed (red) circles.

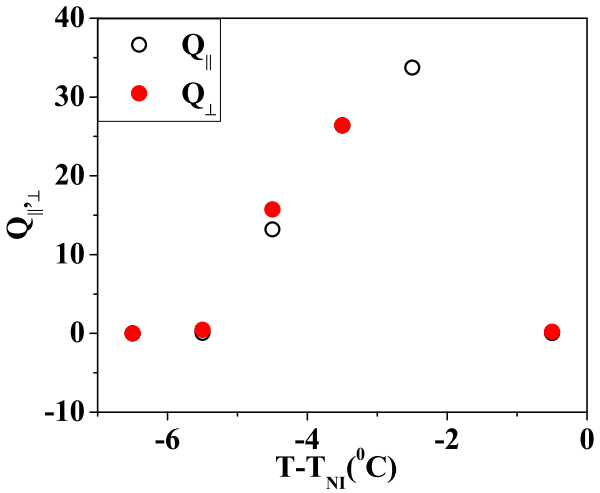

Figure 4.11: Quality factor (Q) vs ΔT of precessional motion of $(\hat{\mathbf{n}})$ in different regimes of nematic phase of 8CB liquid crystals. $(Q_\|)$ is shown by open circles and $(Q_\perp)$ is shown by closed (red) circles.

As the colloidal particle passes through 8CB liquid crystals medium, the precessing nematic director "pushes back" creating long time correlations in the particle trajectory. This memory leads to sub diffusive behavior. In any disordered or complex medium, colloidal particle gets navigated through disordered structures, when the colloidal probe is of the same diameter as of the wavelength of disordered structures. VACF(C_v), which describes the intrinsic memory of the dynamical structures is used in determining diffusive behavior of the colloidal particle. The $C_{v\parallel}$ and $C_{v\perp}$ have shown the profound nature of the precessional motions of the nematic director. The amplitudes of these precessional motions in the parallel direction are very much in agreement with the precessional motion amplitudes measured using bulk rheometer. The amplitudes of precessional motions of the nematic director in the perpendicular direction was measured for the first time and observed a continuous decrease in these peak amplitudes. Also, the amplitudes of isotropic and anisotropic precessional motions in various structures with in the nematic phase were observed and they are in well agreement with the previous literature. Further, we have measured microstructural properties of the 8CB liquid crystals in its nematic phase by fitting the oscillatory motion present in the VACF of 8CB liquid crystals with the under damped harmonic oscillations. To our knowledge, such an attempt using Brownian motion of the colloidal sphere in the tumbling nematics is attempted for the first time. We believe that, this is a necessary and successive step after the experimental measurements by T. Turiv et.al.,[13].

In the next chapter, these tumbling nemato dynamics of 8CB liquid crystals are understood in terms of the dissipation of energy during the tumbling molecular reorientations. Also, by analyzing the difference in the power law variation of storage modulus with respect to frequency the different structural regimes nematic phase (just below NI transition temperature), tumbling nematic phase are differentiated and near the Sm-C transition are differentiated.

BIBLIOGRAPHY

[1] P.M. Chaikin, T.C. Lubensky, "Principles of condensed matter physics", First south asian paperback edition (1998).

[2] M. H. J. Hagen, I. Pagonabarraga, C. P. Lowe, and D. Frenkel, Phys.Rev.Lett., **78**, 19 (1997).

[3] R. Kubo, M. Toda, and N. Hashitsume, "Statistical Physics II", Springer-Verlag, Berlin, (1998).

[4] R. Kubo, Rep. Prog. Phys. **29**, 255 (1966).

[5] Frederic Mondiot, Jean-Christophe Loudet, Olivier Mondain-Monval, and Patrick Snabre, Phys. Rev. E **86**, 010401(R) (2012).

[6] C. R. Safinya, E. B. Sirota, and R. J. Piano, Phys. Rev. Lett., **66**, 15 (1991).

[7] C. R. Safinya, E. B. Sirota, R. Plano, and R. F. Bruinsma, J. Phys.: Condens. Matter., **2**, SA365 (1990) .

[8] K. Negita, J. Chem. Phys. **105**, 7837 (1996).

[9] K. Negita, M. Inoue, and S. Kondo, Phys.Rev. E., **74**, 051708 (2006).

[10] D.F. Gu and A.M. Jamieson, J.Rheol., **38(3)**, 1994.

[11] Dennis J. Ternet, Ronald G. Larson, L. Gary Leal, Rheol Acta **38**, 183 (1999).

[12] P.T. Mather, D.S.Pearson and R.G.Larson, Liquid crystals, **20(5)**, 539 (1996).

[13] T. Turiv, I. Lazo, A. Brodin, B. I. Lev, V. Reiffenrath, V. G. Nazarenko, O. D. Lavrentovich, Science, **342**, 1351 (2013).

[14] V.S.R. Jampani, "Surface coupling agent (DMOAP) for colloidal liquid crystals".(online material)

[15] M. karabot, I. Muevi, Soft Matter **6**, 5476, (2010).

[16] G.Marrucci, Macromolecules, **24**, 4176 (1991).

[17] S. Dhara, Y. Balaji, J. Ananthaiah, P. Sathyanarayana, V. Ashoka, A. Spadlo, and R. Dabrowski, Phys. Rev. E., **87**, 030501(R) (2013).

[18] Jahnig, F. and F. Brochard, J. Phys. (Paris) **35**, 301 (1974).

[19] Jaka Fajar Fatriansyah and Hiroshi Orihara, Phys. Rev. E., **88**, 012510 (2013).

[20] Tongcang Li and Mark G. Raizen, Ann. Phys. (Berlin), **115** (2013).

[21] Jimaan San, Johan T. Padding, and Ard A. Louis, Phys. Rev. E., **79**, 051402 (2009).

5

MICRORHEOLOGY IN TUMBLING NEMATICS OF 8CB LIQUID CRYSTALS

5.1 INTRODUCTION

Microrheological studies in understanding the flow behavior in nematic phase of liquid crystals are not rigorous. Although there were many theoretical explanations and experimental measurements in shear rheology. In shear rheology experiments, Ericksen-Leslie-Pondou(ELP) theory was used in understanding various regimes in the nematic phase of 8CB liquid crystals.

In nematic phase of liquid crystals, the average orientation of molecules is determined by the nematic director $(\hat{\mathbf{n}})$[1]. This director field is coupled to the velocity field or flow field **V(r,t)**. The dissipation of energy in liquid crystals strongly depends on the microscopic constituent molecules alignment and orientation. The direction of orientation of $(\hat{\mathbf{n}})$ characterizes the nematic stress tensor (α_i) Where $i = 1$ to 6. Miesowicz viscosities η_1, η_2, η_3 depends on (α_i). The sign of the viscosity coefficient α_3 determines the flow aligning behavior of the NLC. The sign of α_2 is always negative in case of nematic liquid crystals, so, if α_2, α_3 satisfy a condition, such that $\alpha_2/\alpha_3 > 0$, a flow alignment takes place, with director orientation at an angle $\tan\theta = \sqrt{\alpha_2/\alpha_3}$. In standard liquid crystals like 5CB, with sequence of phases as crystal(cr), nematic(N) and Isotropic(I) fluid, then flow alignment occurs with the director at a characteristic angle with respect to the flow direction even at low shear fields, in the whole nematic phase [2]. For $\alpha_3 > 0$, the director is forced to rotate continuously by the hydrodynamic torques even at low shear field. The director rotation angle θ will always increase with strain and an indefinite oscillatory response is predicted [3]. Jahnig, and Brochard [4] observed that, if a liquid crystal possess a phase sequence as crystal(cr), smectic A(Sm-A), nematic(N), and Isotropic phases, then it will have positive α_3, in its nematic phase near the Sm-A to N transition temperature, since α_3, has a positive divergence at T_{SmA-N}. In 8CB liquid crystals,

phase sequence occurs as cry-Sm-A-N-I, so for $\alpha_3 > 0$, nematic phase is of the tumbling type in these liquid crystlas. It is well known that [2], [5], [6], in 8CB liquid crystals, along with phase transitions, there exists several structures in its nematic regime. Basically, the orientation or the isotropic and anisotropic precessional motions of the director around the velocity or the flow gradient directions determines the phases in the nematic regime. Earlier, from theoretical[7], [8], and experimental measurements by [3] in which apparent viscosity with shear rate and with variation in temperature in 8CB liquid crystals, it was observed that, there exists tumbling motions of the director that dominates the whole nematic regime. They also observed the tumbling oscillation periodicity as a strong function of temperature. This same tumbling motion in the nematic phase of 8CB liquid crystals was explained more precisely by K. Negita et.al.[5]. Various structures are mentioned in their paper with different notations. Here we follow the same notations in representing about the structures and these structures were explained as: In the temperature region just below the N-I transition point, a flow alignment of the director occurs with its direction near the flow direction(y-axis). That means, liquid crystals in this regime behave as a flow aligning nematogens. Below this region of temperatures $\frac{\alpha_2}{\alpha_3}$ becomes negative to make the flow alignment of the director impossible, leading to $a-b, a_m, a_s, a(b)$ and a_c structures succesively with their stable regions depending on the temperature and shear rate. In these regions of structures tumbling motion is expected to occur [3]. The $a-b$ structure is composed of coexistent a and b structures. Below this temperature, precessional motions around the x axis are induced, leading to $a_m, a_s, a(b)$ and a_c structures with their precessional motions characterized by $n_y(t)^2/n_{y0}^2 + n_z(t)^2/n_{z0}^2 = 1$. Here $n_y(t) = n_{y0}\cos(\omega_0 t)$ and $n_z(t) = n_{z0}\sin(\omega_0 t)$ are components of the director $n(t) = (n_x(t), n_y(t), n_z(t))$ precessing around the x-axis with an angular frequency of $\omega_0 = [\dot{\gamma}^2(-\alpha_2\alpha_3^R)/\gamma_1^2]^{\frac{1}{2}}$. $\dot{\gamma}$ is the shear rate, α_3^R is the renormalized viscosity coefficient of α_3 including the effect of the S_A fluctuations, and $\gamma_1 = \alpha_3 - \alpha_2$. Further, the precessional motions in each structure are explained as:
1)a_m strucure: anisotropic precession with larger amplitude in the y-direction with $(n_{y0} > n_{z0})$. 2)a_s structure: isotropic precession with equal amplitude in the y and z direction $(n_{y0} = n_{z0}$. 3)$a(b)$ struc-

ture: anisotropic precession with larger amplitude in the z direction ($n_{y0} < n_{z0}$. 4)a_c structure: anisotropic precession with its larger amplitude of motion deflected along the z-axis ($n_{y0} << n_{z0}$) and in the S_A phase, the formation of the layer structure makes the precessional motion impossible.

All the above description of structural regimes are using ELP theory and critical nematodynamics in bulk rheology and X-ray diffraction measurements. In this chapter, a real space(insitu) measurement using Brownian motion of microsphere of the diameter of the same size as of the structures formed by the orientations of director ($\hat{\mathbf{n}}$). This measurement of Brownian motion in tumbling nematic phase is first of its kind. The microsphere motion in liquid crystals is in analogy to motion in a harmonic trap, because of the defect formed around the microsphere. In such case, the dissipative force describes the average effect on the Brownian motion of bead in liquid crystals. Hence it is important to measure $G^{'}$ and $G^{''}$ with out using ELP theory of shear rheology in 8CB liquid crystals.

5.2 THE EXPERIMENT

Silica microshperes of 0.98 μm are coated with Octadecyl dimethy(3-trimethoxysilylpropyl)ammonium chloride(DMOAP, Sigma Aldrich) for a specific molecular alignment [11] in the 8CB liquid crystals(Sigma Aldirich). These colloidal spheres are dispersed in 8CB liquid crystals. Two coverslips of 130μm in thickness are coated with AL-1254, and for planar alignment, the AL-1254 coating is rubbed in the opposite directions which will be used as opposite facets in the sample cell with the thickness of the cell being 23μm. 8CB liquid crystals phase transitions(cooling):I at 41.5$\circ C$ to N at 34.8 $\circ C$. Uniform dispersion of particles motion is verified in a polarizing microscope(Nikon Eclipse, TE-2000U) with a 40X objective. Brownian motion of an isolated particle is tracked with an appropriate computer program with in an inverted polarizing microscope (Nikon Eclipse, Ti-U) using a 100X objective. The experimental measurement of micro viscosity is very similar to our previous paper [12]. The Brownian motion of an isolated micro sphere is video recorded for about 5 minutes and analyzed. The analysis for calculating microrheological parameters like G′ and G″

is from [9],[10], [13]. More description on the G' and G'' was given in chapter 3. Measurements are repeated with in the same and different cells.

5.3 RESULTS AND DISCUSSION

When a microsphere of $0.98\mu m$ diameter moves in the nematic phase of liquid crystal, the fluctuating director $(\hat{\mathbf{n}})$ displaces or biases the thermal motion of the microsphere. Suppose, a fluctuative director$(\hat{\mathbf{n}})$ displaces the sphere to its left by a distance $\Delta\mathbf{x}$, this displacement temporarily increases the elastic energy density on the left side. So, there occurs a difference in the elastic energy densities between left and right side. This leads to a restoring elastic force F = -K $\Delta\mathbf{x}$/d. 'd' is the diameter of the sphere. This force slows down the diffusion of the microsphere [14]. Thermal motion of the microsphere in liquid crystals is in analogy with motion of a sphere in a trap. That means, motion of sphere is included with elastic forcess of the trap. Micro spheres with dipolar defects generally undergo these restoring elastic forces. In our experiment, the gap size of the cell is very large compared to the bead diameter(d) which leads to dipolar defects of the nematic director around microsphere[11]. If this microsphere displaces through structures are of the order of diameter of sphere($\sim 1\mu$ m), the thermal motion of the sphere constrained. This leads to anomalous Brownian motion of the microsphere.

In isotropic fluids, the mean square displacement (MSD) of the Brownian motion of a spherical particle is linear in time τ. Whereas in case of complex fluids such as entagled actin filament networks etc., the Brownian motion is anomalous, mostly due to the infrequent large jumps that the particle makes between distinct pores in the network[15]. Hence the MSD follows a power law behaviour with $\langle \Delta r^2(t) \rangle \propto \tau^{\alpha}$. When $0 < \alpha < 1$ the nature is sub-diffusive and when $\alpha > 1$ it is super-diffusive, over a lag time τ. Recently, sub-diffusive and super-diffusive motion in 5CB liquid crystals have been reported by measuring time variation of $\left(\langle \Delta r^2(t) \rangle\right)$ [14]. Here, we show from the thermal motion of the colloidal particle, how precessional motions of the director and the collective molecular reorientations affect the Brownian motion. We

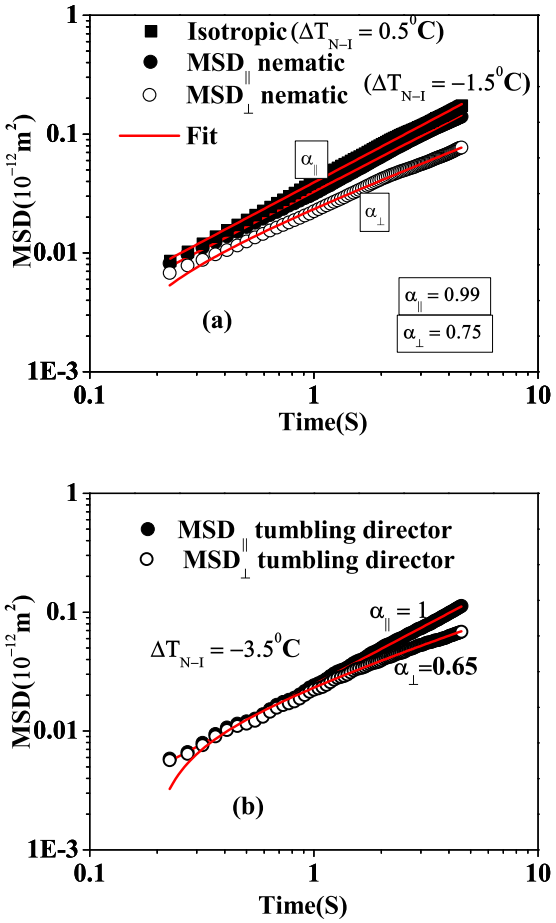

Figure 5.1: MSD vs time for (a) Isotropic(solid square) ($\Delta T_{N-I} = +0.5^{\circ}C$) and nematic phase(closed and open circles for parallel and perpendicular MSD) ($\Delta T_{N-I} = -1.5^{\circ}C$) and (b) In case of tumbling nematic director(closed and open circles for parallel and perpendicular MSD) at ($\Delta T_{N-I} = -3.5^{\circ}C$) of 8CB liquid crystals. solid line(red colour) represents the power law fit.

also show that there exists a non-linear behaviour of $\langle \Delta r^2(\tau) \rangle \propto \tau^{\alpha}$ with respect to time-lag and that the exponent α varies in values.

In figure 5.1 (a), with in isotropic regime, at $\Delta T = 0.5^0 C$, the parallel and perpendicular components both show linear increase in the value of α, this shows the normal diffusive nature of the liquid crystals in the isotropic regime. On lowering the temperature leading to just below N-I transition point, flow alignment of the director is known to occur with its direction near the flow direction as mentioned in [5]. Further decrease in temperature to $\Delta T = -1.5^{\circ} C$, there it shows anisotropy in the MSD Vs time as shown in fig.5.1(a). In the log-log plot, parallel component does possess linear behavior with MSD vs time and fits well with linearly increasing curve and perpendicular component show subdiffusive behavior and fits well with power law rise in time and the value of $\alpha = 0.77$. In the temperature regime where the precessional motion of the director $(\hat{\mathbf{n}})$ is expected to occur along different axial directions, in 8cb liquid crystals case at $\Delta T = -3.5^0 C$, still the parallel component of $\left(\langle \Delta r^2(t) \rangle\right)$ show linear increase with increase in time and perpendicular component exhibits non-linear increase in α value as shown in figure 5.1 (b), and shows subdiffusive behavior with α value being equal to 0.65. As the temperature is reduced to go close to Sm-A translations, again here parallel component has value of $\alpha = 1$ in the MSD vs time graph and perpendicular component has non-linear growth with $\alpha = 0.8$ which is again subdiffusive behavior at $\Delta T = -5.5^0 C$. Overall, MSD Vs time lag graphs of 8CB liquid crystal does show a trend with the decrease in temperature. That is, through out, as the temperature changes, In the parallel direction to the nematic director, the MSD curve does show linear raise with time. Whereas, in the perpendicular direction it does show nonlinear rise in time with $\langle \Delta r^2(\tau) \rangle \propto \tau^{\alpha}$ with exponent α value varying in the power law fitting. The error bars for this α values are larger with the repeated measurements.

Many of the condensed matter systems are either time dependent or frequency dependent. Dynamic properties of the condensed matter systems are mostly harmonic oscillator like modes. Information about the dissipation of harmonic oscillators energy into incoherent degrees of freedom is reflected in the sign of the viscous forces that leads to decay of amplitude of motion in time.

From the measured thermal motion of the silica beads, viscoelastic shear moduli(storage modulus(G') and loss modulus (G'')), using generalised Stokes-Einstein equation can be computed. G$'$ and G$''$ represent the fraction of energy induced by the deformation imposed on the material. A fraction of energy is lost by the viscous dissipation in case of loss modulus(G$''$), and, is stored elastically in case of storage modulus(G$'$). G$'$ and G$''$ were computed using the equations given in Ref.[10], given below, as a function of rate of deformation ω. By expanding the equation of motion of Mean square displacement around $t = 1/\omega$, the translational parameter β is defined as [10]

$$\beta(\omega) = \left.\frac{\langle d \ln \Delta r^2(t)\rangle}{d \ln t}\right|_{t=\frac{1}{\omega}} \tag{5.1}$$

and the Fourier transform of this MSD equation would lead to give G$'(\omega)$ and G$''(\omega)$ as

$$\begin{aligned} G'(\omega) &= |G^*(\omega)| \cos\left(\frac{\pi\beta(\omega)}{2}\right) \\ G''(\omega) &= |G^*(\omega)| \sin\left(\frac{\pi\beta(\omega)}{2}\right) \end{aligned} \tag{5.2}$$

Where $|G^*(\omega)| = k_B T/\pi a \langle \Delta r^2(\frac{1}{\omega})\rangle \Gamma[1+\beta(\omega)]$, and 'a' the radius of the probing bead.

Here, we present the microrheological properties (elastic modulus G', viscous modulus G'') in the nematic phase of 8CB liquid crystals. In liquid crystals, the average orientation of liquid crystal molecules is determined by the director ($\hat{\mathbf{n}}$). Hence, the effect of collective molecular reorientations on Brownian motion of colloids in nematic liquid crystals is determined by the direction of orientation of ($\hat{\mathbf{n}}$). Just below nematic to isotropic transition temperature, in $b^{'}$ regime, at ($\Delta T_{N-I} = -0.5^{\circ}C$), a flow alignment of the nematic director ($\hat{\mathbf{n}}$) occurs with its direction with a small angle near the flow direction(Y-axis). Such flow alignment also occurs in 5CB liquid crystals. In figures 5.3, at high frequencies, $G''(\omega) > G'(\omega)$, represents a material that is more viscous than elastic and is a viscoelastic liquid. Usually, at low frequencies, $G'(\omega) > G''(\omega)$, is a viscoelastic solid[16]. The power law dependence of frequency of $G'(\omega)$, $G''(\omega)$ in both parallel and

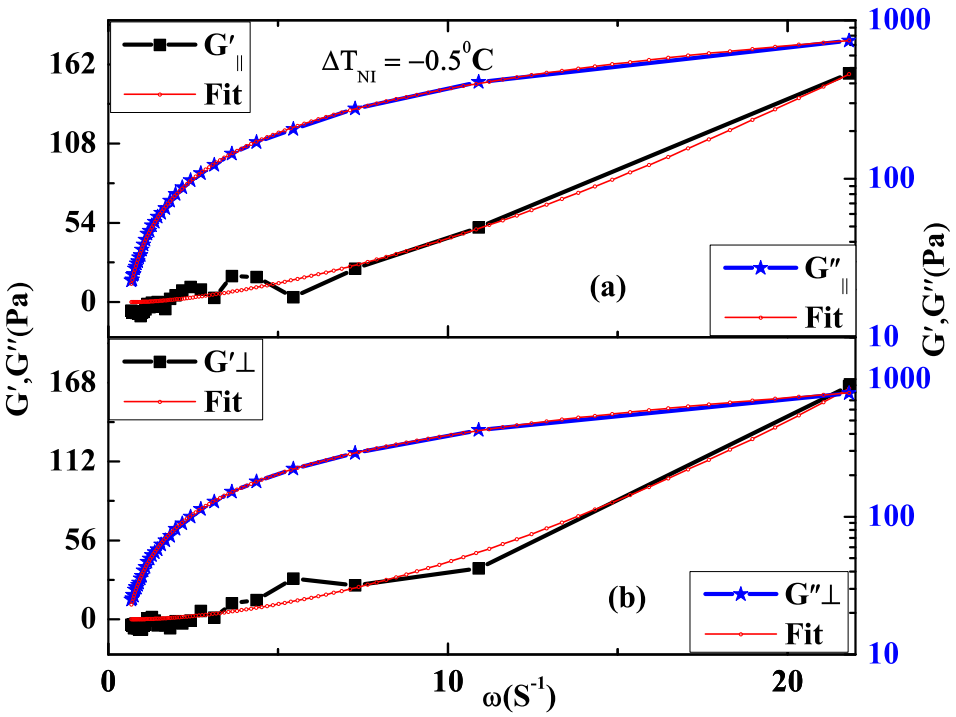

Figure 5.2: In nematic phase of 8CB liquid crystals, at ($\Delta T_{N-I} = -0.5°C$), $G'_{\|}$ and $G''_{\|}$ represent the parallel components of G' and G''. Here, G' is solid square(black colour) and G'' is star(blue colour).(b) $G'_{\perp}$ and $G''_{\perp}$ represents perpendicular components of G' and G''. Thin line(red colour) with a small open circle shows fitting.

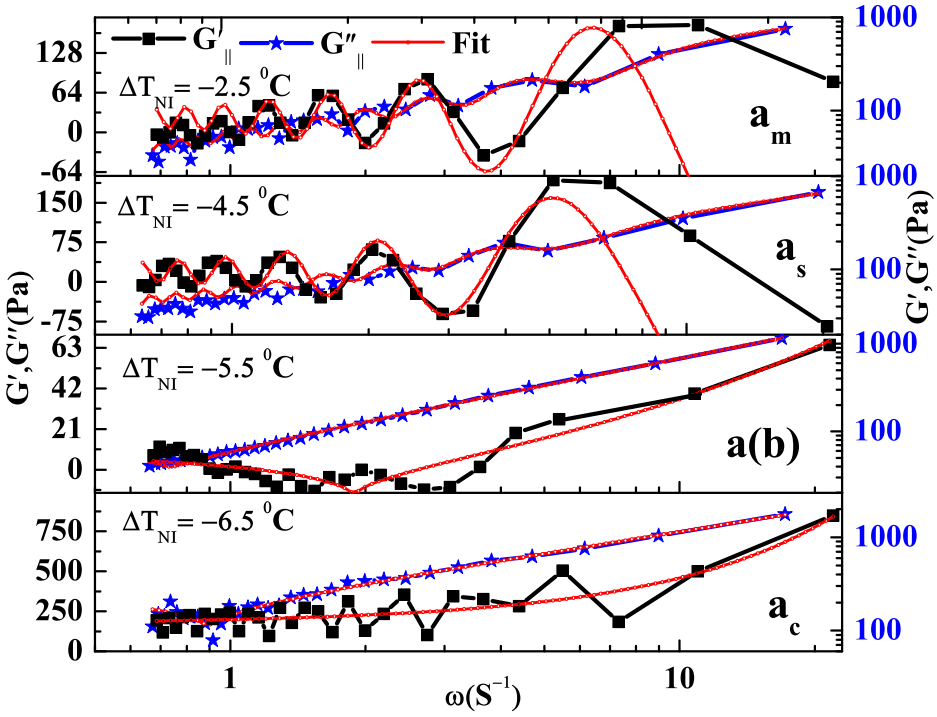

Figure 5.3: In nematic phase of 8CB liquid crystals, parallel components of elastic ($G_{\|}^{'}$) and viscous modulus ($G_{\|}^{''}$) vs frequency (ω) of different regimes($a_m, a_s, a(b), a_c$). Here, $G^{'}$ is represented by line with solid square(black colour) and $G^{''}$ is represented by line with star(blue colour). Thin line(red colour) with a small open circle shows fitting.

.

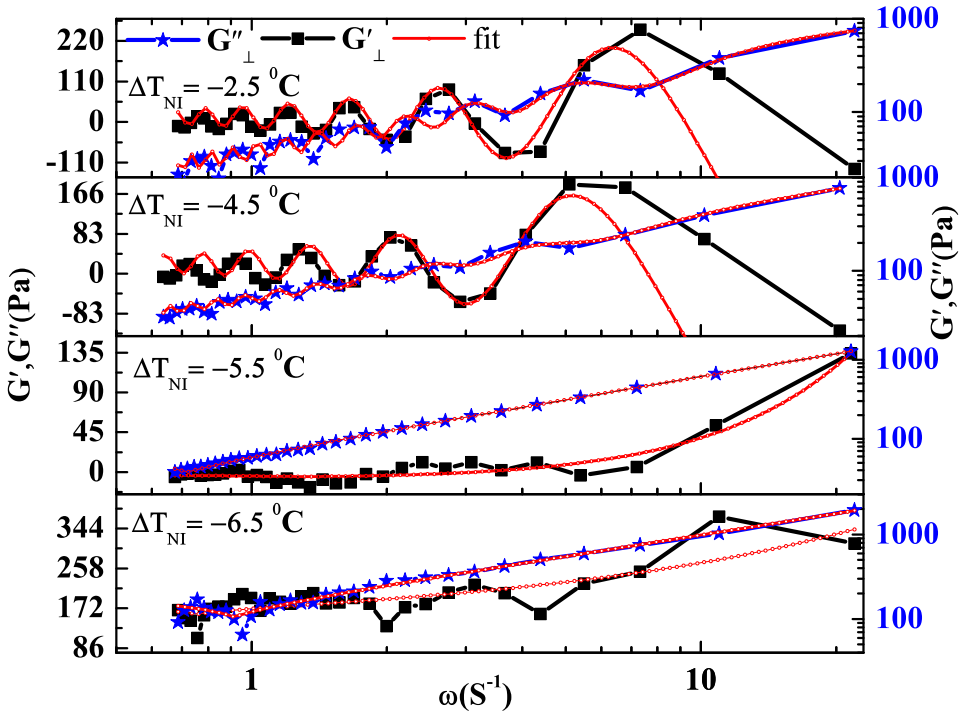

Figure 5.4: In nematic phase of 8CB liquid crystals, perpendicular components of elastic ($G^{'}_{\perp}$) and viscous modulus ($G^{''}_{\perp}$) vs frequency (ω) of different regimes($a_m, a_s, a(b), a_c$). Here, $G^{'}$ is represented by line with solid square(black colour) and $G^{''}$ is represented by line with star(blue colour). Thin line(red colour online) with a small open circle shows fitting.

perpendicular directions to the orienatation of $(\hat{\mathbf{n}})$ are shown with their corresponding fits. From the curve fitting, it represents

$$\begin{aligned} G'(\omega)_{\parallel} &\sim \omega^{1.5} \\ G'(\omega)_{\perp} &\sim \omega^{1.6} \\ G''(\omega)_{\parallel,\perp} &\sim \omega^{0.88} \end{aligned} \tag{5.3}$$

This power law dependence in b' regime clearly represents, how G' values vary with frequency in the pure nematic phase of liquid crystals. So, similar power law dependence also can be expected in 5cb liquid crystals.

According to C.R. Safinya et.al.[6], the orientational state of $(\hat{\mathbf{n}})$ is determined by the interplay between viscous force, elastic and fluctuation torques due to fluctuating smectic clusters acting on it. In shear rheology, the elastic torques gets neglected. As temperature is reduced towards T_{N-Sm-A}, shear flow tends to tilt the smectic cluster layers formed. This changes the layer spacing and gives rise to the restoring force. Here, in microrheology, using single particle tracking technique, elastic or storage modulus and viscous modulus show the effect of tumbling nematic director. Here,the reason for the tumbling effects in 8cb liquid crystals below $a-b$ regime is because of presmectic translations. As the temperature decreases, these smectic layers gets rearranged and hence there exists compression on to the central portion of the liquid crystals. Because of the quasistaic compression on to the liquid crystal layers in the central portion of the sample cell, this could necessarily affect the equilibrium structure in two different ways.

1. The gap between the layers inside the central portion of the sample cell would either be increased or decreased in order to adopt to the variations of the gap size.

2. In order to relax from the elastic stress of the layers, the radius of the dislocation loops would be either be increased or decreased[17].

In simple words, the layers that are close to the wall boundaries, gets rearranged with the changes in temperature. In process, the elastic energy density increases between layers. Hence, In a_m, a_s and $a(b)$ regimes, chiral nematic phase which arises because of tilted smectic C clusters is expected.

In liquid crystals, the average orientation of liquid crystal molecules is determined by the director $(\hat{\mathbf{n}})$. Hence, the effect of collective molecular reorientations on Brownian motion of colloids in nematic liquid crystals is determined by the direction of orientation of $(\hat{\mathbf{n}})$. In 8CB liquid crystals cell, the parallel and perpendicular orientations to $(\hat{\mathbf{n}})$ represent Y(flow) and Z(flow gradient) directions respectively. As the nematic director does precessional motion to Y and Z directions, consequently, the thermal motion of the microsphere gets affected or biased by the precessional motion of the director. Hence, in the amplitude and periodicity of the microrheological properties, amplitude and periodicity of the precesional motion of the director $(\hat{\mathbf{n}})$ is profound. Amplitude and periodicity of $G'(\omega)_{\parallel}$ in figure 5.3 show strong temperature dependence. These characteristics of $G'(\omega)_{\parallel}$ are similar to the apparent viscosity η vs shear strain as in a paper by D.F. Gu et.al.[3]. Amplitude of harmonics increase first from a_m regime to a_s regime and then decreases rapidly in $a(b)$ regime and then again increases in a_c regime more steeply. But, from figure 5.4 amplitude of harmonics of $G'(\omega)_{\perp}$ decreases from a_m regime to $a(b)$ regime and then increases in a_c regime. The periodicity of the harmonics are present in a_m and a_s regimes of both $G'(\omega)_{\parallel}$ and $G'(\omega)_{\perp}$. In a_m regime, as the components of the director show $(n_{y0} > n_{z0})$. Here, $G'(\omega)_{\parallel}$ show anisotropy with $G'(\omega)_{\perp}$ and $G'(\omega)_{\parallel} > G'(\omega)_{\perp}$. This represents, anisotropy in $G'(\omega)_{\parallel}$ and $G'(\omega)_{\perp}$ is clearly a consequence of precessional motion of the director $(\hat{\mathbf{n}})$ being larger in the Y-direction than in the Z-direction. In a_s regime, $G'(\omega)_{\parallel} = G'(\omega)_{\perp}$. This is a consequence of isotropic precession of $(\hat{\mathbf{n}})$ with equal amplitude in both Y and Z-directions $(n_{y0} = n_{z0})$. In $a(b)$ regime, $G'(\omega)_{\parallel} < G'(\omega)_{\perp}$. This is a consequence of anisotropic precession with lesser amplitude in the Y-direction than in the Z-direction $(n_{y0} < n_{z0})$. In a_c regime, both $G'(\omega)_{\parallel}$ and $G'(\omega)_{\perp}$ does show larger values. Here, $G'(\omega)_{\parallel} \gg G'(\omega)_{\perp}$. This is in contrast to the anisotropic precession of $(\hat{\mathbf{n}})$, with very large amplitude in the Z-direction $(n_{y0} << n_{z0})$. This is actually a crossover between values of $G'(\omega)_{\parallel}$ and $G'(\omega)_{\perp}$. Since a_c regime is very close to nematic-smectic transition, smectic layers form temporary clusters. Hence, the elastic energy density among these layers increases. Since, these temporary smectic layers are in the perpendicular direction(Z-axis), the difference in the elastic energy density between the central plane(Y-axis) and temporary smectic clusters in the Z-axis creates restoring elastic force

on the microsphere. This slows down the diffusive motion of the microsphere along the parallel direction and it results in increasing the elastic or storage modulus $G'(\omega)_{\parallel}$. Further, the dependence of elastic modulus $G'(\omega)$ on ω is measured directly by curve fitting.

$$G'(\omega)_{\parallel,\perp} = G_{\circ}(\omega)_{\parallel,\perp} * \omega_{\parallel,\perp} * sin\left(\frac{\gamma_p}{\omega_{\parallel,\perp}}\right) \tag{5.4}$$

The distribution of this $G'(\omega)$ vs ω represents the solution of equation of motion of coupled harmonic oscillator in both Y and Z-directions in a_m and a_s regimes. From the X-ray scattering experiments by C.R. Safinya et.al. [6], they discovered that precessional motin of director $(\hat{\mathbf{n}})$ follows the equation of motion of coupled harmonic oscillators. Hence, the amplitudes of solutions $(G_{\circ}(\omega)_{\parallel,\perp})$ of $G'(\omega)$ could directly represent the amplitude of precessional motion of $(\hat{\mathbf{n}})$. Also, we can conclude that, in these regimes the presence of the pre tilted smectic C clusters, the G' values follow equ. 5.4.

On further lowering the temperature towards smectic A phase of 8CB liquid crystals, the presence of pre smectic A type clusters or layers leads to a different kind of power law dependence of G' with ω. in $a(b)$ regime, $G'(\omega)$ vs ω followed power law dependence.

$$G'(\omega)_{\parallel} = G_{\circ}(\omega)_{\parallel} * \omega_{\parallel}^{0.5} \tag{5.5}$$

and

$$G'(\omega)_{\perp} = G_{\circ}(\omega)_{\perp} * \omega_{\perp}^{1.3} \tag{5.6}$$

Also, in a_c regime,

$$G'(\omega)_{\parallel} = G_{\circ}(\omega)_{\parallel} * \omega_{\parallel}^{1.7} \tag{5.7}$$

$$G'(\omega)_{\perp} = G_{\circ}(\omega)_{\perp} * \omega_{\perp}^{0.6} \tag{5.8}$$

These equations 5.5,5.6,5.7,5.8 show anisotropy in power law dependence of $G'(\omega)$ vs ω in both parallel and perpendicular directions. In $a(b)$ regime, the power law dependence of ω in $G'(\omega)_{\parallel}$ vs ω is similar to the power law dependence of $G'(\omega)_{\perp}$ in a_c regime. The power law dependence of $G'(\omega)_{\perp}$ is similar to power law dependence of $G'(\omega)$ vs ω in b' phase 5.3. This shows how the orientation of director is

tumbling between Y(b-axis) and Z(a-axis)directions. In a_c regime, from equation5.7 represents the precessional motion of the director being large to the Z direction. Also, the effect of pre smectic A type layers on elastic modulus (G') variation with frequency (ω) is observed in $a(b)$ and a_c regimes.

Further, in a_m and a_s regimes, $G''(\omega)$ vs ω in parallel and perpendicular directions fits with

$$G''(\omega) = a * \omega + b * x^n * sin^2\left(\frac{c}{\omega}\right) \tag{5.9}$$

and in $a(b)$ and a_c regimes, $G''(\omega)$ follows power law dependence with ω. In $a(b)$ regime,

$$\begin{aligned} G''_{\parallel} &\simeq \omega^{0.94} \\ G''_{\parallel} &\simeq \omega^{0.95} \end{aligned} \tag{5.10}$$

In a_c regime,

$$\begin{aligned} G''_{\parallel} &\simeq \omega^{0.74} \\ G''_{\parallel} &\simeq \omega^{0.85} \end{aligned} \tag{5.11}$$

Also, we computed the dynamic viscosity (η'') values from G''/ω in both parallel and perpendicular directions to the director $(\hat{\mathbf{n}})$. The characteristics of (η'') are very similar to bulk rheology viscosity values[2]. But, we observed a crossover between $\eta''_{\parallel}$ and $\eta''_{\perp}$. Similar crossover between $\eta_{\parallel}$ and $\eta \perp$ in the micro viscosity values of bent core liquid crystals near N-Sm-A transition were observed in our previous paper[12].

As in figure5.5, a_c regime being near to smectic region, the thermal motion of the microsphere in the parallel directions(Y-direction) is highly restricted by more smectic layer formations. In more details, one can understand this restriction of thermal motion of microsphere. since the cell is rubbed to promote specfic molecular alignment, the larger smectic layer planes in a_c regime are oriented perpendicular to the rubbing direction and are large enough to restrict the thermal motion of microsphere. Hence, the self diffusion of the microsphere in the direction perpendicular to the layer plane is lower than in parallel direction as a result $\eta''_{\parallel}$ can diverge.

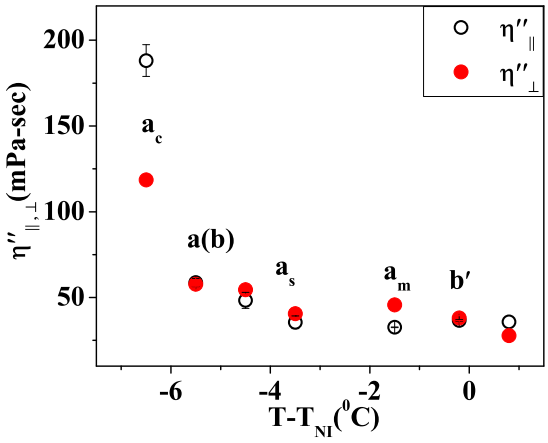

Figure 5.5: Temperature dependent variation of dynamic viscosity($\eta^{''}$). $\eta_{\parallel}$ and $\eta_{\perp}$ are represented with open circles and closed circles(red colour).

5.4 CONCLUSIONS

Instead of following ELP theory, a different approach was followed in addressing the motion of a tumbling nematic director ($\hat{\mathbf{n}}$). By comparing the coupled harmonic oscillator motion with depenendence of $G^{'}$ on ω gave the complete description of ($\hat{\mathbf{n}}$) in different structural regimes of nematic 8CB liquid crystals. All the regimes of 8cb liquid crystals are clearly differentiated by elastic modulus (G') variation with frequency ω. In b' regime, flow in nematic phase of liquid crystals is expected to be similar to 5cb liquid crystals. Here (G') varies with ω as, $G'(\omega) \sim \omega^{1.5}$. In a_m and a_s regimes, with the presence of tilted pre smectic C clusters, the (G') values varies with ω as $G'(\omega)_{\parallel,\perp} = G_{\circ}(\omega)_{\parallel,\perp} * \omega_{\parallel,\perp} * sin\left(\frac{\gamma_p}{\omega_{\parallel,\perp}}\right)$. On further lowering the temperature towards smectic A phase, pre smectic A layers can be expected in $a(b)$ and a_c regimes. In these regimes (G') values varies with ω with a power law dependence. Hence, this micro rheological measurements proved to be a simple method to differentiate different regimes with pure nematic flow behavior, presence of tilted smectic C clusters, smectic A layers of 8cb liquid crystals.

Microrheology in tumbling nematics..

.

BIBLIOGRAPHY

[1] P.G. de Gennes, "The physics of Liquid crystals", 2nd ed., Oxford University Press, Oxford, (1993).

[2] K. Negita, J. Chem. Phys. **105**, 7837 (1996).

[3] D. F. Gu and A. M. Jamieson, J. Rheol., **38(3)**, (1994).

[4] Jahnig, F. and F. Brochard,J. Phys. (Paris) **35**, 301 (1974).

[5] K. Negita, M. Inoue, and S. Kondo, Phys.Rev. E **74**, 051708 (2006).

[6] C. R. Safinya, E. B. Sirota and R. J. Piano, Phys. Rev. Lett. **66**, 15 (1991).

[7] G. Marrucci, Macromolecules, **24**, 4176 (1991).

[8] W. H. Han and A. D. Rey, Journal of Rheology, **39**, 301 (1995).

[9] Balaji Yendeti, G. Thirupathi, Ashok Vudaygiri, and R. Singh, Eur. Phys. J. E, **37**, 70 (2014).

[10] Thomas G. Mason, Rheol. Acta **39**, 371 (2000).

[11] M. Skarabot and I. Musevic, Soft Matter, **6**, 5476, (2010).

[12] S. Dhara, Y. Balaji, J. Ananthaiah, P. Sathyanarayana, V. Ashoka, A. Spadlo, and R. Dabrowski, Phys. Rev. E **87**, R30501 (2013).

[13] Todd M. Squires and Thomas G. Mason, Ann. Rev. Fluid Mech. **42**, 413 (2010)

[14] T. Turiv, I. Lazo, A. Brodin, B. I. Lev, V. Reiffenrath,V. G. Nazarenko, O. D. Lavrentovich, Science, **342**, 1351 (2013).

[15] I.Y. Wong, M. L. Gardel, D. R. Reichman, Eric R. Weeks, M.T. Valentine, A. R. Bausch, and D. A. Weitz, Phys.Rev.Lett., **92**, 17 (2004).

[16] Denis Wirtz, Annu. Rev. Biophys. **38**, 301 (2009)

[17] P.C. Martin, O. Parodi, P.S. Pershan, Phys. Rev.A., **6**, 6 (1972).

6

MICRORHEOLOGICAL PROPERTIES OF BENT-CORE NEMATIC LIQUID CRYSTALS

6.1 INTRODUCTION

In microrheology experiments, thermal motion of a colloidal particle of micrometer size probes the local environment of the complex fluids. Microscopic structural properties of the complex fluids may change locally with the applied stress by this colloidal particle. The thermal motion of the colloidal particle, brings a difference in the elastic energy densities of the material locally. If the colloidal particle motion is on to the left side, with the applied stress, elastic energy density increases on this side. Hence, the elastic behavior of the material becomes rate dependent. In these experiments, the fraction of energy induced by the deformation imposed on the material are represented by elastic modulus (G') and viscous modulus (G''). Except few [1, 2], microrheological experiments in thermotropic liquid crystals are rare.

A variety of different phases have been found with increasingly complex molecular structures ever since the liquid crystals discovery in 1880s. Nearly 45 years ago, Freiser[3], has described theoretically(using mean field approximation), that, in asymmetric molecules, a first order transition from the isotropic to uniaxial state followed, at lower temperatures by a second order transition to a biaxial state. Since then, there has been much attention in this topic, because of static and dynamic properties and with fast switching applications. The molecular axes are oriented along the director in the uniaxial nematic (N_u) phase. In the biaxial nematic (N_b) phase, an additional orientational order exists along a second director. In case of bent core liquid crystals, space symmetry and order parameter considerations have characterized several phases[4],[5]. The phase diagram of bent-core molecules exhibit, isotropic (I), uniaxial nematic (N_u), biaxial nematic (N_b), the orientationally ordered but optically isotropic tetrahedratic (T), Tetra hedratic nematic (N_T) phase is neither uniaxial nor biaxial, but, exhibits fourfold improper rotation in variance consisting of a

rotation through $(\pi/2)$ about Z-axis followed by an reflection and chiral tetrahedratic nematic (N_T^*) phase, exhibits periodic spatial modulations of the direction of molecular alignment. The transitions from the phases (N_b), (T) and the (N_T) to the (N_T^*) phase are with D_{2d} symmetry and are of second order transitions.

In general, nematic (N) liquid crystals are uniaxial. These uniaxial liquid crystal molecules, although they are not cylindrically symmetric, freely rotate about the long molecular axes. Whereas, in case of bent core liquid crystals (BLC) the shape of BLC are compared with a bow, and the molecule's overall long axis with the string (wing span), and the apex of the core defines the direction of the "bend" with respect to the direction of the arrow. Unlike the orientation of the conventional (N_u) phase with perfect symmetry cancellation, in the (N_b) phase, there is spontaneous symmetry breaking of the continuous rotational symmetry about the nematic director $(\hat{\mathbf{n}})$. This is because of mutual tendency of banana-shaped molecules to induce a local bend director with a negative bend elastic constant [6]. This kinked geometry of the molecules strongly frustrates the disorder and hence it is uncommon to find a purely orienational order in bent core nematic liquid crystals. Hence, it shows many uncommon physical properties, such as, biaxial nematic phase [7], flexoelectric [8], sign inversion of elastic anisotropy [9], larger shear and rotational viscosities [10]. The rotational viscosity γ_1 measured is ten times larger than for calamitic compounds and observed this is primarily due to the shpae of the molecule. However, a home built nanoliter rheometer by Bailey et.al.[2] to measure shear dependent viscosities. They reported Newtonian behavior in the lower shear rate range $(\dot{\gamma} \leq 2000 s^{-1})$ and non-Newtonian behavior at higher shear rates. Further, non-Newtonian flow in the optically isotropic liquid phase was observed. This behavior was attributed to the existence of nanostructured, fluctuating clusters composed of a few smectic like layers. Dynamic light scattering (DLS) measurements by D.Wiant et.al., [11] have observed the same phenomenon in the optically isotropic phase. To understand these smectic fluctuations, recent measurements of passive visocosities through out the nematic phase in A131 bent-core liquid crystals, have revealed strong temperature dependence of passive viscosities than bulk viscosities [12]. Also, the effect of presmectic fluctuations are observed much higher than the N-Sm-C transition temperature than commonly seen in Calamitic liq-

uid crystals. In chapter 5, measurements of microrheological (storage (G') and viscous modulus (G'')) properties of 8CB liquid crystals have found the variation in storage modulus G' with the tumbling nematic director ($\hat{\mathbf{n}}$). It was observed that the values of elastic modulus G' varies from negative to positive values representing the tumbling behavior of ($\hat{\mathbf{n}}$). These negative values of G' are the consequences of the non-Newtonian flow behavior. Further, a simple approach has been followed by comparing with the dissipation properties of coupled harmonic oscillator to describe the elastic modulus during the tumbling motion of the nematic director.

There had been an assumption that is, describing the discrimination between orientational director fluctuations and tumbling orientations could be very difficult due to the partial overlapping between the characteristic times typical of these motions. Here we present the microrheological properties of bent-core liquid crystals of single particle tracking experiment, this technique differentiates properties of bent-core liquid crystals between tumbling motion and orientational director fluctuations. The advantage of single particle tracking experiments to give directional dependent results is helpful to differentiate these characteristics. Symmetry properties of bent core liquid crystals are verified with their physical rigidity nature.

6.2 THE EXPERIMENT

Experimental instrumentation is very similar to those mentioned in the previous chapter 2. After recording the Brownian motion, the calculation for mean square displacement(MSD) and G', G'' was also described in the same chapter.

6.3 RESULTS AND DISCUSSION

The thermal motion of the colloidal particle is measured in two dimensions along the parallel direction(rubbing direction of the alignment layers)(($\mathbf{n} \parallel$)) and perpendicular direction ($\mathbf{n} \perp$) to the nematic director ($\hat{\mathbf{n}}$). From the measured thermal motion of the colloidal particle, the mean square displacements (MSDs) are computed. Elastic mod-

ulus (G') and viscous modulus (G'') of a material can be computed along (($\mathbf{n} \parallel$)) and ($\mathbf{n} \perp$) [13, 14, 15, 16, 17]. Here, we present the (G') and (G'') of bent core liquid crystals through out its nematic and isotropic phases. A fraction of energy is lost by the viscous dissipation in case of loss modulus(G''), and, is stored elastically in case of storage modulus(G'). G' and G'' were computed using the equations given in Ref.[14], given below, as a function of rate of deformation ω. By expanding the equation of motion of Mean square displacement around $t = 1/\omega$, the translational parameter β is defined as [14]

$$\beta(\omega) = \left. \frac{\langle d \ln \Delta r^2(t) \rangle}{d \ln t} \right|_{t=\frac{1}{\omega}} \tag{6.1}$$

and the Fourier transform of this MSD equation would lead to give G'(ω) and G''(ω) as

$$\begin{aligned} G'(\omega) &= |G^*(\omega)| \cos\left(\frac{\pi\beta(\omega)}{2}\right) \\ G''(\omega) &= |G^*(\omega)| \sin\left(\frac{\pi\beta(\omega)}{2}\right) \end{aligned} \tag{6.2}$$

Where $|G^*(\omega)| = K_B T / \pi a \langle \Delta r^2(\frac{1}{\omega}) \rangle \Gamma[1 + \beta(\omega)]$, and 'a' the radius of the probing bead. The physical properties of complex fluids can be characterized by the change in slope of elastic modulus (G') with respect to ω.

$$G'(\omega) \simeq a * \omega^x \tag{6.3}$$

Distinct situations of physical rigidity can be identified :

- If the value of $'a'$ is +ve and larger, and if values of $G'(\omega)$ does not vary with ω, this behavior corresponds to solid behavior.
- x being +ve, and is greater than 1, represents viscoelastic liquid behavior.
- If the value of $'a'$ is +ve and smaller, and if values of $G'(\omega)$ does not vary with ω, this is viscoelastic solid behavior.
- If x being +ve and if it is less than 1, represents viscoelastic solid behavior.

- In addition we observed an unusual situation of both a and x being negative. This results in G' being negative. Which is an anomalous behavior and generally not observed in bulk rheology measurements. This case occurs with the dissipation of energy during the deformation induced by the material on to the colloidal particle.

The ultimate importance of knowing microrheological properties is in understanding the formation of microstrucres in complexfluids. The *insitu* probing of the colloidal particle describes the real space microstructural formations. Since, bent-core liquid crystals have many applications like fast switching applications, for electro optic devices [18], it is of priority to the scientific community to understand the physical properties with in various structural transformations of the nematic phase of bent core liquid crystals. Theoretical studies [3], space symmetry predictions [4, 5] and experimental studies using X-ray scattering [6], Dynamic light scattering [11] NMR spectroscopy [19, 20], Raman spectroscopy [21] have confirmed the existence of several exotic phases such as

(a) An orientationally ordered, yet optically isotropic phase.

(b) Both uniaxial and biaxial phases.

(c) A spontaneously chiral nematic phase.

(d) Macroscopically polar nematic phase.

Microrheological properties in the nematic phase of the bent core liquid crystals would characterize the physical properties of bent core liquid crystals. Here, we present the microrheological properties in the isotropic and nematic phase of A131 bent-core liquid crystals. The phase transiton temperatures in our measurements of bent core liquid crystals (cooling): Isotropic (I) at 178.5 ◦ C to Nematic (N) at 120 ◦ C to Sm-C. Close to N-Sm-C phase, the Brownian motion of the colloidal particle are highly restricted. This is because, the smectic layer planes in the temporarily fluctuating clusters are oriented perpendicular to the rubbing direction of the planar alignment. In this case, the fluctuating clusters are large enough and the diffusion of the microparticle reduces. To avoid microscopy resolution issues in these measurements, Brownian motion data close to nematic-smectic phase is not considered.

6.3.1 *Isotropic phase*

Three previous important experimental results [2], [11], [19] and their hypotheses to explain the unusual behavior in isotropic phase of bent-core liquid crystals(BCLCs) :

(1) A peculiar behavior in the isotropic phase of BCLCs was first observed in the NMR measurements [19]. This unusual behavior claimed to have a homogeneous nature, thus indicating the presence of reorientational motions much slower than in conventional isotoropic liquid crystalline phases. Two hypotheses were proposed to explain the slow motions in the isotropic phase of BCLCs. (a) hindering of molecular reorientations due to the bent shape of molecules and, in particular to the presence of local and temporary entanglements. (b) restricted motions due to the presence of local organized clusters, where BCLCs are packed and as a consequence, limited in their molecular motions.

(2) In DLS correlation function measurements by D.Wiant et.al., [11] have observed contributions from coexisting order parameter and nematic (director) fluctuations in the isotropic phase of bent core liquid crystals. This was attributed to nanostructural organization of the isotropic phase, which is based on molecular clusters or some short range structural association of the bent core molecules. These clusters have larger surface area and more isotropic (spherical) in shape which experience less change in excluded volume as a consequence of nematic orientational order.

(3) In nanolitre rheometer experiments [2], shear thinning was observed in the isotropic phase of BCLCs. It was claimed that, this could be due to the kinked shape of the molecules, which tend to lock them into layered (or smectic-like) clusters which are known as "cybotactic groups" and these are of few nano meters in size. These bent-core nematics preserve these cybotactic smectic clusters and their nature is like small "squishy" spheres even in the isotropic phase. Even though they are pure compounds, they have similar rheology to dilute particles suspensions. Hence, shear thinning behavior was observed.

The major advantage with microrheological experiments is, direction dependent measurements. Our microrheological experiment results, in the isotropic phase ($\Delta T_{N-I} = +1.5^{\circ}C$), at 180°C, of bent-core liquid crystals, are in concurrence with the above three experimental

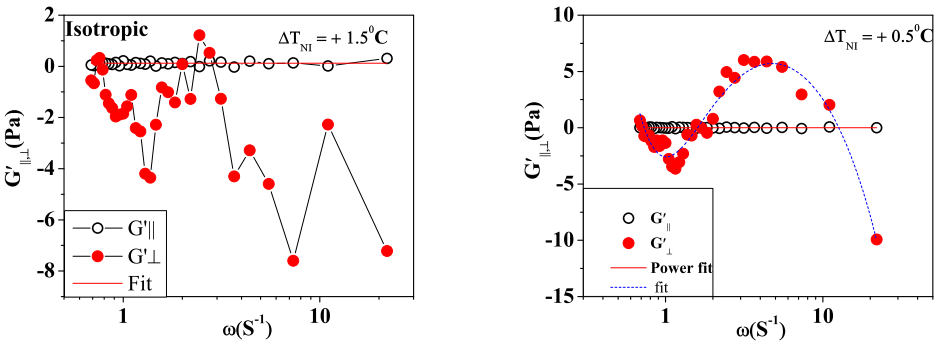

Figure 6.1: Elastic modulus (G') in the parallel and perpendicular direction to the director $(\hat{\mathbf{n}})$ at $(\Delta T_{N-I} = 1.5°C, \Delta T_{N-I} = 0.5°C)$. Scale is linear on Y-axis and logarithmic on X-axis. parallel and perpendicular components are represented with open and closed circles respectively.

results and their hypotheses. The values of elastic modulus (G') in both parallel and perpendicular directions are measured. As in fig.6.1, the value of $G'_{\|}$ is constant with respect to frequency. Whereas, $G' \perp$ has values fluctuating from positive to negative values. This shows a clear anisotropic nature in the known optically isotropic regime. From equation 6.3, $a \simeq 0$, represents the elastic modulus (G') similar to suspension of squishy sphere's elastic modulus. The values of $(G') \sim 0$ represents visco elastic solid behavior and these values matches with the elastic modulus (G') of suspension of squishy spheres[22]. In fig. 6.1, mean value of $G'_{\|} = 0.11$ Pa represents that the probing colloidal sphere is in the environment surrounded by particle clusters with rigidity close to polystyrene particles suspensions. Also, the colloidal probe (silica sphere) is in near contact with these particle clusters. Even in nanoliter rheometer experiments as described by C.Bailey [2] et.al., these particle clusters are compared with "squishy" spheres. Considering these particulate suspensions as the cybotactic groups is an interesting phenomenon of their results. Results of $G' \perp$ in fig. 6.1 is in concurrence with this behavior. In particular, these cybotactic groups show tilted orientation because of the kink shape of the bent core molecules. Hence, the diffusion of the colloidal particle in the $(\mathbf{n} \perp)$ shows change in the values of elastic modulus which entails the possibility for the fluctuations of the orientation of molecules. Also,

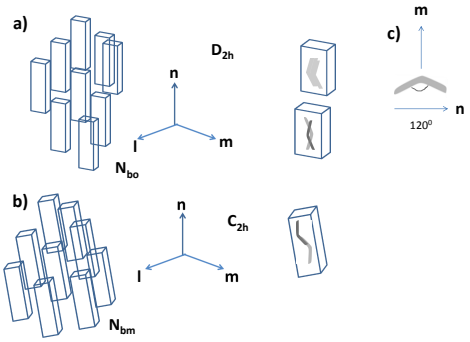

Figure 6.2: Fig. (a) represents orthorhombic biaxial nematic phase with (D_{2h}) symmetry of bent core molecules. Fig (b) represents monoclinic biaxial nematic phase with (C_{2h}) symmetry. Fig.(c) represents "bow" shape of the bent core liquid crystal molecules and the corresponding two orientational axes of these molecules.

at $\Delta T_{N-I} = 0.5^{\circ}C$, the mean value of $G'_{\parallel} \simeq 0$ and $G'_{\perp}$ has fluctuations. Which represents the similar behavior through out the isotropic phase. Similar arguments to understand the tumbling nematic director in 8CB liquid crystals is made in our previous chapter 4. This shows the existence of memory effects in the isotropic phase of BCLCs. Which is a very rare phenomenon that occurs in complex fluids with isotropic nature. This phenomenon further need to be investigated in future. Further, in this chapter, we understand the presence of different exotic phases in the nematic phase of BCLCs by analyzing the variation of elastic modulus $(G^{'})$ with frequency (ω) in a similar way as was done in chapter 5.

6.3.2 *Nematic phase*

In the uniaxial(N_u) nematic phases, the molecular axes are oriented along the director $(\hat{\mathbf{n}})$, but, in the biaxial (N_b) phases, there exists an additional director $(\hat{\mathbf{m}})$, which is perpendicular to $(\hat{\mathbf{n}})$. That means, in the N_u phase, the molecules are rotationally disordered around the long axis whereas in the N_b phase, this rotation is restricted. Which leads to a time averaged board-like shape of the molecules. At high temperatures, nematic phases have relatively small clusters of

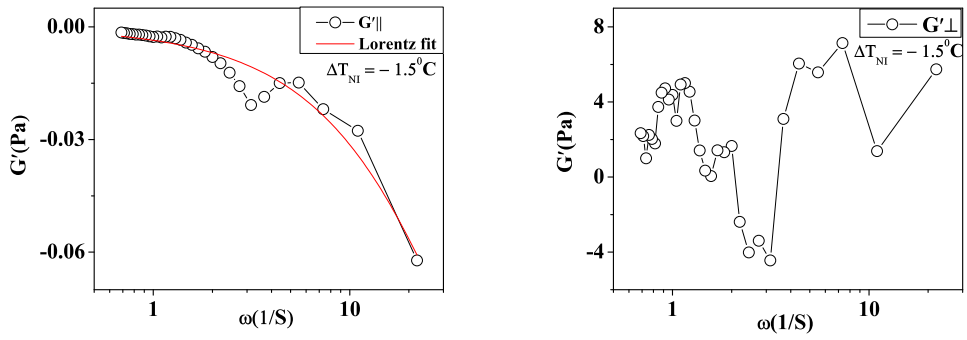

Figure 6.3: Elastic modulus (G') in the parallel and perpendicular direction to the director ($\hat{\mathbf{n}}$) at ($\Delta T_{N-I} = -1.5°C$). Scale is linear on Y-axis and logarithamic on X-axis

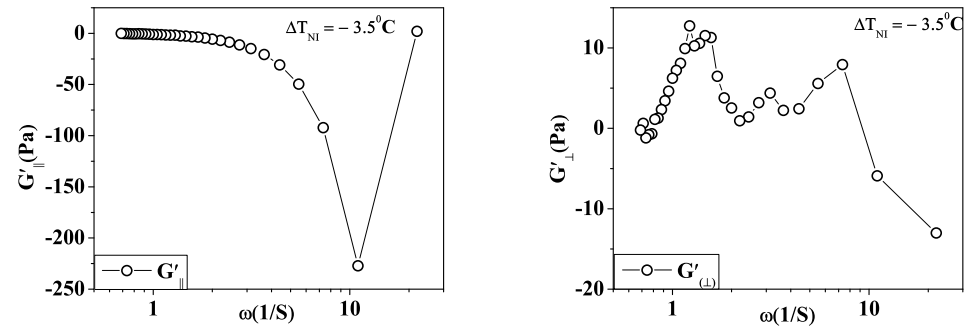

Figure 6.4: Elastic modulus (G') in the parallel and perpendicular directions to the director ($\hat{\mathbf{n}}$) at ($\Delta T_{N-I} = -3.5°C$). Scale is linear on Y-axis and logarithamic on X-axis

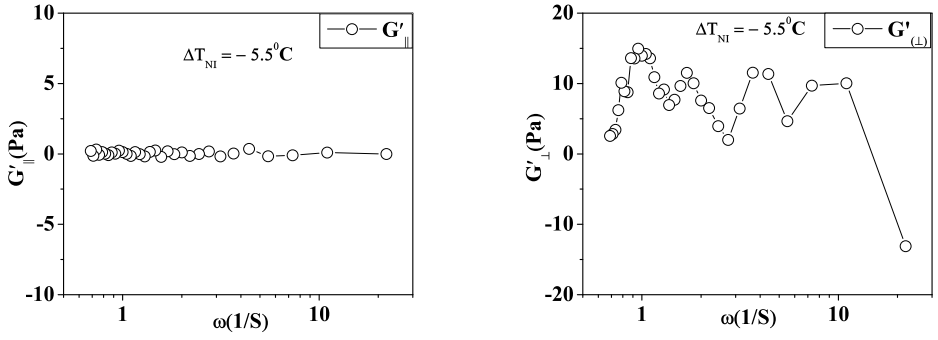

Figure 6.5: Elastic modulus (G') in the parallel and perpendicular directions to the director $(\hat{\mathbf{n}})$ at $(\Delta T_{N-I} = -5.5°C)$. Scale is linear on Y-axis and logarithamic on X-axis

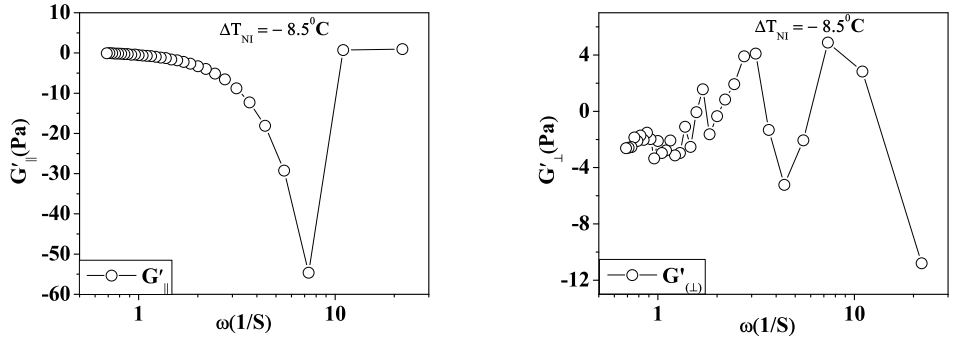

Figure 6.6: Elastic modulus (G') in the parallel and perependicular directions to the director $(\hat{\mathbf{n}})$ at $(\Delta T_{N-I} = -8.5°C)$. Scale is linear on Y-axis and logarithamic on X-axis

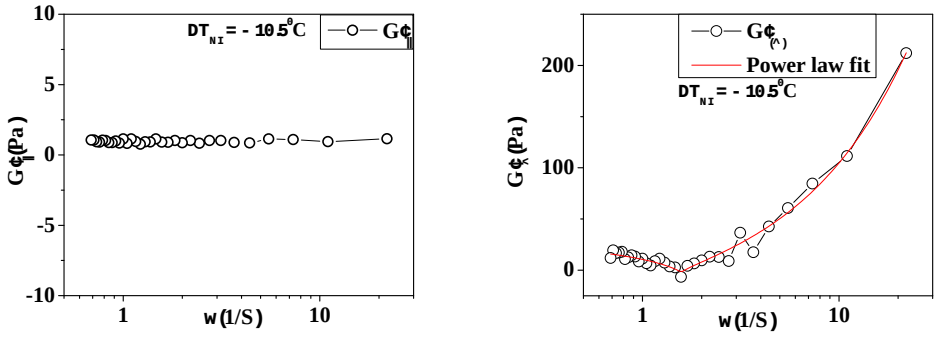

Figure 6.7: Elastic modulus (G') in the parallel and perpendicular directions to the director $(\hat{\mathbf{n}})$ at $(\Delta T_{N-I} = -10.5°C)$. Scale is linear on Y-axis and logarithmic on X-axis

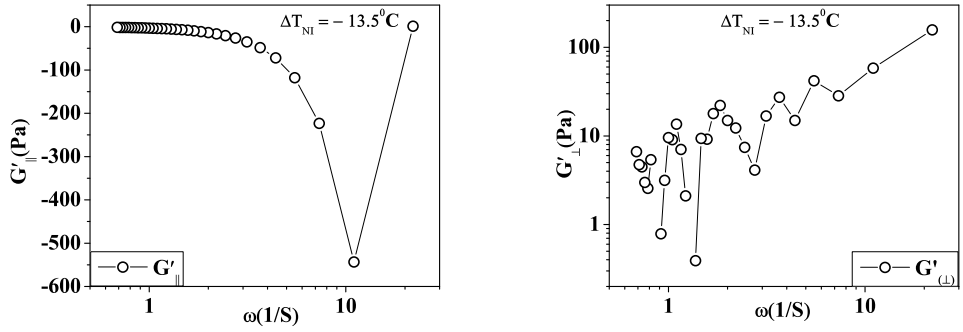

Figure 6.8: Elastic modulus (G') in the parallel direction to the director $(\hat{\mathbf{n}})$ at $(\Delta T_{N-I} = -13.5°C)$. Scale is linear on Y-axis and logarithamic on X-axis

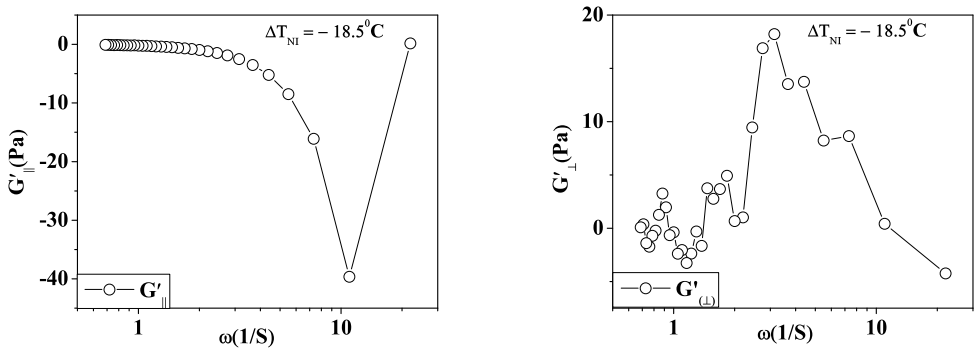

Figure 6.9: Elastic modulus (G') in the parallel and perpendicular directions to the director $(\hat{\mathbf{n}})$ at $(\Delta T_{N-I} = -18.5°C)$. Scale is linear on Y-axis and logarithamic on X-axis

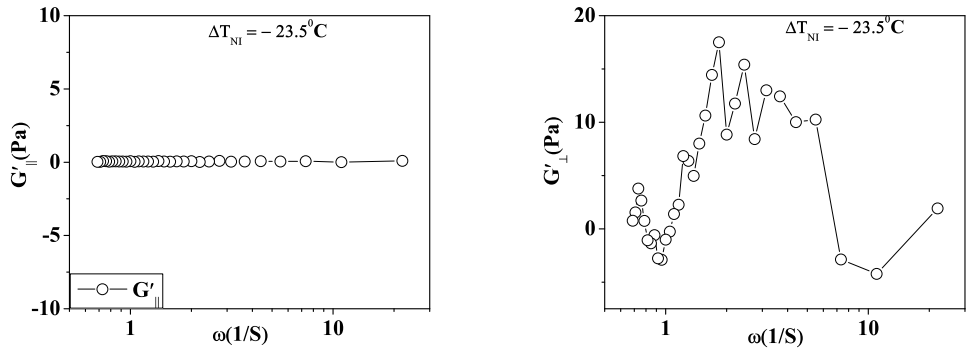

Figure 6.10: Elastic modulus (G') in the parallel and perpendicular directions to the director $(\hat{\mathbf{n}})$ at $(\Delta T_{N-I} = -23.5°C)$. Scale is linear on Y-axis and logarithamic on X-axis

nano particle size, and these clusters grow in size with decreaseing temperature. As the size of these clusters increases, these clusters become the dominating entities, which align parallel to each other and parallel to the surfaces. After increasing to a particular size, the clusters do prefer an orientation with the layer planes parallel to the substrate surface.

In nematic phase of bent-core liquid crystals, bent core molecules aggregate to form clusters. Cluster formation is mainly caused by the seggregation of the alkyl chains and supported by the kink shape of the molecules. In uniaxial state, there exists two different phases N_u and $N_{u'}$ with respect to the response of these clusters to transverse aligning stimulus. In the N_u phase, the stimulus addresses individual molecules and hence shows marginal effects on biaxial ordering. This phase is considered to be with nearest neighbor correlations between molecules and cybotactic nematic phase without proper local biaxiality in the Sm A clusters (N_{uCybA}), or with SmC like clusters with weak internal biaxiality (N_{uCybC}). Whereas, $N_{u'}$ is an intermediate nematic phase between uniaxial and biaxial. In this phase molecules are intimately correlated. The relative ordering of these molecules defines a set of directors locally. On lowering the temperature, these cybotactic clusters can undergo thermotropic transition to a spontaneously biaxial state (N_b). Biaxial clusters in the nematic phase of bent core liquid crystals are identified as "cybotactic clusters" or "Cybotactic nematics". The primary directors of these cybotactic clusters spontaneously orient along a particular direction $\mathbf{n}$. Their transverse directors are randomly distributed to form uniaxial state $(N_{u'})$ [23]. In some nematic liquid crystals, certain pretransitional effects of a smectic phases or some stable structural features through out the temperature range of nematic phase are observed. These cybotactic nematics are two types.

1. Cybotactic nematic phases of Sm A-type with Sm A like structures in the clusters (N_{cybA}).

2. Skewed cybotactic nematic phase composed of Sm C like clusters (N_{cybC}).

The clusters formed of the Smecitc A type are uniaxial. Freezing of rotation of the molecules along the long axis in smectic A phase leads to biaxial SmA_b. This restricted rotation of molecules in Sm A clusters

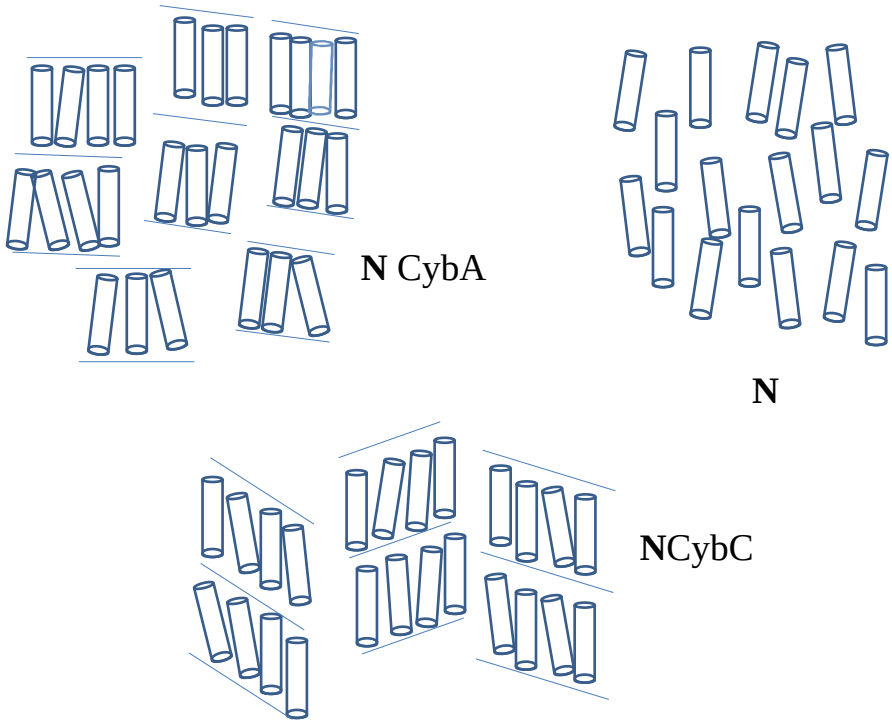

Figure 6.11: cybotactic clusters

could lead to local biaxiality $(N_{u'cybAb})$. In N_{cybC} phases, the tilt in Sm C type clusters and intrinsic hindrance of rotation of molecules along their long axes manifests biaxiality. Biaxiality that arises because of the tilt of the Smectic clusters will have long range correlation. This phase is considered as "improper" biaxiality. However, the rotation around the long axis could also be hindered in the SmC clusters. In this way, by combining the biaxiality due to tilt and biaxiality originating from the hindered rotation around the long axis leads to "double biaxiality" or "proper local biaxiality" $(N_{u'cybCb})$. In this notation, tilt in smectic C clusters is prescribed by 'C' and hindered rotation by 'b'.

In the cybotactic clusters, a rigid layer formation of molecular structures can be expected. In the direction perpendicular to primary director, because of the layer like formations by the cybotactic smectic clusters(CLS), an increase in their volume constraints the motion of the colloidal particle in the perpendicular direction. This leads to tumbling reorientations of CBLCs. Dynamic light scattering (DLS) experiments have interpreted the presence of slow collective motions, such as order director fluctuations in the vicinity of N-I transitions [24]. The hydrodynamics of the colloidal sphere is in more analogy with the motion of a colloidal particle in a confined cylindrical volume [25], [26]. Further, $G'_{\perp}$ fits with the behavior of equation for energy dissipation of a coupled harmonic oscillator. Just below nematic - isotropic transition temperatures have relatively small clusters and these CLS grow in size with the decreasing temperature. Hence, with the temperature dependence, there exists a complex relation between molecular structural features, cluster size and tilt angle [27]. This complex relation determines the dissipative properties (elastic or storage modulus, viscous or loss modulus). The uni axial and uni axial - bi axial transformations in the nematic phase of bent core mesogens was well addressed[19], [20], [28] in NMR diffusometry experiments and other literature [29] [30]. The DLS measurements by Jakli et.al., [24] had first evidenced the director fluctuations being 100 times slower than observed in the typical nematics based on cylindrical molecules. This behavior was attributed to cybotactic clusters. A theoretical approach to analyze NMR relaxation times by Domenici et.al.,[28] have concluded (a)fast internal reorientations affecting the lateral wings of the bent core Liquid crystal (BLC) molecules. (b) very slow dynamics of out of plane motions of the molecules. They also suggest that, collective motions in BLC are much

slower than that in calamitic BLCs. These phenomena were attributed to restricted molecular motions because of the aggregation and packing properties of bent-shape liquid crystals. Verena G. et.al.,[30] have suggested that, the unusual fluctuating and dynamically changing fluid behavior is due to a combination of calamitic molecular shape with a considerable transverse dipole leads to unusual strength and combination of molecular interactions. The description of nematic phases of bent core mesogens by Keith et.al., [27] had given a clear description of stepwise transition from cybotactic nematic phases to different types of non-polar phases. Also an intermediate state with the cybotactic clusters composed of elongated but not fused bent-core liquid crystal molecules was interpreted.

In microrheology, slow dynamics accompanied by a large decrease in the single particle mobility is profound in disordered many-body systems. A mechanical coupling between the particle and structures generated in the above mentioned various phases, is measured as an oscillatory elastic response of the particle and thereby, decomposition of this transmitted stress into elastic and viscous components. In case of bent-core liquid crystals, in this experiments, the long axis(wing span direction of the liquid crystal molecules) of the director of cybotactic clusters is along the rubbing direction of the sample cell. At temperatures from 177° C ($\Delta T_{N-I} = -1.5°C$) to 155° C ($\Delta T_{N-I} = -23.5°C$), 1)'in plane' rotation 2)'restricted' rotation 3)'flip' rotations takes place with thermotropic transitions. The centre of mass of the molecules in cybotactic clusters may not lie in the transverse plane of the whole molecule and small tilts are expected to occur. In these 'in plane' rotations, cybotactic clusters rotates, with the 'bow axis' fixed. In case of restricted rotation, clusters will be at rest, and, the average wingspan direction of the clusters faces one another. So, the elastic energy density among the layers on left side is same as on the right side. Hence the net elastic energy difference will be zero. In the other flip rotations case, these clusters completely rotates or flips from left handedness to right handedness. From high temperatures to lower temperatures, the growth in the size of clusters is expected, hence, the order parameter increases. These clusters in the N_u phase will have small 'in plane' rotations. During these small reorientations, dissipation of elastic energy will be continuous and is also reversible. which is uniaxiality behavior. So, the value of G' decreases with small 'in plane' rotations

(elastic energy decreases with motion). But, at some temperatures, in the $N_{u'}$ phase, additional discontinuous and irreversible changes also occurs. Though this is not a phase transition, but is a realignment. As a consequence of the growing cybotactic clusters with decreasing temperature. The total 'in plane' reorientation (flip) of the molecule or clusters will lead to these discontinuous process. That means, with the bow axis or transverse axis fixed, the whole cluster reorients to its opposite direction. After, reorientation, the wing span axis of this reoriented cluster and another cluster beside this face each other. So, locally, the net elastic energy density becomes zero. In this total process, discontinuity arises because of the reorientation of the cluster. So, discontinuity is expected in the values of G'. In the direction perpendicular to the rubbing direction $\mathbf{n}\perp$, since the cybotactic clusters lie in the plane parallel to the liquid crystal molecule aligning direction $\mathbf{n}\parallel$, the fluid or motion of the colloidal (probing) particle in the direction perpendicular to the cybotactic clusters gets confined and hence the motion of the colloidal particle in this direction gets confined with in the gap of the growing clusters and their re orientations. This occurs in $(N_{u'cybCb})$ phase showing the presence of restricted orientation and tilted smectic clusters. The hydrodynamics of confined colloidal motion is well understood concept [25]. Infact, in calamitic liquid crystals like 8CB liquid crystals, the passive microrheological properties are well studied [4]. As the temperature decreases, these cybotactic clusters gets rearranged and hence there exists compression on to the central portion of the liquid crystals. This could necessarily affect the equilibrium structure in two different ways. $a)$ The gap between the layers inside the central portion of the sample cell would either be increased or decreased in order to adopt to the variations of the gap size. $b)$ In order to relax from the elastic stress of the layers, the radius of the dislocation loops would be either be increased or decreased[11]. The structures formed in this process vary dynamically. This similar variation in bent core liquid crystal structures can be identified with G' varying similar to G' in tumbling nematic phase. At certain other temperatures, restricted rotational motion but with smectic A clusters can be identified as G' being parallel in the restricted rotation plane and with a variation in frequency similar to a_c regime in 8cb liquid crystals as mentioned in chapter 5. In bent core liquid crystals, this

occurs in $(N_{u'cybAb})$ phase. In our measurements, we observed three fundamental transitions: $N_u \rightarrow N_{u'}$, $N_{u'} \rightarrow N_b$ and $N_u \rightarrow N_b$.

At high temperatures in the nematic phase of bent core liquid crystals, with rotationally disordered biaxial clusters, the rotational disorder of the clusters around $\mathbf{n}\|$ leads to macroscopic uniaxiality. Restricted rotation around $\mathbf{n}\|$, but without polar order, leads to simplest type of biaxial nematic phase (N_b) with orthorhombic symmetry. From the analysis mentioned above, we realized that at just below NI transition temperature 177° C or ($\Delta T_{N-I} = -1.5°C$), G' values in $\mathbf{n}\|$ direction varies continuously with frequency with small 'in plane' rotations and is with small G' values. In the perpendicular direction, weak internal biaxiality with smectic C clusters representing the uniaxiality (N_{uCybC}) phase. An important point to mentioned here is, G' values in $\mathbf{n}\|$ direction are constant upto certain frequency and then slowly decreases to negative values. In shear rheology negative values of G' is meaning less. Because, in shear rheology, external force acts on the material and whence deformation in the material under shear is expected. But, in microrheology, instead of deformation of the material by the probing colloidal sphere, rotational force by different types of rotation of the molecules or clusters of the bent core liquid crystals along with surface anchoring effects acts upon the motion of the colloidal particle. Hence, negative values of G' can be expected. These results are observed in repeated experimental measurements. Further, this argument needs to be supported by theoretical investigation on these negative values of G'.

6.3.3 *Proof of "spontaneous" biaxiality*

The tilted organization in the cybotactic clusters ($N_{u'cybC}$ phases) could only lead to N_b phases with C_{2h} symmetry (N_{bm} phases). To be precise, "proper" biaxiality can be proved in the presence of a reference system provided by the organization of molecules in SmC clusters with frozen rotation around $\mathbf{n}\|$. Therefore, the proof of spontaneous biaxiality is in

1. In the $\mathbf{n}\|$ direction, there should be significant restricted rotation of clusters.
2. In the $\mathbf{n}\perp$ direction, organization of molecules in SmC clusters.

At 173° C ($\Delta T_{N-I} = -5.5°C$) and at $\Delta T_{N-I} = -5.5°C$ consequences of restricted rotation around $\mathbf{n}\|$ can be observed representing biaxiality with monoclinc symmetry. In this case, since the cybotactic clusters have their wingspan direction facing each other, values of $G' \|$ is constant with respect to frequency. The values of $G' \|$ from these graphs are 0.03 Pa. This represents the visco elastic solid properties of these clusters in the parallel direction. In the perpendicular direction, thermal motion of BCLCs is under rigid confinement. This results in smectic C clusters with tilt or chiral nematic phase is similar to tumbling motion observed in the nematic phase of calamitic 8CB liquid crystals. That means, thermal motion of the colloidal particle in BCLCs with monoclinic symmetry shows "proper biaxiality" in $(N_{u'CybCb})$ phase. Clearly in the perpendicular direction, the resultant chirality behavior of G' observed is similar to G' in the a_m phase of 8CB liquid crystals.

Clearly, At 168° C ($\Delta T_{N-I} = -10.5°C$) the $G' \|$ values are constant with frequency. This represents, significantly restricted rotation along $\mathbf{n}\|$ direction. Which shows the viscoelastic solid behavior. But, the amplitude of G' is positive. Mean value of G' is 0.97 Pascals. But, is close to the rigidity values of 'polystyrene' behavior [22]. In the perpendicular direction to the director, the power law dependence of G' on ω shows,

$$G'(\omega) \simeq \omega^{3/4} \tag{6.4}$$

which is clearly a significance of presence of smectic A clusters. To confirm the presence of Sm A clusters, our previous microrheology results of 8CB liquid crystals becomes useful. There is a clear difference in G' vs ω values of b' regime and the $a(b)$, a_c regimes. b' regime is just below the NI transition temperature of 8CB liquid crystals, $a(b)$ and a_c regimes are close to Sm A phase. In b' regime, $G'(\omega) \simeq \omega^{3/2}$ and in $a(b)$ and a_c regimes in the directions in which Sm A layers are expected, $G'(\omega) \simeq \omega^{3/4}$. Hence, at this temperature, for this graphs, presence of SmA clusters in the perpendicular direction leads to a conclusion of $(N_{u'CybAb})$ phase.

Whereas, at other temperatures $\Delta T_{N-I} = -3.5°C$, $\Delta T_{N-I} = -8.5°C$, $\Delta T_{N-I} = -13.5°C$, $\Delta T_{N-I} = -18.5°C$ the values of G' represents intermediate phase between uniaxial and biaxial $(N_{u'})$phase. Clearly,

there is a discontinuity in the values of G' with total flip bringing opposite handedness locally, representing uniaxial-biaxiality behavior. If a cybotactic cluster flips completely, it forms to have opposite handedness with the neighboring clusters. The rotationally disordered biaxial clusters with orthorhombic symmetry will have these flip rotations. This behavior is mirrored in G', which is zero till a certain frequency, after which it continuously decreases, indicating dissipation of elastic energy. At much higher frequency, there is a complete flip or rotation of clusters, which is indicated by a discontinuity of G'. From the above figures, it is clear that, the small 'in plane' re orientations (the angle of 'in plane' orientations is small) show reduction in the value of elastic modulus at the same frequency. But, their amplitude of dissipation does change with temperature. This can be obvious, because, as the cybotactic clusters size increases, more energy gets dissipated during this small reorientation process. Whereas in the total flip re orientations, this reorientation frequency is changing with increase in amplitude of dissipation of the elastic or storage modulus, correspondingly there is decrease in the frequency of reorientations. In the case of total flip 'in plane' reorientations in $G' \parallel$, the tumbling behavior is more dominant in $G' \perp$. Because, this flip orientation leads to more confinement of the fluid in the perpendicular direction. The curves in $G' \parallel$ were fitted to Lorentzian curves which indicates that these are dynamic fluctuating systems. The curves in $G' \perp$ were fitted to energy dissipation curves for a time dependent coupled harmonic oscillator curves. This dynamic variation of $G' \perp$ with frequency ω is

$$G' \perp (\omega) = \omega^p * sin^n(1/\omega) \tag{6.5}$$

Where P shows the power law behavior and n represents the nematic alignment (Physically, it represents confined motion of the colloidal particle) behavior. The presence of tilted Sm C clusters will lead to this chirality in the perpendicular direction. This phenomena without restricted rotation along the parallel direction and with presence of tilted Sm C clusters behavior is known as "improper biaxiality". It has $G'(\omega)$ dependence in the perpendicular direction given by equation 6.5. This clearly represents that, in the perpendicular direction to the nematic director, bent-core liquid crystals show tumbling behavior as calamitic liquid crystals. Hence, the sequential effect is memory effects of bent-core liquid crystals in this temperature range.

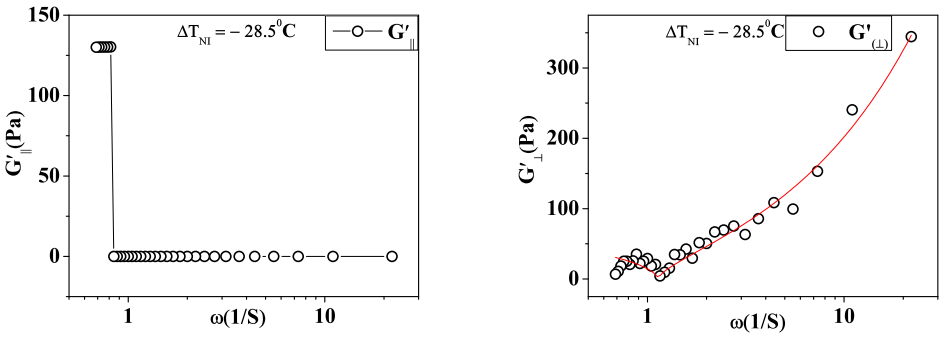

Figure 6.12: Elastic modulus (G') in the parallel direction to the director $(\hat{\mathbf{n}})$ at $(\Delta T_{N-I} = -28.5°C)$. Scale is linear on Y-axis and logarithamic on X-axis

In the above mentioned temperature range, 177° C $(\Delta T_{N-I} = -1.5°C)$ to 155° C $(\Delta T_{N-I} = -23.5°C)$, we have shown the consequences of small 'in-plane' rotation of the clusters around the molecules long axis $\mathbf{n}\|$ direction which leads to an uniaxial nematic phase (N_u) with tetrahedral symmetry. Restricted rotation because of the opposite (left and right) or same (left or right) handedness of the molecules which leads to biaxiality with orthorhombic symmetry. Flip rotations of the molecules during the rotation, they show uniaxial and with the complete flip rotation they show biaxial behavior which leads to uniaxial-biaxiality with nematic-tetrahedratic symmetry [5]. Theoretically it was proved that, along with these, there exists another biaxial nematic phase with monoclinic C_{2h} symmetry (N_{bm}) phase.

This conclusion is supported by another method that measures the correlation between liquid crystal molecules which is given below.

6.3.4 *Out of plane orientations*

As the temperature decreases, further, the size of BCLCs increases, at a particular temperature, instead of 'in-plane' rotations, these BCLCs completely 'tilt' to the out of plane direction.

As in the above figures, at $(\Delta T_{N-I} = -28.5°C$, in the parallel direction to the director $(\hat{\mathbf{n}})$, G' value has a sudden discontinuity. This represents dissipation of energy during the 'tilt' of the BCLCs to out

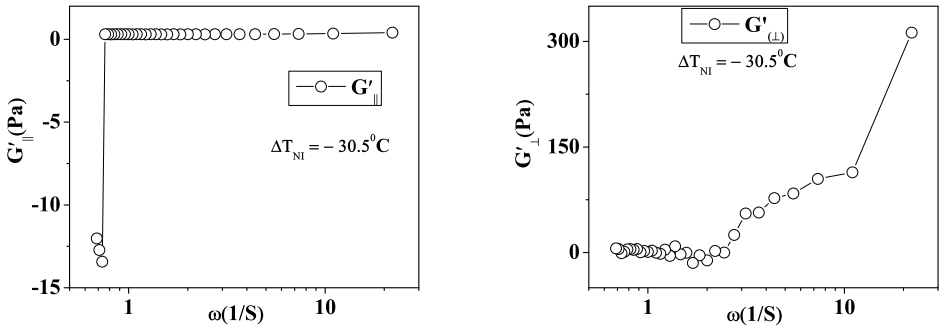

Figure 6.13: Elastic modulus (G') in the parallel direction to the director $(\hat{\mathbf{n}})$ at $(\Delta T_{N-I} = -30.5°C)$. Scale is linear on Y-axis and logarithamic on X-axis

of plane geometry. In the perpendicular direction to the director $(\hat{\mathbf{n}})$, the frequency dependence of $G' \perp$ is $G'(\omega) \simeq \omega^{0.63}$ representing the presence of Sm A layers.

6.3.5 *Surface anchoring effects*

In the graphs, from 148° C or $(\Delta T_{N-I} = -30.5°C)$ to 130° C or $(\Delta T_{N-I} = -48.5°C)$, amplitude of dissipation of energy is relatively small. This could be because the colloidal particles are coated with DMOAP, which promotes homeotropic alignment of the bent-core molecules. On the surface of the microsphere, the free rotation of the molecules along the long axis is restricted due to steric hindrance. So, they are pinned in a facilitating formation of permanent smectic clusters or layers around the micro sphere. Because of this reason, the hydrodynamic radius of the micro sphere could become significantly larger than the actual radius due to the large cloud of the distorted nematic around the micro sphere. In addition, the smectic layering effect can increase with decreasing temperature due to a kind of condensation of the clusters around the micro sphere. Which effectively increases the diameter of the micro sphere with decreasing temperature. Further, the important question here is, why the 'in-plane' (small rotations, complete flip) and 'out of plane' orientations (tilt) show relatively less dissipation of energy compared to previous

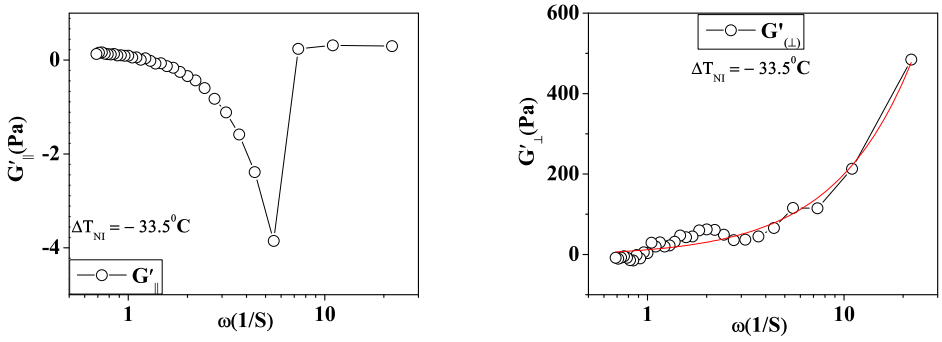

Figure 6.14: Elastic modulus (G') in the parallel and perpendicular directions to the director $(\hat{\mathbf{n}})$ at $(\Delta T_{N-I} = -33.5°C)$. Scale is linear on Y-axis and logarithmic on X-axis

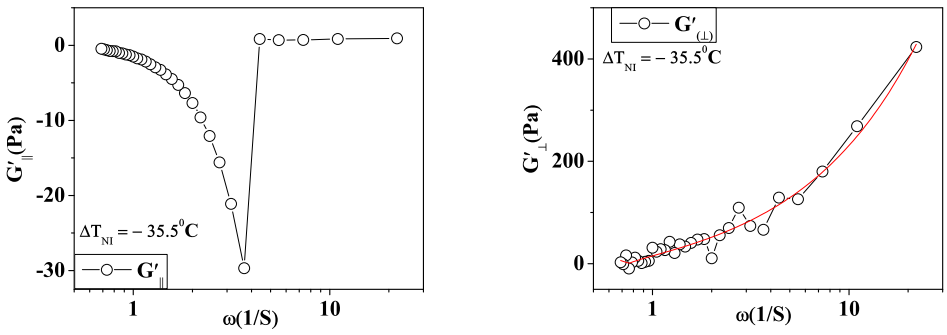

Figure 6.15: Elastic modulus (G') in the parallel and perpendicular directions to the director $(\hat{\mathbf{n}})$ at $(\Delta T_{N-I} = -35.5°C)$. Scale is linear on Y-axis and logarithmic on X-axis

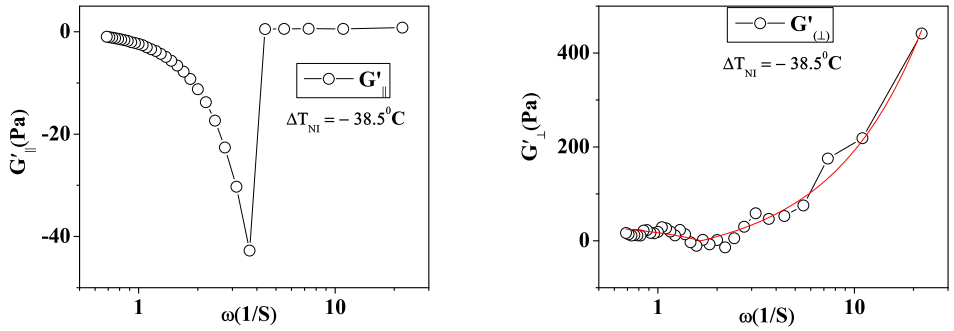

Figure 6.16: Elastic modulus (G') in the parallel and perpendicular direction to the director $(\hat{\mathbf{n}})$ at $(\Delta T_{N-I} = -38.5°C)$. Scale is linear on Y-axis and logarithmic on X-axis

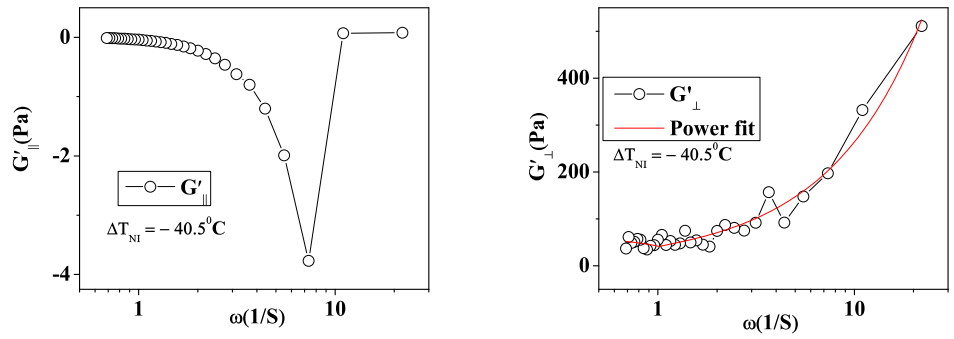

Figure 6.17: Elastic modulus (G') in the parallel and perpendicular directions to the director $(\hat{\mathbf{n}})$ at $(\Delta T_{N-I} = -40.5°C)$. Scale is linear on Y-axis and logarithamic on X-axis

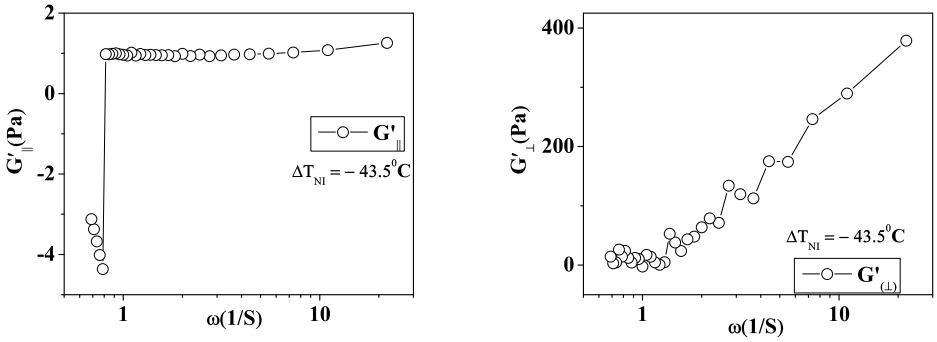

Figure 6.18: Elastic modulus (G') in the parallel and perpendicular directions to the director $(\hat{\mathbf{n}})$ at $(\Delta T_{N-I} = -43.5°C)$. Scale is linear on Y-axis and logarithamic on X-axis

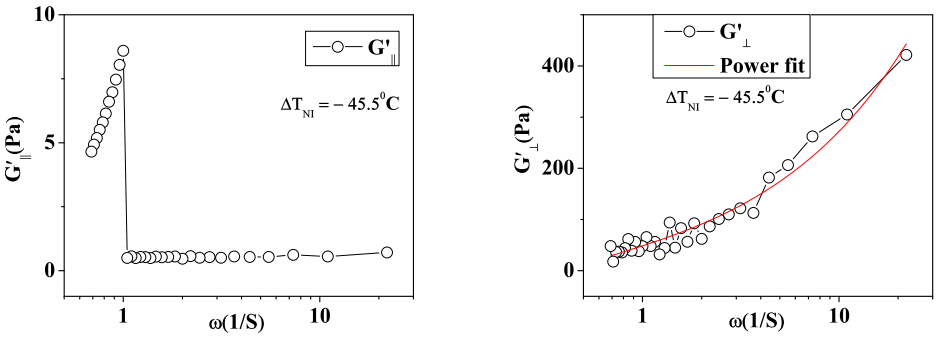

Figure 6.19: Elastic modulus (G') in the parallel and perpendicular directions to the director $(\hat{\mathbf{n}})$ at $(\Delta T_{N-I} = -45.5°C)$. Scale is linear on Y-axis and logarithamic on X-axis

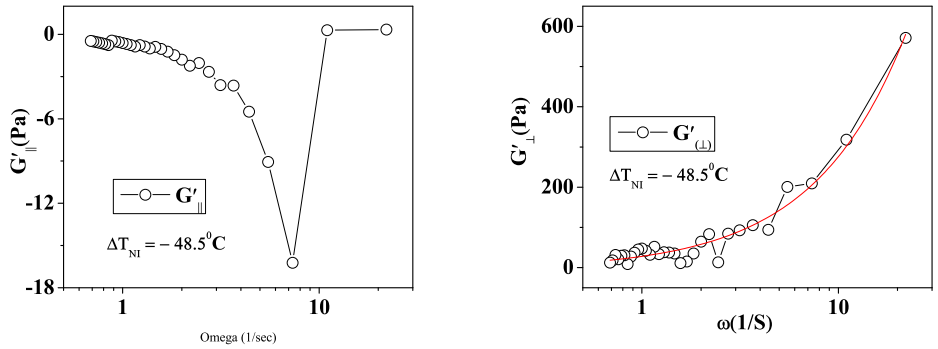

Figure 6.20: Elastic modulus (G') in the parallel and perpendicular directions to the director $(\hat{\mathbf{n}})$ at $(\Delta T_{N-I} = -48.5°C)$. Scale is linear on Y-axis and logarithamic on X-axis

temperatures? There could be two reasons for the less dissipation of energy: 1) Since the size of the colloidal particle increases, diffusive motion of the colloidal particle decreases. which leads to relatively small dissipation of elastic energies during their 'in-plane' and 'out of plane' rotations . 2) The rotation of the colloidal particle has surface influence (surface anchoring effects) from the planar surface alignment on the surface of the coverslips and homeotropic alignment on the colloidal particle. Since the cell is rubbed for planar alignment, it can be expected that the smectic layer planes in the temporarily fluctuating clusters are oriented perpendicular to the rubbing direction. In this case, the cybotactic clusters are large enough and the self diffusion of the micro particle reduces.

The clusters surrounding these large size colloidal particle feels a kind of 'torque' forces, which arises because of the homeotropic alignment on the colloidal sphere and planar alignments on the cover slips. Here, the dipole moment of pinned liquid crystals molecules surrounding the sphere, and the dipole-moment of smectic layering planes in the temporarily fluctuating clusters are in opposite directions. The torque force due to these dipole moments drives the 'in-plane' and 'out of plane' orientations. Hence, there could be reduction in the absorption of energy. This leads to less dissipation of energy during the rotation of BCLCs. Further, in the perpendicular direction, the power law dependence of the $G' \perp$ on frequency has shown

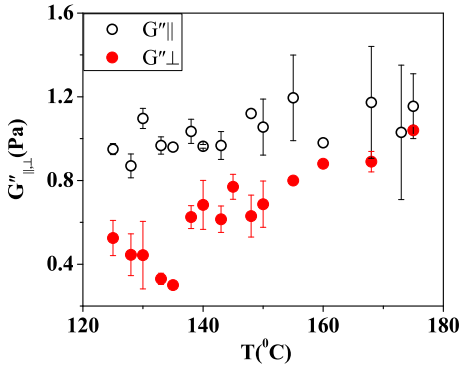

Figure 6.21: Elastic modulus (G'') in the parallel and perpendicular directions to the director ($\hat{\mathbf{n}}$) for temperatures from 180◦ C to 125 ◦ C at ($\Delta T_{N-I} = -48.5°C$).

the values of power of ω being with in 0.45 to 1. This indicates the presence of smectic clusters in the perpendicular direction to the director. Another significant behavior to be noticed in 'out of plane' orientations is, at $\Delta T_{N-I} = -28.5°C$, at very low frequencies, $G' \parallel$ values are parallel to ω, where as at other temperatures, close to smectic phase ($\Delta T_{N-I} = -43.5°C, -45.5°C,$) that show out of plane orientations, the G' vs ω shows a large dependence on ω. Both positive and negative slopes are observed. This represents, for out of plane orientations, at very low frequencies of G' vs ω, at $\Delta T_{N-I} = -28.5°C$, physically bent-core liquid crystals has viscoelastic solid nature and at other temperatures, it has viscoelastic liquid nature. These physical properties at very low frequencies gives a clue about the existence of cybotactic clusters at $\Delta T_{N-I} = -28.5°C$, and small smectic clusters at other temperatures. Hence, because of their large size of the cybotactic clusters, the frustration among these clusters bring an 'out of plane' orientation and when small smectic clusters are present, close to smectic phase, surface anchoring has important role in describing the rotational motion of the clusters.

6.4 VISCOUS MODULUS(G")

$G'' = \eta\omega$ that means, G'' possess characteristics similar to viscosity of bent core liquid crystals. Viscosity of bent core liquid crystals was described in chapter 4. Here the power law dependence of G'' on ω is in figure.

6.5 CONCLUSIONS

The microrheological measurements reveal the slow dynamics of kink shaped bent core molecules. Both in isotropic and nematic phase, the physical nature of the bent core liquid crystals and their corresponding symmetry properties from the theoretical predictions are confirmed. In the isotropic phase, the presence of cybotactic clusters are confirmed by the nature of their physical rigidity. Because of these cybotactic clusters, parallel component of G' exhibits the rigidity nature similar to particulate suspensions. Where as in the perpendicular direction, G' shows fluctuations similar to fluctuations in the nematic phase of calamitic liquid crystals. In the nematic phase of bent core liquid crystals, the small and total flip orientations of these kink shaped bent core liquid crystals, leads to dissipation of energy which results in the negative values of storage modulus (G') of the colloidal particle motion and is a consequence of small flip orientations of the bent core molecules. These negative values of G' observed are expected to be consequences of deformation induced by the rotation of bent core liquid crystal molecules on to the colloidal particle. G' vs ω in the parallel direction fits well with the Lorentzian curvature which represents the dynamical nature of these liquid crystals. Further, this fitting confirms the theoretical predictions of the uniaxial symmetry. Also, the values of G' being constant with change in frequency in the parallel direction which is a consequence of restricted rotation of the molecules and the variation of G' values with change in frequency in the perpendicular direction which is similar to G' vs ω in calamitic liquid crystals, this confirms the theoretical prediction of the orthorhombic and monoclinic symmetry of the liquid crystals molecules. Also, the value of G' becoming negative and then becoming constant with respect to frequency confirms the uniaxial to biaxial symmetry transformation

which is a consequence of total flip orientation. Further, an important observation is, proper biaxiality which is a consequence of monoclinc symmetry. G' value being constant with respect to frequency in the parallel direction and the remark of presence of tilted SmC clusters in the perpendicular direction lead to show the "proper biaxiality" nature. The observation of G' being constant with respect to frequency in the parallel direction to the director which is a consequence of the restricted rotation of bent core molecules. In perpendicular direction to the director, the dependence of G' on ω which represents variation of G' on ω follows simple power law behavior and the values of this power being < 1 represents, the presence of smectic A layers. In A131 bent core liquid crystals, $150^{\circ}C$, was assumed to be a temperature at which biaxiality can be predicted. But, results of microrheological measurements has shown this as a consequence of total out of plane orientation of the bent core liquid crystal molecules. At this temperature, the sudden jump in the G' value from being constant with change in the frequency and then again becoming constant and that value being equal to zero in the parallel direction. This jump represents the out of plane orientation of the cybotactic clusters formed. This out of plane orienation is due to larger size of cybotactic clusters and the frustration among these cybotactic clusters. In the perpendicular direction, G' vs ω follows power law behavior which represents the presence of smectic A layers. The presence of smectic cluster behavior is a consequence of orthorhombic symmetry. Further, as the size of cybotactic clusters grow with the decrease in temperature, the surface anchoring effects play the role in reducing the dissipation of elastic energy during the in plane and out of plane orientations of liquid crystals in the parallel direction. But, in the perpendicular direction, consequence of Smectic A clusters is observed. These measurements could not identify polar order of the molecules.

BIBLIOGRAPHY

[1] Mohammad Mydul Alam and Raffaele Mezzenga, Langmuir **27**, 6171 (2011).

[2] C.Bailey, K.Fodor-Csorba, J.T.Gleeson, S.N. Sprunt, and A. Jakli, Soft Matter, **5**, 3618 (2009).

[3] M.J.Freiser, Phys.Rev.Lett. **24**, 19 (1970).

[4] T. C. Lubensky, Leo Radzihovsky, Phys. Rev. E., **66**, 031704 (2002).

[5] Lech Longa, Grzegorz Pajk, and Thomas Wydro1, Phys. Rev. E, **79**, 040701(R) (2009).

[6] E.Dozov, Euro.Phys.Lett., **56**, 247(2001).

[7] Bharat R. Acharya, Andrew Primak, and Satyendra Kumar, Phys.Rev.Lett., **92**, 14, (2004).

[8] J. Harden, B. Mbanga, N. Eber, K. Fodor-Csorba, S. Sprunt, J. T. Gleeson, and A. Jakli, Phys. Rev. Lett., Phys. Rev.Lett., **97**, 157802, (2006).

[9] P. Sathyanarayana, M. Mathew, Q. Li, V. S. S. Sastry, B. Kundu, K. V. Le, H. Takezoe, and Surajit Dhara, Phys. Rev. E **81**, 010702(R) (2010).

[10] E. Dorjgotov, K. Fodor Csorba, J. T. Gleeson, S. Sprunt and A. Jakli, Liquid Crystals, **35**, 149-155, (2008).

[11] D. Wiant, S.Stojadinovic, K. Neupane, S. Sharma, K.Fodorcsorba, A.Jakli, J.T. Gleeson and S. Sprunt, Phys. Rev. E **73**, 030703 (2006).

[12] S. Dhara, Y. Balaji, J. Ananthaiah, P. Sathyanarayana, V. Ashoka, A. Spadlo, and R. Dabrowski,Phys. Rev. E **87**, 030501(R) (2013).

[13] T. G. Mason, T. Gisler, K. Kroy, E. Frey, D. A. Weitz, J. Rheol. **44**, 917 (2000).

[14] Thomas G. Mason, Rheol. Acta **39**, 371 (2000).

[15] Todd M. Squires and Thomas G. Mason, Ann. Rev. Fluid Mech., **42** 413 (2010).

[16] Denis Wirtz, Annu. Rev. Biophys., **38** 301 (2009).

[17] Balaji Yendeti, G.Thirupathi, Ashok Vudaygiri, Rajendra singh, Eur. Phys. J. E, **37** 70 (2014).

[18] Jesus Etxebarria and M. Blanca Ros, J. Mater. Chem., **18**, 2919 (2008).

[19] Valentina Domenici, Marco Geppi, Carlo Alberto Veracini, Robert Blinc, Andrija Lebar, and Bostjan Zalar, J. Phys. Chem. B **109**, 769 (2005).

[20] Mario Cifelli and Valentina Domenici, Phys. Chem. Chem. Phys., **9**, 1202 (2007).

[21] M.S.Park, B.J.Yoon, J.O.Park, Veena Prasad, S.Kumar, M.Srinivasarao, Phys.Rev. Lett. **105**, 027801 (2010).

[22] Prerna sharma, Shankar Ghosh and S.Bhattacharya, Nature Physics **4**, 960 (2008).

[23] Carsten Tschierske and Demetri J. Photinos, J. Mater. Chem., **20**, 4263 (2010).

[24] S. Stojadinovic, A. Adorjan, S. Sprunt, H. Sawade, A. Jakli, Phys. Rev. E **66**, 060701(R) (2002).

[25] Jimaan Sane, Johan T. Padding, and Ard A. Louis, Phys. Rev. E, **79**, 051402 (2009).

[26] Guillaume Gueguen, Nicolas Destainville, and Manoel Manghi, Eur. Phys. J. E, **37**, 76 (2014).

[27] Christina Keith, Anne Lehmann, Ute Baumeister, Marko Prehma and Carsten Tschierske, Soft Matter, **6**, 1704 (2010).

[28] Valentina Domenici, Diego Frezzato, and Carlo Alberto Veracini, J. Phys. Chem. B , **110**, 24884, (2006) and Valentina Domenici, Soft Matter, **7**, 1589, (2011).

[29] Oriano F., Vesna Stanic, Sofia I. Torgova, Alfredo Strigazzi, Nicola Scaramuzza, Claudio Ferrero, Igor P. Dolbnya, Thomas M. Weiss, Roberto Berardi, Luca Muccioli, Silvia Orlandi, and Claudio Zannoni, Adv. Funct. Mater. **19**, 25922600 (2009). Oriano Francescangeli and Edward T. Samulski, Soft Matter, **6**, 2413 (2010).

[30] Verena Gortz, Christopher Southern, Nicholas W. Roberts, Helen F. Gleeson and John W. Goodby, Soft Matter, **5**, 463 (2009).

[31] P.C.Martin,O.Parodi,P.S.Pershan, Phys. Rev.A., **6**, 6, (1972).

[32] M. karabot, I. Muevi, Soft Matter, **6**, 5476, (2010).

7

DIFFUSING DIFFUSIVITY IN LIQUID CRYSTALS

7.1 INTRODUCTION

It is commonly assumed about the random motions of the colloidal particles in thermal bath are to follow a normal or Gaussian distribution. In such case, mean square displacement(MSD) of the Brownian motion is $\langle \Delta r^2(t) \rangle \propto \tau$, known as Fickian diffusion. Thermal motion or diffusion of colloidal particle in an orientationally ordered fluid is anisotropic[1]. It was well proved that[2],[3],[4], in anisotropic fluids, MSD varies non-linearly with time$\langle \Delta r^2(t) \rangle \propto \tau^{\alpha}$. B. Wang et.al.[5][6] have proved that in many systems, MSD varies linearly with time, which is typical of normal diffusion, but accompanied with a non-Gaussian probability distribution of displacements G(x,t), whose Gaussian center and tails combine in three different ways, depending on their relative position. A non-Gaussian distribution of displacements with exponential tails at short times, with exponents that scale with the square root of time as $\lambda(t) \propto \sqrt{t}$. It was concluded that, the distribution of displacement probability is exponential for large amplitudes of Brownian motion. Another possible category is, the central and tail portions are both Gaussian but are of different diffusion constants or with different variance. Further, the interpretation of non-Gaussian distribution was described as convolution of Gaussian, independently diffusive processes(distribution of diffusive processes). Inverting the non-Gaussian probability distribution of probe displacements the distribution of diffusivities were characterized as the slow and fast diffusive processes. Recently, Mykyta V.C.et.al.[7] had given a generic model for phenomena like "anomalous yet Brownian" diffusion. In their model, there is diffusivity memory but no direction memory in the particle trajectory such model leads to both linear MSD and a non-Gaussian G(x,t) at short times.

In this chapter, considering the effect of director deformations around a sphere in the particle trajectory as the colloid passes through liquid crystals and also, the elastic force [2] by the fluctuative splay on

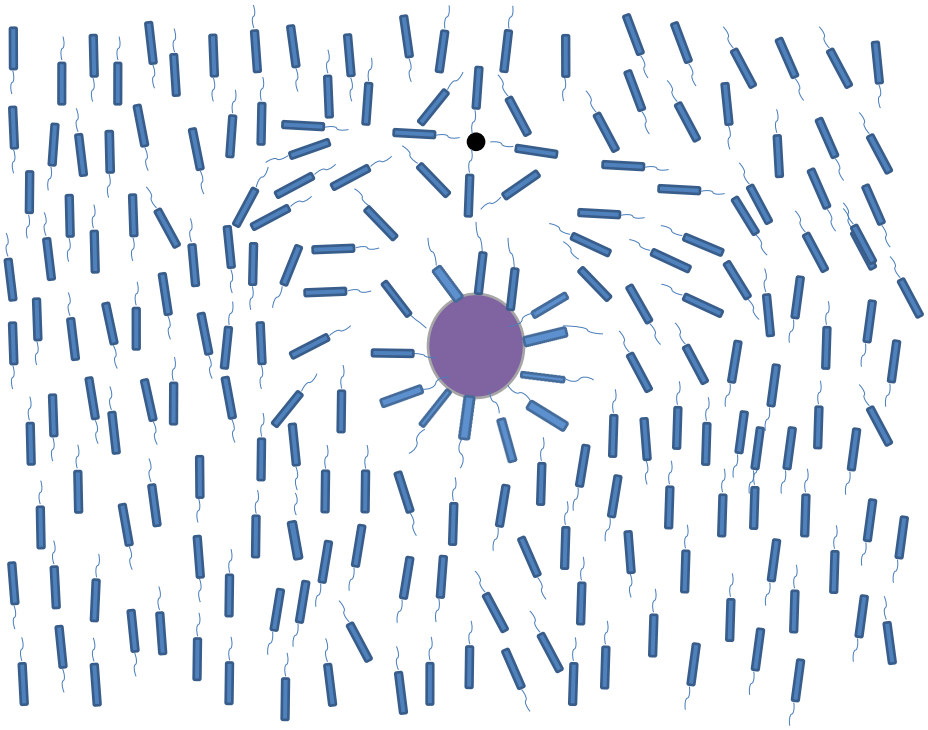

Figure 7.1: colloidal particle in liquid crystals

the sphere, we analyzed the diffusivity of the colloidal particle in liquid crystals. The diffusivitiy of colloidal particle in 8CB liquid crystals with their tumbling nematic director $(\hat{\mathbf{n}})$ at certain temperatures[8] in the nematic phase is analyzed. The nomenclature used for the description of structures in the nematic phase of 8CB liquid crystals is similar to that was mentioned by K. Negita et.al.[8]. This chapter is about the analysis on anomalies in diffusion of colloidal particle in liquid crystals.

7.2 RESULTS AND DISCUSSION

There was an assumption that, if the probability distribution of the motion of a colloidal particle in single particle tracking(SPT)experiments, is non-Gaussian, then the factors that are responsible for the non-Gaussian distribution of displacements should also be responsible for the non-linear behavior $(\langle \Delta r^2(t) \rangle \propto \tau^{\alpha})$ of the MSD. In several other

works[5],[6] it was proved, this assumption is incorrect. The time dependence of linearity in MSD possessing non-Gaussian probability distribution is popularly known to be the "anomalous yet Brownian diffusion". Recently, a generic model was proposed for such cases by M.V. Chubynsky et.al.[7]. In their model, the particle trajectory is chosen to have diffusivity memory but no direction memory which leads to both linear MSD and a non-Gaussian distribution of displacements at short times. For the random walks without direction memory, but with diffusivity memory, the instantaneous effective diffusion coefficient of a particle changes slowly or diffuses with or without bias. Such diffusive behavior was termed as "diffusing diffusivity". This corresponds to the environment of the particle changing gradually by its own or because the particle moves to a different environment.

In 8CB liquid crystals, the tumbling motion of the nematic director is well understood using shear rheology methods [8],[9],[10]. Here, in fig. 7.2 we present, the time dependence of the MSD from the thermal motion of the colloidal particle in the parallel and perpendicular directions to the nematic director $(\hat{\mathbf{n}})$ of 8CB liquid crystals.

Figure 7.3, represents VACF (C_v) Vs time in parallel and perpendicular directions to director. At $\Delta T_{N-I} = -2.5^{\circ}C$, MSDs show linear behavior with time in the parallel and perpendicular directions. Whereas the corresponding C_v in figure 7.3 represents the long range correlations in the diffusive behavior for these particular cases. This behavior is similar to the observation of "anomalous yet Brownian diffusion" on lipid tubules[5].

In the nematic phase of 8CB liquid crystals, because of the presmectic translations at temperatures from $\Delta T_{N-I} = -2.5^{\circ}C$ to $\Delta T_{N-I} = -5.5^{\circ}C$, few layered structures formed close to the glass cell boundaries, gets rearranged due to the differences in elastic energy density with changes in temperatures[11]. This leads to gaps in the form of compressions and rarefractions in central portion of the equilibrium structures of the liquid crystals. Hence the the particle trajectory of a colloidal particle in such oscillatory nematic director does posses random motion without direction memory, but with diffusivity memory. So, the diffusion of colloidal particle in tumbling nematic 8cb liquid crystals can be regarded as the best example for "anomalous yet Brownian" diffusion. In fact as it was described in chapter 7, even the colloidal particle motion in bent-core liquid crystals does show

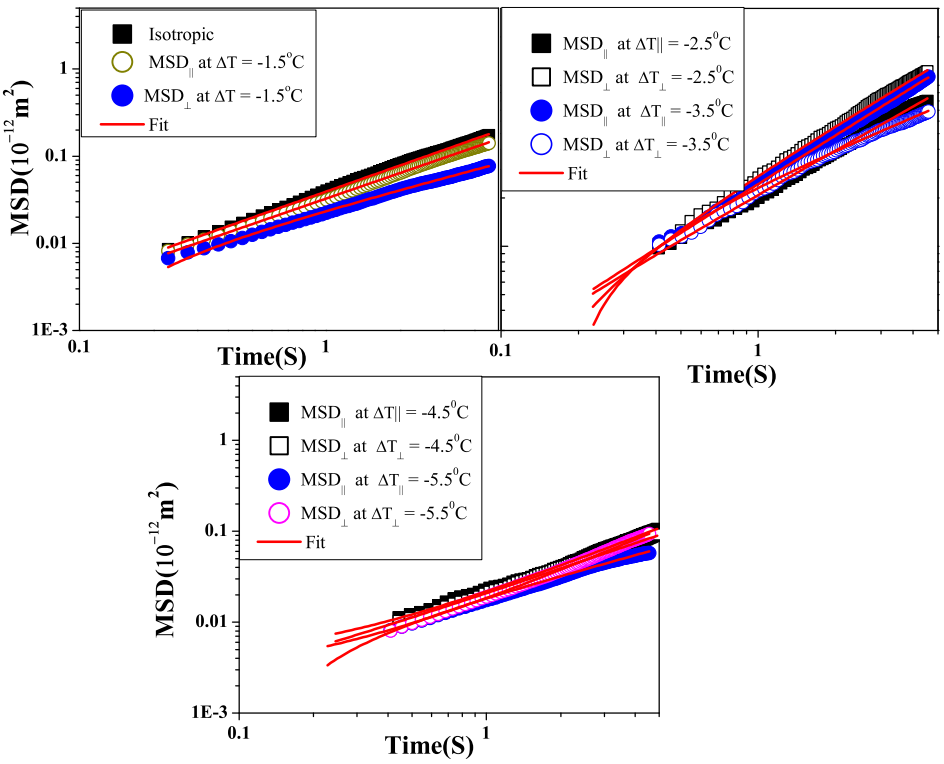

[h!]

Figure 7.2: MSD $< x^2 >$ Vs Time in the parallel and perpendicular direction to the director $(\hat{\mathbf{n}})$ for temperatures from $(\Delta T_{N-I} = -1.5°C)$ to $\Delta T_{N-I} = -6.5°C$. Scale is logarithamic on X and Y-axis.

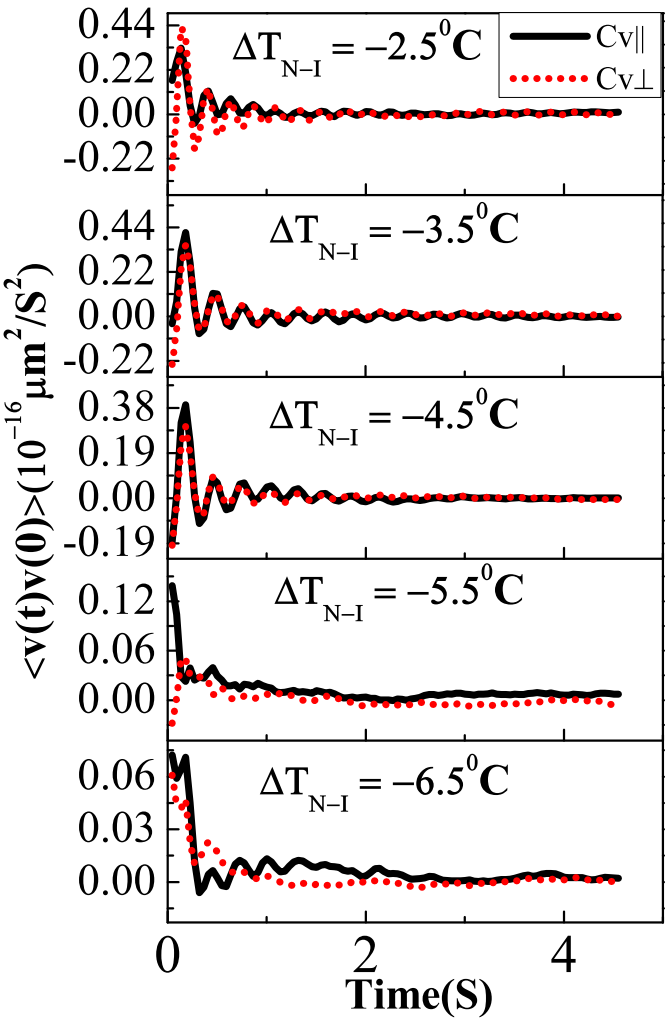

Figure 7.3: VACF(C_v) Vs Time in the parallel and perpendicular direction to the director ($\hat{\mathbf{n}}$) from temperatures at ($\Delta T_{N-I} = -2.5°C$) to ($\Delta T_{N-I} = -6.5°C$) . Scale is linear both on X and Y-axis. parallel components are represented with solid lines and perpendicular components are represented with short dots respectively.

anomalous behavior with their elastic modulus. In that case, it was observed that, the effective slow diffusion of colloidal particle is due to the slow fluctuations of the temporarily smectic clusters whose layer normal is parallel to the rubbing direction.

From the MSD graphs, and from the corresponding VACF C_v, one can find that, for temperatures at $\Delta T_{N-I} = -2.5^{\circ}C$, the MSD is linear for both parallel and perpendicular directions to $(\hat{\mathbf{n}})$ and C_v shows diffusive motion of the colloidal particle being oscillatory both in $C_{v\parallel}$ and $C_{v\perp}$. But, at $\Delta T_{N-I} = -3.5^{\circ}C$, though $C_{v\parallel}$ and $C_{v\perp}$ show oscillatory diffusive motion(amplitude and periodicity in $C_{v\parallel}$ and $C_{v\perp}$ are same) but their corresponding MSD are different in different directions. $\text{MSD}_{\parallel}$ show linear behavior and $\text{MSD}_{\perp}$ show non-linear behavior. Curve fitting with power law $\langle \Delta r^2(t) \rangle \propto \tau^{\alpha}$ gives $\alpha_{\parallel} = 1.0$ and $\alpha_{\perp} = 0.65$. Which represents normal diffusive nature in parallel direction and sub diffusive nature in perpendicular direction to the director. Also, at $\Delta T_{N-I} = -4.5^{\circ}C$, MSD shows linearity in both parallel and perpendicular directions. But, the corresponding diffusive nature being oscillatory.

This similar behavior can be observed in bent-core liquid crystals(BLC). The kink shape of the BLCs leads to cluster formation which results in dynamic behavior in the diffusion of colloidal particles in the bent core liquid crystals. The 'in-plane' and 'out of plane' rotational motions of bent core liquid crystal molecules leads to their slow dynamics. As the temperature reduces in the nematic phase of BLCs, the size of the layers around the colloidal particle increases and hence the change in its transport properties.

Figure 7.4, represents the MSD of a colloidal particle in bent core liquid crystals. MSD varies linearly with time in both parallel and perpendicular directions to $(\hat{\mathbf{n}})$. Fig. 7.5 represents velocity auto correlation functions $C_{v\parallel}$ and $C_{v\perp}$. Positive values of $C_{v\parallel}$ with limited variations in time, represents restricted rotation of molecules along the parallel idrection. This leads to normal diffusion of colloidal particle. The tumbling correlated motion in the perpendicular direction represents chirality in the collective molecular orientations in the nematic phase of bent core liquid crystals. This chirality leads to sub diffusive motion of colloidal particle. Overall, these results supports an argument, that is, the systems governed by a generalized Langevin

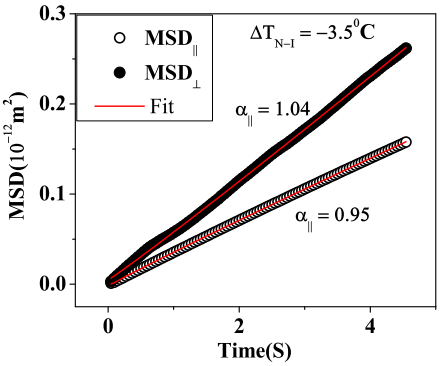

Figure 7.4: MSD $< x^2 >$ Vs Time in the parallel and perpendicular direction to the director $(\hat{\mathbf{n}})$ for temperatures at $\Delta T_{N-I} = -3.5°C$. Scale is linear on X and Y-axis.

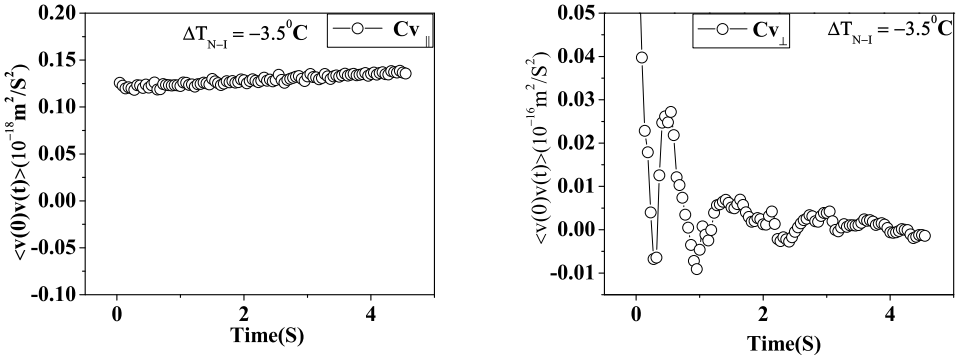

Figure 7.5: VACF (C_v) Vs Time in the parallel and perpendicular direction to the director $(\hat{\mathbf{n}})$ at $\Delta T_{N-I} = -3.5°C$.

equation with long range memory can be normal, sub diffusive or super diffusive[12].

Slowly varying, anisotropic fluctuations of the environment leads to the non-Gaussian features in the probability distribution of the positions of the colloidal particle at slower timescales. If the MSD is linear, and is of non-Gaussian distribution of particle displacements, in such case, as mentioned in B.Wang et.al.[5], the hypothetical diffusion coefficients D_{Gauss} and D_{tail}, which represent the behavior of central portion of the non-Gaussian distribution, that can be approximated by $G_c(x,t) \propto exp[\frac{-x^2}{2\sigma^2(t)}]$ with width σ, x is one-dimensional displacement and the tail in the non-Gaussian behavior is approximated by $G_t(x,t) \propto exp[\frac{-(x)}{\lambda(t)}]$ with λ being the characteristic decay length. Further they proposed that, depending on the characteristics of the exponential tails, whether it is larger or smaller than the average diffusivity, $G_t(x,t)$ is made into four categories. Among these four categories, depending on the relative position of the Gaussian center and their exponential tails they can combine in three different ways and also, there can be both central and tail portions that are Gaussian, but are of different variances.

The thermal motion of the colloidal particle in bent core liquid crystals does show anomalous diffusion characteristics [1]. An analysis on the non-Gaussian features profound during and near the critical transitions of the bent core(BC) liquid crystal and 8CB liquid crystals is presented as shown in figures 7.6, 7.7. In BC liquid crystals, at, $\Delta T_{N-I} = -47.6^{\circ}C$, the effective diffusion of the colloidal particle is due to the slow fluctuations of the temporarily smectic clusters whose layer normal is parallel to the rubbing direction. Consequently, the diffusion in the parallel direction to $(\hat{\mathbf{n}})$ was observed to have the tail parts being significantly differing from the Gaussian features of the central portion and in the perpendicular direction, histogram of the Brownian motion of the colloidal particle fits well with the Gaussian. From figure 7.6, further analysis on the non-Gaussian features shows that, the central portion and tail portions does fit with different Gaussian. Which is exactly the fourth category of the non-Gaussian features [5]. The central (D_{Gauss}), and tail D_{tail} portions of the non-Gaussian has different diffusion constants ($D_{Gauss} = 0.79 \times 10^{-15} m^2/sec$ and $D_{tail} = 11.72 \times 10^{-15} m^2/sec$) referring to the complex static heterogeneity in

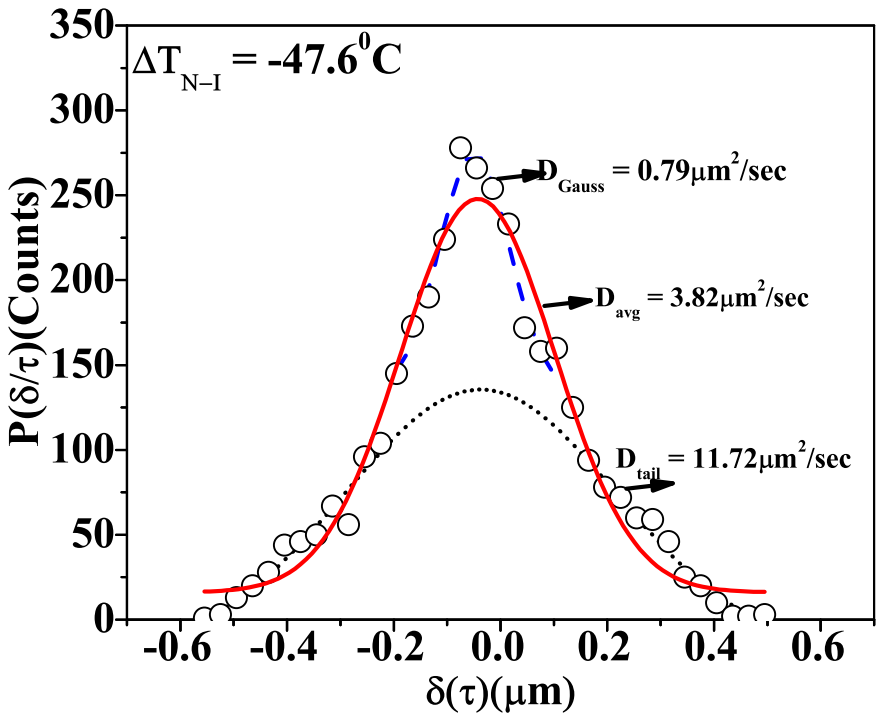

Figure 7.6: Probability distribution of displacements Vs positions of the particle in the parallel and perpendicular direction to the director $(\hat{\mathbf{n}})$ for temperatures at $\Delta T_{N-I} = -47.6°C$. Scale is linear on X and Y-axis.

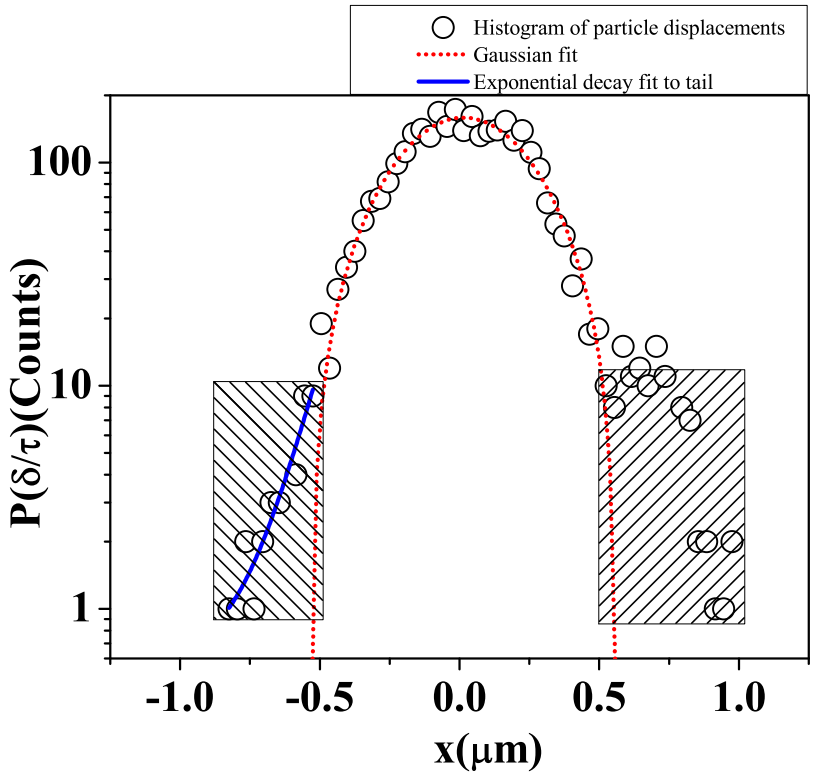

Figure 7.7: Probability distribution Vs positions of the particle in the parallel and perpendicular direction to the director $(\hat{\mathbf{n}})$ for temperatures from $(\Delta T_{N-I} = -3.5^{\circ}C)$. Scale is logarithmic on Y-axis and linear on X axis.

the liquid crystal medium. Infact, this Bent core liquid crystals, has the other three categories present in other repeated measurements.

Also, in chapter 4, the diffusion of colloidal particle was analyzed in the twisted structures of 8CB liquid crystal. The oscillatory amplitude and periodicity in the diffusion of the colloidal motion varies with temperature. Brownian motion possess isotropic and anisotropic oscillatory amplitude behavior in parallel and perpendicular directions at different temperatures. In such case, the diffusion of colloidal particle undergoes dynamical heterogeneity in the medium. Figure 7.7, shows the histogram with non-Gaussian features of Brownian motion of the colloidal particle at $\Delta T_{N-I} = -5.5^{\circ}C$. These two figures 7.6, 7.7 resembles the three categories that were mentioned by B.Wang et.al.[5]. In these histograms, both in figures 7.6 and 7.7, the central portions of the non-Gaussian behavior features the Gaussian nature $G_c(x,t) \propto exp[\frac{-x^2}{2\sigma^2(t)}]$. But, the tail portions fits with exponential decay with $G_t(x,t) \propto exp[\frac{-(x)}{\lambda(t)}]$ with λ being the characteristic decay length. In fig. 7.7, the fitting in central portion with Gaussian curve gives the diffusion constant to be $14 \times 10^{-15} m^2/sec$ and tail portion with exponential decay gives $\lambda = 0.09\mu m$. This characteristic decay length λ is proportional to the square root of elapsed time t[5].

Systems with dynamic heterogeneity, can be analyzed by decomposing complex processes into normal modes. Bo Wang et.al.[5] interpreted the non-Gaussian diffusion by the convolution of Gaussian, independently diffusive processes as, $G(x,t) = \int P(D) \cdot g(\frac{x}{D}) \cdot dD$ Where $P(D)$ reflects the temporal correlation of microscopic fluctuations and $g(\frac{x}{D}) = \frac{1}{\sqrt{4\pi Dt}} \exp(-\frac{x^2}{4Dt})$. This convolution process is the common approach followed in signal processing. But, the distribution of diffusivities $P(D)$ is computed from Lucy's[13] iterative algoritham. $P(D)$ is a mathematical transform of orthogonal fluctuation modes. $P(D)$ characterizes whether diffusion is slow or fast in the medium.

Recently, Turiv et.al.[2] have used the memory function or velocity auto correlation function (VACF) to understand the distribution of diffusivities in different liquid crystals. Also, in recent literature [14], VACF (C_v) has been used in understanding the ballistic Brownian motion in air and liquids. Even though non-Gaussian features of probability distribution of displacements describes the anomalies in the diffusivities, it is difficult to obtain further information on microstruc-

tural properties of the material from this analysis. But, the ultimate interest of understanding the anomalies in the Brownian diffusion should be in microstructural information. Moreover, in a recent paper by David et.al. has proved the failure of Gaussian diffusion approximation in complex fluids [15]. In the process of understanding the complex dynamics of liquid crystals, we realized that analyzing the results of C_v is relatively easy and it not only infers the anomalies in diffusion but it gives information about the structural dynamics of complex dynamics. As described in chapter 4, the collective tumbling molecular orientations of 8cb liquid crystals leads to the oscillatory motions of the colloidal particle along nematic director in the tumbling phase ($\Delta T_{N-I} = -2.5^0C$ to $\Delta T_{N-I} = -5.5^0C$) of the 8CB liquid crystals. The amplitude and periodicity of these oscillations depends on, frustration in the liquid crystal moleculear layers. Also, these precessional motions of the director $(\hat{\mathbf{n}})$ can be quantified by fitting these VACF with the equation for the VACF of particle with time dependent harmonic oscillations .

7.3 CONCLUSIONS

The concept of diffusing diffusivity is best observed in liquid crystals. To interpret the concept of diffusing diffusivity, VACF is used. Since, the invalidity of Gaussian diffusion approximation is observed in many complex fluids, considering VACF is a better alternative to understand the anomalous diffusion behavior and micro structural properties of complex fluids.

BIBLIOGRAPHY

[1] S. Dhara, Y. Balaji, J. Ananthaiah, P. Sathyanarayana, V. Ashoka, A. Spadlo, and R. Dabrowski, Phys. Rev. E **87**, R30501 (2013).

[2] T. Turiv, I. Lazo, A. Brodin, B. I. Lev, V. Reiffenrath,V. G. Nazarenko, O. D. Lavrentovich, Science **342**, 1351 (2013).

[3] I.Y.Wong, M. L. Gardel, D. R. Reichman, Eric R.Weeks, M.T. Valentine, A. R. Bausch, and D. A.Weitz, Phys.Rev.Lett. **92**,17(2004).

[4] Balaji Yendeti, G. Thirupathi, Ashok Vudaygiria, and R. Singh, Eur. Phys. J. E, **37**, 70 (2014).

[5] Bo Wang,James Kuo and Steve Granick, Nat.Mat., **11**, 481 (2012).

[6] Bo Wang, S. M. Anthony, S. C. Bae, and S. Granick, Proc. Natl. Acad. Sci. U.S.A. **106**, 15160 (2009).

[7] Mykyta V. Chubynsky and Gary W. Slater, Phys. Rev.Let. **113**, 098302 (2014).

[8] K. Negita, J. Chem. Phys. **105**, 7837 (1996).

[9] D.F.Gu and A.M.Jamieson, J.Rheol. **38** 3 (1994).

[10] G. Marrucci, Macromolecules, **24**, 4176 (1991).

[11] P.C.Martin, O.Parodi, P.S.Pershan, Phys. Rev.A., **6**, 6 (1972).

[12] Rafael Morgado and Fernando A. Oliveira, Phys. Rev. Let. **89**, 10 (2002).

[13] Lucy,L.B. Astron.J. **79**, 745 (1974).

[14] Tongcang Li and Mark G. Raizen, Ann. Phys. (Berlin), **525**, 281 (2013).

[15] George David Joseph Phillies, Soft Matter, **11**, 580 (2015).

Diffusing diffusivity..

8

FIELD DEPENDENT ANISOTROPIC MICRO RHEOLOGICAL AND MICROSTRUCTRUAL PROPERTIES OF FERROFLUIDS

8.1 INTRODUCTION

Magnetic fluid contains colloidal ferromagnetic nanoparticles in carrier liquids like water, kerosene, Toluene etc. In presence of an external magnetic field, individual particles align to form long chains of nano particles along the direction of the applied field [1]. This modifies the fluid properties of the sample. High enough fields can even achieve a phase transformation, showing an almost solid-like behaviour. Furthermore, the system is anisotropic and values for the parameters along the field are different from those values for perpendicular to the field. The extent of this anisotropy can be measured by passive microrheology. The underlying physics behind such a behaviour can be better understood by studying the microrheological properties of these magnetic fluids.

The chain formation typically happens when the dipole moment induced due to the external field exceeds the average thermal energy $k_B T$ of the nanoparticles. At high fields, the chains are typical $10-20$ μm long and are easily visible under microscope. The external field also causes a torque on each particle given by $\mu \mathbf{M} \times \mathbf{H}$, which constraints their rotation about axis perpendicular to the magnetic field. This causes an additional friction, and hence an increased viscosity [2]. At higher fields, all particles are effectively pinned against rotation, which leads to an anisotropy.

Magnetic fluids have several interesting engineering, bio-medical and scientific applications [3, 4, 5, 6]. Hence it has been a subject of several studies earlier, which attempt to understand the diffusive characteristics of ferrofluids. Magnetic field dependent viscosities, referred as Magneto-viscous effect (MVE), have been studied in macroscopic regime theoretically [7, 8] as well as experimentally[2, 9]. Mertelj et. al. have recently reported about 4 times increase of the storage modulus

along the external magnetic field in maghemite samples, although their measurements for anisotropy in MVE were inconclusive due to a larger statistical variation [1]. But earlier theoretical predictions, such as by Morozov[10], and following capillary viscometer experiments [2, 9] showed a clear anisotropy. Odenbach et. al, explained the anisotropy in MVE as due to structures formed along the field. When flow was perpendicular to the applied field, these structures offered stronger hindrance, resulting in higher viscosity [9].

We present here measurements of microrheological properties of a $Mn_{0.75}Zn_{0.25}Fe_2O_4$ (MZF) ferrofluid by recording the thermal motion of a silica microparticle suspended in it. MZF is a soft ferrite and its nanoparticles are well useful for ferro fluids. Bulk magneto-viscous measurements show a transition from non-Newtonian to Newtonian as shear rates are increased from 0.1 to 1000 s^{-1} at different magnetic fields. Magneto-viscosity exhibits a hysteresis at constant shear rates[11].

Mn-Zn ferrofluids are applicable in magnetic valve controls, fluid transformers, shock absorbers, hypothermia etc., because of its suitable magneto-rheological and electro-rheological properties [5, 6]. Following standard approach of passive micro-rheology, thermal motion of a silica bead was recorded in a home-built inverted microscope and analysed using video tracking software. The trajectories of the probe particle thus measured yields the local probe response and the linear visco elasticity. From these measured values of viscosity, we derive other relevant parameters by following relationships given in earlier works - such as elongational flow coefficient λ_2 [12, 13], coefficient of dissipative magnetization α [8], magnetization relaxation time constant τ [14] etc. For all these measurements, 6 different field measurements, for each field 6 different trajectories and 4 different sample cells with different concentrations ranging from 16% ratio by weight to 4% ratio by weight are considered. All error bars in these measurements are statistical.

8.2 THE EXPERIMENT

Soft ferrimagnetic $Mn_{0.75}Zn_{0.25}Fe_2O_4$ ferro fluid was synthesized by a soft chemical approach of coprecipitation [15, 16]. The size distribution

of nanoparticles was analysed using TEM micro graphs. The electron diffraction pattern shows single phase of the system of nanoparticles (see figure 8.3. The uniformly dispersed Mn-Zn ferrite nanoparticles in Ethylene Glycol (EG) were used for micro rheological measurements. Magnetization measurements of the sample shows a saturation at as low as 0.24 T and a superparamagnetic nature with zero coercivity and zero remnance - as seen in figure 8.2

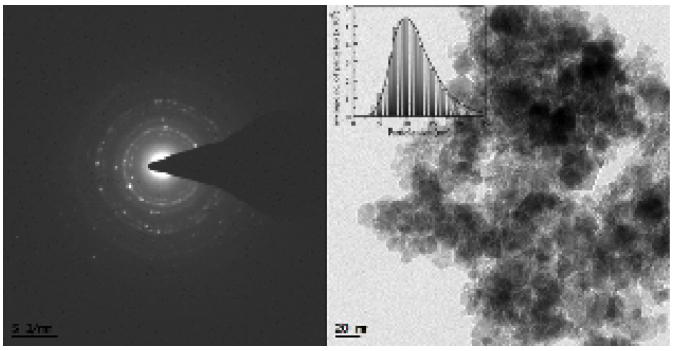

Figure 8.1: TEM images of nanoparticle. Inset shows histogram for particle size distribution

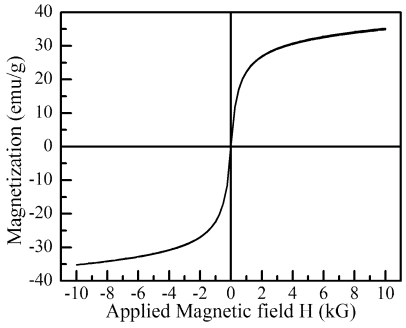

Figure 8.2: M-H curve for the sample at room temperature, showing superparamagnetic nature with zero coercivity

From this sample, 50 μl of this magnetic nano particle solution, 1 ml of water and 20 μl of N,N-Dimethyl-N-Octadecyl-3-aminopropyltrimethoxysilyly chloride(DMOAP) are mixed thoroughly by vortexing for 20 minutes to get uniform alignment of octadecyl chains on the surface of these magnetic nano particles. This addition of DMOAP is for steric stabilization of the nanoparticles. On addition of DMOAP, one would

observe a foam layer on the top of the solution, because of the silane. This mixture is further centrifuged to remove excess solution from nano particles and 1 ml of water is added to this nano particles to wash out the remained silane,then again mixed, centrifuged to remove the excess solution with nano particle aggregates. This process is done $3-4$ times until there is no foam layer. Samples with different concentrations, ranging from 4% to 16% ratios by weight of nanoparticles were prepared from this stock, by adding different amounts of distilled water to this stock solution. To each of these sample solutions, 2 to 5 μl of suspension of silica beads (average diameter 2.34 μm) in water and 30 to 50 μl of Polyethylene glycol(PEG) solution is added. These samples were taken into a glass cell, made by microscope coverslips sealed on all sides with double sided tapes of thickness 100 μm. This sample cell is placed in a home built inversion microscope with 100X, 1.4 N.A., oil immersion microscope objective (Olympus, UPLSAPO series). A homogenous magnetic field with electromagnets is arranged in such a way magnetic field is in the parallel direction with the sample cell and with a gap between the two coils being 20 mm. The gradience in field with in this gap is less than 1 mT at a magnetic field strength of 240 mT.

The thermal motion of the silica bead in this sample is recorded using a normal CCD camera (Watec 90, 512×512 pixels) and a frame grabber card (National Instruments IMAQ NIPCI-1209), at a rate 30 frames/sec acquisition speed and analyzed. A freely available particle tracking software with facility of auto tracking the bead in a video frame in which a template and its associated target are defined is used which becomes useful in analysing the highly concentrated nanoparticle solution [17] The position of the silica beads in the magnetic nano particle solution was determined by this off-line analysis with an accuracy of $\pm$ 55 nm. The probability distribution of the thermal motion of the particles were fitted with a Gaussian curve. The probability that the silica bead would diffuse to a certain distance δx in this magnetic fluid in the time interval 't' is $P = P_0 \exp(-(\delta x)^2/\Delta^2 t)$. Here P_0 is the normalization constant and Δt is the width of the Gaussian distribution (see figure 8.5). From this, the diffusion coefficients of the silica bead are determined in the parallel and perpendicular directions of the application of the field with $D_{\parallel,\perp} = \Delta^2_{\parallel,\perp}(t)/4t$ [18]. The cor-

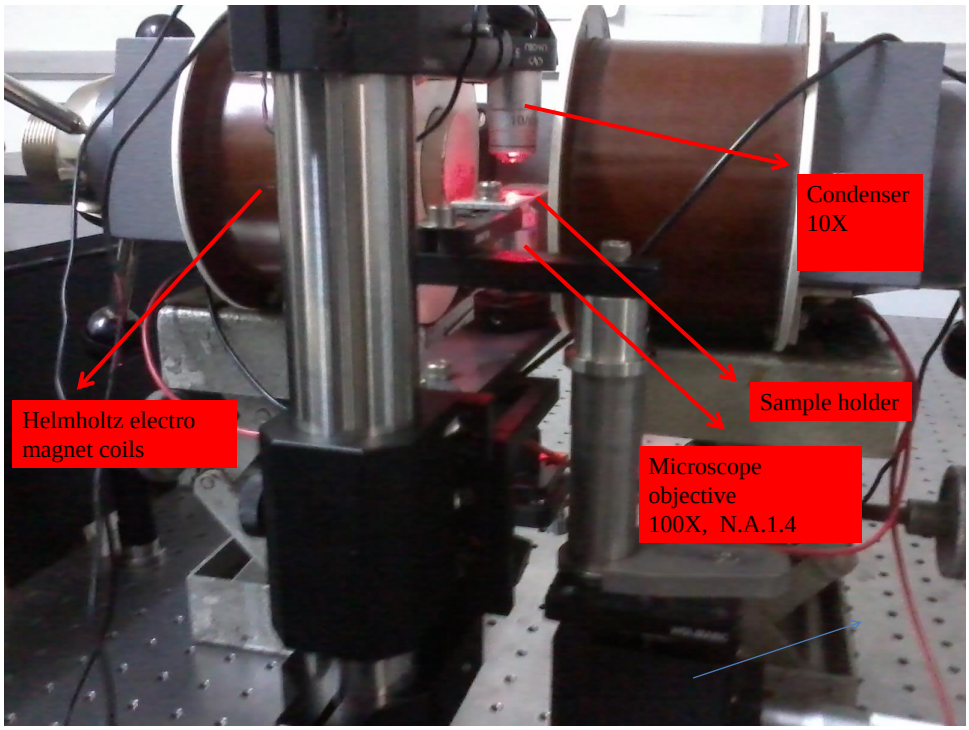

Figure 8.3: Home built microscope with sample cell in magnetic filed with helmholtz coil

responding parallel and perpendicular viscosities of the sample are measured using the Stokes-Einstein relation

$$\eta_{(\parallel,\perp)} = \frac{k_B T}{6\pi D_{(\parallel,\perp)} r}, \tag{8.1}$$

where 'r' is radius of the micro bead.

All relevant micro-rheological parameters of the ferrofluid are derived from these data as explained in the following section.

8.3 RESULTS AND DISCUSSION

8.3.1 *Magnetic properties*

Super paramagnetic particles under the action of an external magnetic field, acquire induced magnetic dipoles and these dipoles interact to

form long chains. This interaction energy between these magnetic dipoles is given by [19],

$$U = \frac{\mu_0 m^2}{4\pi r^3}[1 - 3\cos^2\theta] \tag{8.2}$$

Where $\mu_0 = 4\pi \times 10^{-7} N/A^2$ is the magnetic permeability of free space, m is the magnetic dipole moment, r is the distance between the two magnetic dipoles and θ is the angle between the applied external magnetic field and the line joining between the centres of the two magnetic dipoles. Since, this dipole-dipole interaction energy is dependent on θ value, anisotropic structures with long chain formations are formed in these super paramagnetic fluids. This interaction is dominant over a characteristic length scale λ_B, in comparison to length scale of thermal effects, given by

$$\lambda_B = \left(\frac{\mu_0 m^2}{2\pi k_B T}\right)^{\frac{1}{3}}. \tag{8.3}$$

The above equation comes from the ratio between the dipole-dipole interaction energy U and thermal energy k_BT. The minimum energy configuration is when θ=0, and when the interparticle distance is almost equal to the diameter of the particles 'r' the interaction energy equation (8.2) becomes

$$U_{\min} = \frac{\mu_0 m^2}{2\pi d^3 k_B T} \tag{8.4}$$

where 'd' is the distance between the centres of magnetic nano particles. From the above equation it is very clear that, the field induces a magnetic moment in the nanoparticles and hence influences the interaction parameter between the magnetic nano particles. In turn, this influences the rheological properties.

8.3.2 *Micro-rheological properties*

From the thermal trajectories of the probe particles, the time dependence of the mean square displacements(MSDs) in the direction along and perpendicular to the external field and are as shown in (Fig.8.4). As the field strength increases, there is a clear transformation in the slope of these curves. That transformation in slope of these curves

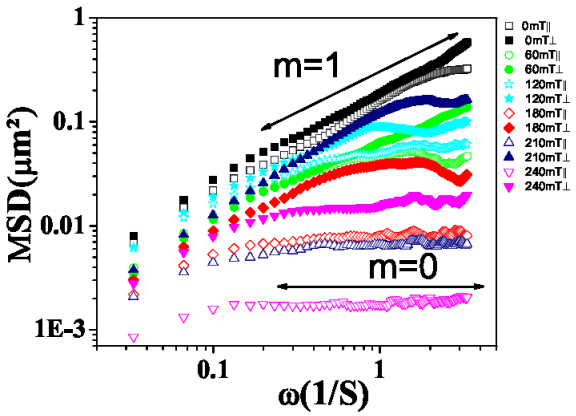

Figure 8.4: Mean square displacements of probe particle in magneto rheological fluid for different external magnetic field strengths. Parallel to the external field (empty) and perpendicular to external field (filled) components are plotted as a function of deformation frequency ω. Nanoparticles form chains along the magnetic field direction. Suggested slope for the curves are represented as m=1 (zero field) and m=0 (high field)

represents the transformation[20] from viscous to viscoelastic and to solid behaviour in the chain formation as the field increases. This is the typical behaviour in repeated measurements. Also, there is increased differences in the MSDs of parallel and perpendicular directions as the field increases. Slope of parallel direction MSDs becomes zero with the increase in field than the slope of perpendicular direction MSDs.

Histograms for thermal trajectories of the bead and a curve fit using a Gaussian curve to them is shown in figure 8.5. Both parallel component (circles) and perpendicular component (closed circles) are shown for low magnetic field (60 mT - Figure 8.5 top) and for a high field (180 mT - Figure 8.5 bottom). It can be seen that the parallel and perpendicular components almost overlap for zero field situation, while the the parallel component has a significantly narrow distribution compared to the perpendicular component in presence of a high field. This indicates that the corresponding diffusion coefficients follow the relation $D_{\perp} > D_{\parallel}$, and the silica bead finds it easier to

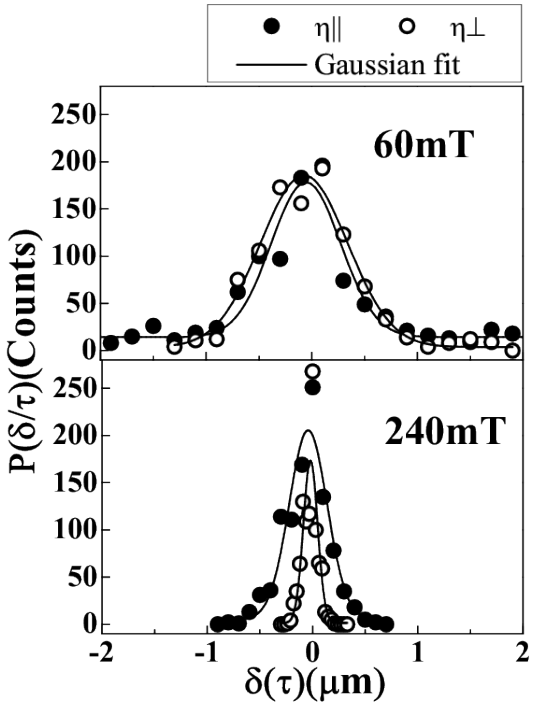

Figure 8.5: (Histogram of particle displacements parallel (open circles) and perpendicular (closed circles) to the magnetic field for τ = 1 s. The solid lines are Gaussian fits. Top figure is for low magnetic field (60 mT). Bottom one is for is for high field (240 mT). Anisotropy between parallel and perpendicular behaviour is clearly visible for high field case.

move in a direction perpendicular to the applied field than in parallel direction.

Figure 8.6 shows parallel and perpendicular viscosities as a function of field, with subfigures (a) - (d) are for different concentrations, as explained in the associated caption. As the field strength increases, the interaction between magnetic nanoparticles dominates the thermal motion of the individual nanoparticles and clusters and they start forming chains. With this, parallel viscosity increases with increasing field. Perpendicular component of the viscosity also increases, but

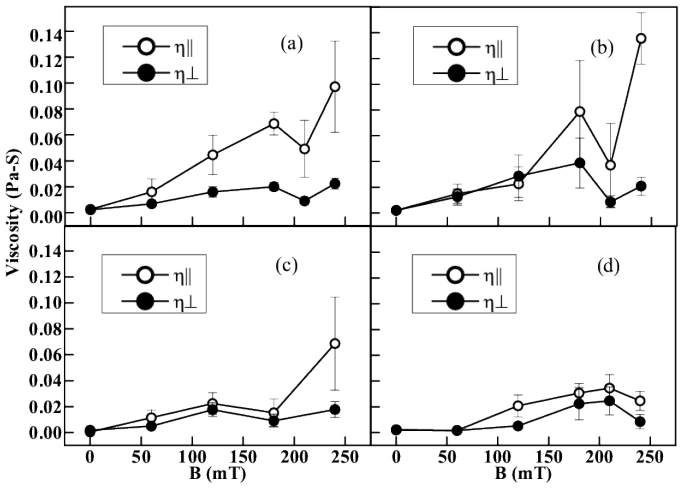

Figure 8.6: Field dependent variation of $\eta_{\|,\perp}$ with varying concentration of superparamagnetic particles. Concentrations are for 16%, 14%, 10% and 8% by weight, respectively for (a), (b), (c), (d)

much more slowly than the parallel component. At very dilute situations such as shown in figure 8.6 (d), the difference between parallel and perpendicular components are very small. But at higher concentrations, the difference between the two components become much larger, at higher fields.

Though there will be very little flow in the sample cell, the thermal motion of the solvent brings a small movement in the magnetic chains which leads to torque acting on the magnetic nanoparticle chains. However, there is an important discussion which is relevant with respect to the distribution of the silica beads among the nanoparticle chains, as given below.

We can distinguish four situations of position of the bead with respect to the chains. (i) During the chain formation, some of these probing beads get caught between two closely lying chains and its movement would be restricted to the region within. (ii) The Silica beads, which are much larger in diameter in comparison to thickness of the chains, sit astride more than one chain. In this case, the bead moves with the chains much like a person sitting on a hammock. The nanoparticles within the chains experience a torque due to the

external field and also interaction between each other. This leads to a collective movement of the chain as a whole and this movement is more in direction perpendicular to the chains than along it. This therefore induces a movement to the bead as well and that results in an anomalously high diffusion coefficient in perpendicular direction. (iii) The third case is a situation where the chains are sparse, at least in some regions and a silica bead is almost touching only one chain. In this case, the beads moves easier in the parallel direction, along the chain, giving a higher value for the parallel component. (iv) Fourth case is when the bead is away from any of the chains and gives a true thermal motion. But in higher magnetic field, this region would have very few nanoparticles since most of them are involved in chain formation and thus the viscosity measured in this region would be mostly that of carrier liquid rather than that of ferrofluid. All these situations are schematically represented in the figure 8.7. For better measurement, we measured thermal motion of different silica beads, spread over all the above situations and then computed their average value. The values shown in figure 8.6 are a result of such a measurement and the statistical variation between these values will obviously be large. This is the reason for such large error bars depicted in the figure 8.6.

In addition, both components of viscosity show a sharp dip at around 210 mT, as seen in figure 8.6. Following the same line of arguments as given in [9], we propose the reason for this dip as follows. When nanoparticles of slightly different sizes are involved, the larger particles become part of the chains at low field strengths. The smaller particles, whose magnetic moments are weaker, require slightly higher fields, so as to be pinned down within the chain. However, due to a lower surface contact, particularly between two nanoparticles of different sizes, the smaller particles are also equally likely to come out of the chain at higher fields and form independent structures. The silica bead has to find pathway between these structures, which would perhaps lead to an increase in perpendicular viscosity but a decrease in parallel viscosity. This situation would lead to a decrease in anisotropy, which is seen at fields beyond 210 mT.

From the measured thermal motion of the silica beads, we can also compute viscoelastic shear moduli(storage modulus(G') and loss modulus (G'')), using generalised Stokes-Einstein equation. G′ and G″

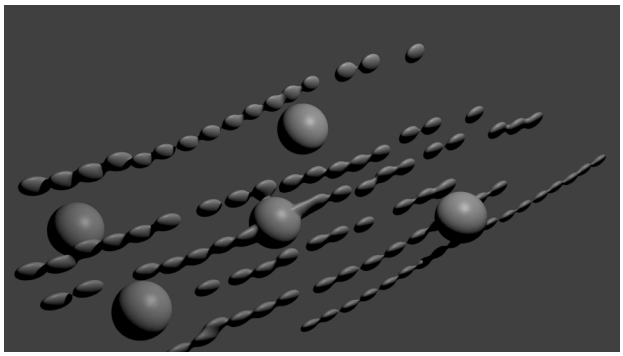

Figure 8.7: A representative rendering of chain formation by magnetic nanoparticles (irregular particles) and the position of silica beads (regular spheres) in relationship to them. Cases mentioned in text as (i), (ii), (iii) and (iv) are clearly seen in figure

represent the fraction of energy induced by the deformation imposed on the material. This fraction of energy is lost by the viscous dissipation in case of loss modulus(G″), and, is stored elastically in case of storage modulus(G′). G′ and G″ were computed using the equations given in Ref.[21], given below, as a function of rate of deformation ω. They are shown in Figure 8.8.

By expanding the equation of motion of Mean square displacement around $t = 1/\omega$, the translational parameter β is defined as [21]

$$\beta(\omega) = \left.\frac{\langle d \ln \Delta r^2(t)\rangle}{d \ln t}\right|_{t=\frac{1}{\omega}} \tag{8.5}$$

and the Fourier transform of this MSD equation would lead to give $G'(\omega)$ and $G''(\omega)$ as

$$\begin{aligned} G'(\omega) &= |G^*(\omega)| \cos\left(\frac{\pi\beta(\omega)}{2}\right) \\ G''(\omega) &= |G^*(\omega)| \sin\left(\frac{\pi\beta(\omega)}{2}\right) \end{aligned} \tag{8.6}$$

Where $|G^*(\omega)| = k_B T/\pi a \langle \Delta r^2(\frac{1}{\omega})\rangle \Gamma[1+\beta(\omega]$, and 'a' the radius of the probing bead.

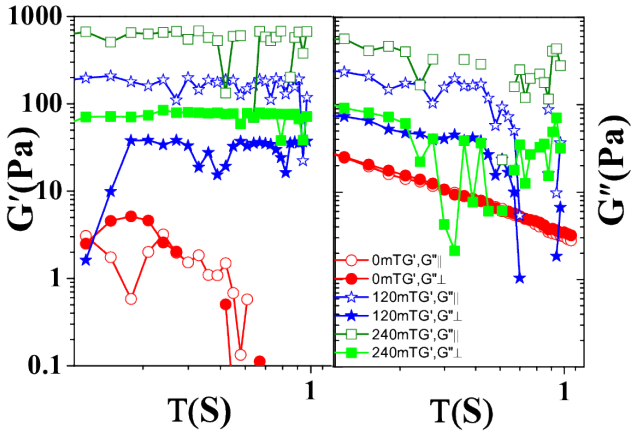

Figure 8.8: (color online) All values of storage (G′) and loss (G″) moduli for different magnetic fields, as a function of time, plotted together for comparison. Empty symbols represent parallel components and filled ones are are corresponding perpendicular components.

Figure 8.9 shows that, at very low fields, G″ dominates G′, indicating a pure diffusive movement of the bead, as appropriate of a viscous fluid. Further $G'_{\parallel}$ and $G'_{\perp}$ are close to each other (and similarly $G''_{\parallel}$ and $G''_{\perp}$) indicating a nearly isotropic behaviour. As field strength increases, the system becomes anisotropic with parallel and perpendicular components becoming different. At intermediate field strengths, $G' \simeq G''$ indicating a viscous to visco-elastic transition. Further increase in field strength results in G′ dominating G″. At this stage, G′ becomes constant with respect to frequency, which is indicative of a purely elastic behaviour as in case of a solid[22].

8.3.3 *Micro-structural properties*

The other important parameters, such as transport coefficient α, the relaxation timescale τ, and elongational flow coefficient λ_2 were also derived using equations from references [12, 8]. Parallel and perpendicular components of each α and τ were derived at the limit of small shear. The two components are equivalent to two distinct situations

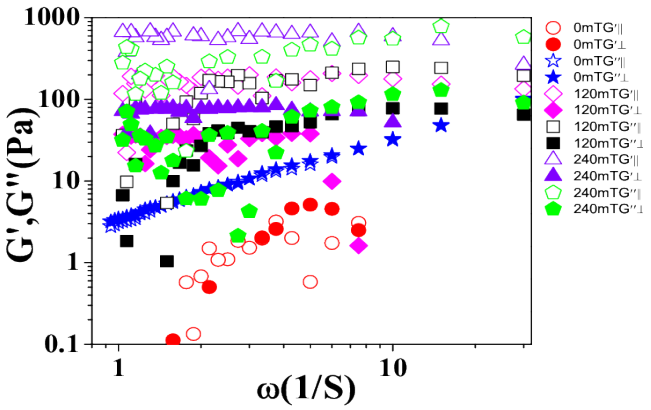

Figure 8.9: Storage (G′) (left) and loss (G″) (right), moduli for different magnetic fields as a function of deformation frequency. It can be noticed that G″ dominates G′ at lower fields. At intermediate fields, their values are closer to each other. At much higher fields G′ becomes significantly higher than G″. Furthermore, at these higher fields, both components become almost constant across deformation frequency ω, indicating a solid like behaviour, due to strong chain formation

mentioned in references [12, 8] , viz., (a) external field is perpendicular to flow velocity and therefore along the flow gradient and (b) external field is along the flow velocity and therefore perpendicular to the flow gradient. In our case, the flow is the small thermal drift of the chains due to external field.

The measured values of viscosities in the parallel and perpendicular direction to the applied external field are substituted in the equation 8.7, this gives λ_2, which accounts for the microstructural properties of ferrofluid with the coupling of symmetric velocity gradient (v_{ij}) [23] to the magnetization relaxation(τ) and it accounts for the elongational flow[13, 24].

$$\frac{\eta_{\parallel}(\xi \to 0)}{\eta_{\perp}(\xi \to 0)} = \frac{(1-\lambda_2)^2}{(1+\lambda_2)^2}(1+\chi)^2 \tag{8.7}$$

Where χ is the magnetic susceptibility.

At higher values of external field, our results show that $\eta_{\parallel}(\xi \rightarrow 0) > \eta_{\perp}(\xi \rightarrow 0)$. This implies that the left side of equation (8.7) is always greater than 1. Rearranging the terms of equation (8.7), this would lead to the result that $\lambda_2 > 0$. This is also in concurrence with results of Odenbach [13, 24] wherein λ_2 is shown to be related to the chain length, which has to be a positive value. However, using equation 8.7, very few of our values for λ_2 were found to be negative. We did not find any reference to this discrepancy in the literature till date. However, we propose that an absolute value of λ_2 be chosen always.

The reaction of the magnetization to changes in field strength and direction, is relaxation of magnetization. In super para magnetic fluids, the smaller relaxation time will dominate the magnetic relaxation behaviour of the fluid. Here, we show how the motional behaviour or viscosity properties of magnetic nanoparticles in solvents is used to derive slow relaxation times of the magnetic nanoparticles. The relationship between viscosity and magnetization relaxation, under limit of zero shear, is given by [8] as,

$$\begin{aligned} \eta_{\parallel} &= \frac{(1-\lambda_2)^2 \tau \chi H_0^2}{4} \\ \eta_{\perp} &= \frac{(1+\lambda_2)^2 \tau \chi H_0^2}{4(1+\chi)^2} \end{aligned} \tag{8.8}$$

Relaxation times τ are obtained by substituting the measured values of $\eta_{\parallel}$ and $\eta_{\perp}$ and the derived values of λ_2, χ and H_0 in the equations 8.8, and are plotted in figure 8.10. While both parallel and perpendicular components of τ decrease at higher field strengths, the perpendicular component decreases by more than 10 times the parallel counterpart. It is well known that the relaxation of magnetization consists of two contributions - the Neel relaxation, arising due to change of intrinsic magnetization within the nanoparticles and the Brownian relaxation, which arise due to rotational diffusion of the particles . Below a critical particle size, the value of Neel relaxation are smaller than that of Brownian relaxations [14]. In a polydispersed ferrofluid solution, the smaller particles have much weaker magnetization and therefore faster relaxation times in comparison to larger particles. Also, the relaxation times for smaller particles would be

more critically dependent upon the external magnetic field, since the inter-particle interaction is lesser. These would allow us to surmise that the parallel component of τ is mostly contributed by the Brownian relaxation rate while the perpendicular component is mostly due to the smaller Neelian relaxation and also due to the smaller particles. This would be possible if at lower fields, the larger particles start forming chains at first and the smaller particles join them only at higher fields.

Another important coefficient, α which is related to the dissipative field(H_D)[8] can be estimated with $\eta = \eta_0 + \frac{1}{4}\alpha B^2$. This α gives the dependence of viscosities of the magnetic fluid. Where η_0 is the viscosity at zero magnetic field.

Figure 8.11 shows that, the α value decreases with the increase in magnetic field strength, which is expected. Because, As the field strength increases, the deviation from the equilibrium magnetization is accounted for by the dissipative field. This dissipative field in turn related to α value using the relation

$$H^D = \alpha \left(\frac{\partial}{\partial t} + v.\nabla - \Omega\times \right) B \tag{8.9}$$

Also, the difference between parallel and perpendicular components shows that, the dissipation of magnetic field is lesser in the parallel direction of the applied field compared to the dissipation in the perpendicular direction. When compared with Shliomi's result, with the equation, $\eta = \eta_0 + \frac{1}{4}\tau MH$ These values of α are comparable to the values of τ. Which shows the reliability of these values. With the diluted magnetic fluids, one cannot calculate this transport coefficient(α) value with this formula, because $\eta \simeq \eta_0$.

8.4 CONCLUSION

We have measured micro-rheological properties of a Manganese Zinc ferrofluid by using thermal motion of a 2.3 micron silica bead suspended in it. The measurements were done using video tracking in a home built inverted microscope. With this, we are able to measure the magnetoviscous effect, and show a field dependent viscosity. While in most of earlier literature explain the anisotropy in terms of shear and torque acting on a single nanoparticle ([25] for example), we propose

a practical consideration of torque on the entire chain, which leads to the anisotropy.

In addition, we are also able to derive, from the statistics of thermal motion, other micro-rheological properties such as the storage modulus G', loss modulus G'' (which together form the complex response modulus $G' + iG''$), elongational flow coefficient λ_2, transport coefficient α and relaxation timescale τ. The coupling parameter λ_2 to the symmetric velocity gradient is calculated from measured viscosity values - absolute value of this parameter is proposed. The range of these values of λ_2 are in good agreement with the previously published values from theoretical and macro-rheological methods [13]. For the first time, values of τ are derived adopting theory to experimental micro-rheology values both in parallel and perpendicular directions. We are able to derive all the rheological and structural parameters of the ferrofluid using a single set of measurements of thermal motion of the probe bead. The values of these parameters are very close to those proposed by theory or those obtained by macro rheology measurements.

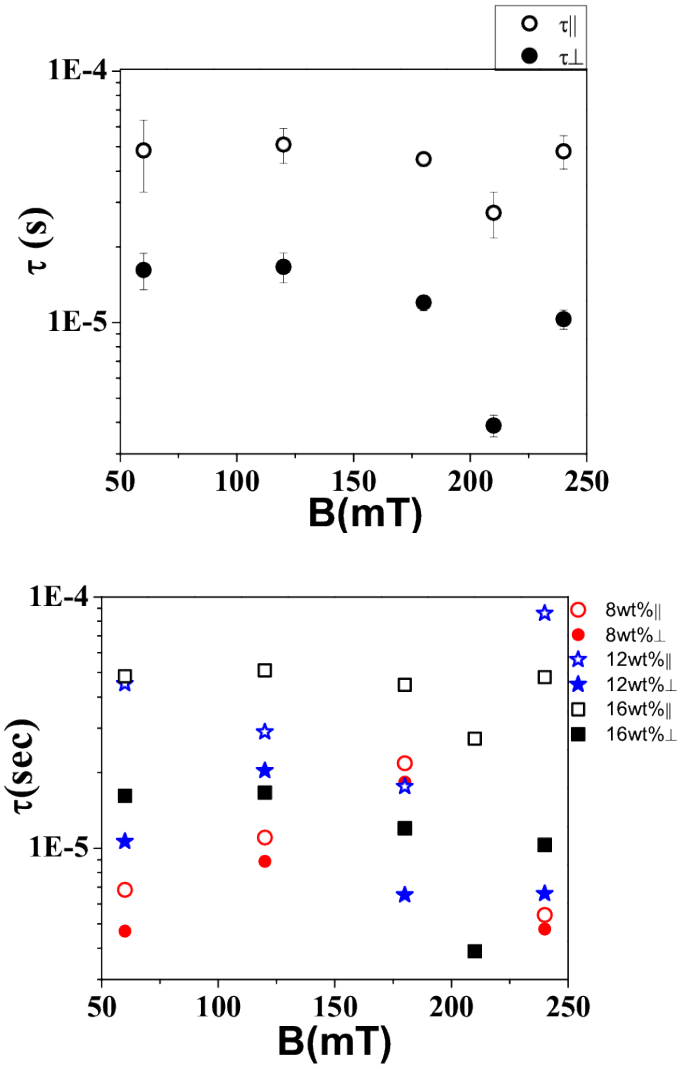

Figure 8.10: Relaxation time scale τ as a function of field (above) and for different concentrations (below). Perpendicular components are indicated by filled symbols and parallel are by open symbols.

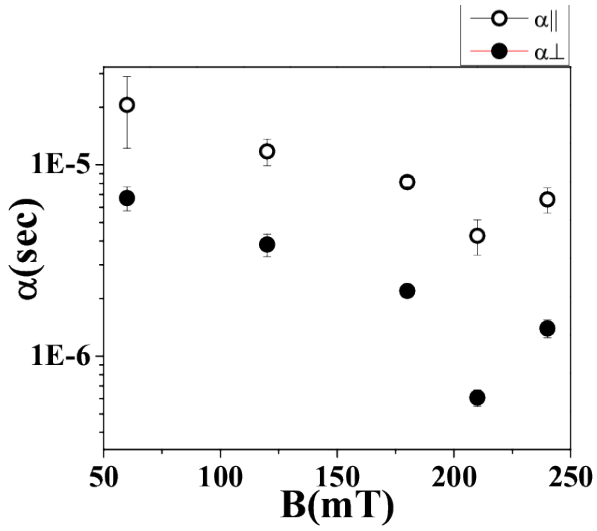

Figure 8.11: Field dependent variation of α

BIBLIOGRAPHY

[1] Alenka Mertelj, Andraz Resetic, Saso Gyergyek, Darko Makovec and Martin Copic, Softmatter, **7**, 125 (2011).

[2] John P. McTague, J. Chem. Phys., **51**,133, (1969).

[3] C. Scherer and A. M. Figueiredo Neto, Brazilian journal of physics, **35** (2005).

[4] Tobias Neuberger, Bernhard Schopf, Heinrich Hofmann, Margarette Hofmann, Brigitte Von Rechenberg, J. Mag. and Mag. Mat. **293**, 483 (2005).

[5] Marcela Gonzales, Kannan M. Krishnan Journal of Magnetism and Magnetic Materials **293** 265 (2005).

[6] Sunghyun Yoon, M. Gonzales-Weimuller, Y. C. Lee and Kannan M. Krishnan, J. Appl. Phys. **105**, 07B507 (2009).

[7] M. Shliomis, Phys. JEPT 34, 1291 (1972).

[8] S. Mahle, P. Ilg, M. Liu, Phys.Rev. E. **77**, 016305 (2008) and references therein.

[9] S. Odenbach, J. Phys. Cond. Matt **23**, 346002 (2011).

[10] K. I. Morozov, J. Magn. Magn. Mater., **122**, 98, (1993).

[11] G. Thirupathi and R. Singh, Physica B: Condensed Matter, **448**, 346, (2014).

[12] Oliver Muller, Dorothea Hahn and Mario Liu, J. Phys. Condens. Matter **18** S2623, (2006) and references therein

[13] S. Odenbach and H. W. Muller, Phys. Rev. Lett. **89**, 037202 (2002).

[14] S. Odenbach, *"Colloidal magnetic fluids"*, Springer Verlag, Berlin Heidelberg, 2009.

[15] G. Thirupathi and R. Singh IEEE Trans Mag **48**, 3630 (2012).

[16] G. Thirupathi, S Saipriya and R. Singh AIP Conf.Proc. **1447**,1129 (2012).

[17] software is freely downloadable from `http:\\www.Opensourcephysics.org`

[18] S. Dhara, Y. Balaji, J. Ananthaiah, P. Sathyanarayana, V. Ashoka, A. Spadlo, and R. Dabrowski, Phys. Rev. E **87**, R030501 (2013).

[19] Jordi Faraudo, Jordi S. Andreu and Juan Camacho, Soft Matter, **9**, 6654 (2013).

[20] Denis Wirtz, Annu. Rev. Biophys. **38** 301 (2009).

[21] Thomas G. Mason, Rheol. Acta **39**, 371 (2000).

[22] Juan Pablo Segovia-Gutierrez, Juan de Vicente, Roque Hidalgo-Alvarez and Antonio M. Puertas, Softmatter **9**, 6970 (2013).

[23] $v_{ij} = 1/2(\nabla_j v_i + \nabla_i v_j$ as per reference [12, 8]

[24] S. Odenbach, H. W. Muller, J. Mag. and Mag. Mat. **289**, 242 (2005).

[25] S. Odenbach, J. Phys. Cond. Mat. **16**, R1135 (2004).

9 CONCLUSIONS AND FUTURE DIRECTIONS

The purpose of this Chapter is to summarize the important results reported and future directions for the progress of the work in this Thesis.

9.1 CONCLUSIONS

The results presented in this thesis can be classified into three major physical descriptions: (a) addressing the tumbling nematic director of the liquid crystals by simply analyzing with a time dependent harmonic oscillator motion. (b) addressing the physical and symmetrical properties of bow shaped liquid crystals by studying diffusion of colloidal particle. (c) addressing the flow properties of ferrofluids under external magnetic field implication. Overall, this Thesis is a study on microrheological, microstructral and micromechanical properties of complex fluids. A striking difference between flow properties of liquid crystals and ferrofluids was observed from this thesis. In nematic liquid crystals, molecules are aligned along the nematic director. In ferrofluids, magnetic nano particles form long chain of particles in the applied field direction. But, in liquid crystals the diffusion of colloidal (probing) particle is more along the perpendicular direction to the nematic director compared to the parallel direction. Whereas, in ferrofluids with the application of field, the diffusion of the colloidal particle is more along the parallel direction than in the perpendicular direction. In this thesis, though nematohydrodynamics are not used in describing the flow properties of liquid crystals, but the theoretical results of zero shear conditions of magneto hydrodynamics are used in describing the flow properties of ferrofluids. In this study of slow dynamics of complex fluids, micro viscosity of bent core liquid crystals, memory effects due to tumbling nematic director in 8CB liquid crystals, microrheological properties of 8CB liquid crystals, microrheological properties of bent core liquid crystals and field dependent anisotropic microrheological and microstructural properties of ferrofluids are reported. The results of single particle tracking experiment

in liquid crystals, without using a valid generalized Stokes-Einstein relation(GSER)which follows Leslie-Ericksen equation is presented. To our knowledge, a quantitative approach for determining the flow properties of nematic liquid crystals with GSER using Leslie-Erickson equations for studying the diffusion properties of a colloidal probe as a funciton of time was not done by considering the material parameters, probe particle anchoring conditons, and director orientation.

9.1.1 *Dynamics of tumbling nematic director in liquid crystals*

In **chapter 4**, to understand the collective molecular orientations in 8CB liquid crystals, an approach to studying the correlation properties of liquid crystal molecules by understanding the parallel and perpendicular components of Brownian motion of colloidal particle was followed. velocity auto correlation function (VACF) which represents the rate of change in the diffusion properties of colloidal particle is used in understanding the dynamics of molecular orientations in 8CB liquid crystals. The consequence of the twisted structures formed in the tumbling nematics of 8CB liquid crystals, are probed by a colloidal particle of the same size as of the size of the structres formed. This leads to probing the amplitudes of twisted structures formed of the dynamics of collective molecular orientations using VACF vs time. An interesting note is, these amplitudes measured from the correlations are in well agreement with the amplitudes of dynamic viscosity measured from bulk rheometers which followed Leslie-Erickson equations. Also, these isotropic and anisotropic behavior of amplitudes of auto correlaion have exactly followed the amplitudes of director from the nemato dynamics. Further, a generic approach by fitting this VACF with time dependent harmonic oscillations, micro structural properties like relaxation time of collective molecular orientations (τ) , frequency (ω) of motion of tumbling director are computed. Also, micro mechanical properties like elastic constant (k), quality factor (Q) of tumbling motion of the director are computed. An intriguing observation by fitting solutions of time dependent harmonic oscilltor motion equations to these correlations is, just below NI transition, the correlation follows underdamped harmonic oscillations, in the tumbling phase, correla-

tion follows coupled and decaying coupled harmonic oscillation. Near Sm-N transition, correlation follows, critically damped oscillation.

In **chapter 5**, frequency dependent mobility of a colloidal particle in tumbling nematics of 8CB liquid crystals is reported. Microrheological parameters storage (G') and loss modulus (G'') which represents the fraction of energy induced by the deformation imposed on the material. Since these micro rheological parameters represents the fourier transform of diffusion of the colloidal particle motion, the G' Vs ω values have followed the characteristics similar to VACF (C_v) vs time (t). The dependence of G' on ω follows the amplitude of motion of a coupled harmonic oscilltor in the tumbling regime. The G' values have shown different dependence on ω in just below NI transition compared to the smectic-nematic (Sm-N) transition temperature. Also, in the nematic phase of 8cb liquid crystals, different regimes with different structural properties were clearly differentiated by analyzing variation of G' with ω. Further, dynamic viscosity (η'') is also computed from the ratio of G'' and ω. Dynamic viscosity in the parallel direction has shown the characteristics similar to the previously measured bulk viscosity values. Near to the Sm-N transition temperature, observed crossover between the parallel and perpendicular components is addressed with how the Brownian motion of the colloidal particle is restricted by the large smectic layers.

9.1.2 *Consequences of irregular shape of molecules in liquid crystals*

In **chapter 3**, the measurements of passive viscosities of bent core liquid crystals are reported. These passive viscosities are measured from the self diffusion of an isolated colloidal particle motion in single particle tracking experiment. Anisotropy in the self diffusion is observed. Relative to active viscosity values in the shear rheology measurement, viscosity values in passive measurements have shown stronger temperature dependence. The effect of presmectic fluctuations are observed much higher than the N-SmC transition temperature than commonly seen in calamitic liquid crystals. A cross over in the viscosity values of parallel and perpendicular components near N-SmC transition temperature is observed which was attributed to the presence of large presmectic cluster layers.

In **chapter 6**, micro rheology technique is used in describing the physical nature of bent core liquid crystals at different temperatures. The kinked shape of bent core molecules which accounts for their packing or aggregation properties leads to show different physical properties. The theoretical predictions of symmetry properties were confirmed through out their transitions from isotropic to nematic and nematic smectic-C phases. In isotropic phase, the rigidity nature along parallel direction to the director, the fluctuations along perpendicular direction to the director are observed and addressed. The small and total flip orientations in the nematic phase are understood in terms of their dissipation of elastic energy in the $(\hat{\mathbf{n}}||)$ direction of uniaxial phase. As the temperature decreases, the size of BCLCs increases which leads to confinement of fluid in the perpendicular direction hence it shows calamitic liquid crystals tumbling behavior. The restricted rotation of bent core liquid crystals with ortho rhombic $D2h$ symmetry and monoclinic C_{2h} symmetry was differentiated by analyzing the variation of G' with *omega*. Also, the total tilt of BCLCs and the consequences in terms of a jump in G' Vs ω was observed. In the lower temperature, as the smectic C phase approaches, the surface anchoring effects and its role in reducing the dissipation of energy during inplane and out of plane orientations is described. At very low frequencies, the slope of G' Vs ω have shown a clear difference between the 'in-plane' and 'out of plane' rotations in the nematic phase at high temperatures and low temperatures.

9.1.3 *Inference on the diffusivity in liquid crystals*

In **chapter 7**, the diffusion of colloidal particle in complex fluids does show characteristics of "anomalous yet Brownian" motion. A recently proposed theoretical model, have characterized these complex fluids that show anomalies in their diffusion. Diffusion of colloidal particle in complex possess diffusion memory but no direction memory in their particle trajectory which is termed as "diffusing diffusivity". The sub diffusive motion of colloidal particle in 8CB liquid crystals, show characteristics of "diffusing diffusivity". Also, it was concluded that, velocity auto correlation function is the better approach to understand

the anomalies in diffusion of colloidal particle in complex fluids by understanding the correlation between the molecular dynamics.

9.1.4 *Field dependent diffusion in ferrofluids*

In **chapter 8**, micro-rheological properties of a Manganese Zinc ferrofluid are measured by using thermal motion of a 2.3 micron silica bead suspended in it. The measurements were done using video tracking in a home built inverted microscope. The magneto viscous effect and the field dependent anisotropy in the viscosity values are observed. While in most of earlier literature explains the anisotropy in terms of shear and torque acting on a single nanoparticle, we propose a practical consideration of torque on the entire chain, which leads to the anisotropy. Also, from the statistics of thermal motion, other micro-rheological properties such as the storage modulus G', loss modulus G'' (which together form the complex response modulus $G' + iG''$), elongational flow coefficient λ_2, transport coefficient α and relaxation timescale τ. The coupling parameter λ_2 to the symmetric velocity gradient is calculated from measured viscosity values - absolute value of this parameter is proposed. The range of these values of λ_2 are in good agreement with the previous literature. For the first time, values of τ are derived adopting theory to experimental micro-rheology values both in parallel and perpendicular directions. We are able to derive all the rheological and structural parameters of the ferrofluid using a single set of measurements of thermal motion of the probe bead.

9.2 FUTURE DIRECTIONS

a) Theoretical approach for colloidal particle motion in liquid crystals with a quantitatively valid generalized Stokes-Einstein equation by solving Leslie-Erickson equations for the frequency dependent motion of collodial particle as a function of anchoring conditions, material parameters, and director orientations needs to be studied.

b) A generic approach which was followed in chapter 3, by using equation of time dependent harmonic oscillatory motion to report various microstructural and micromechanical properties of 8cb liquid crystals can also be verified for diffusion of collodial particle in bio-

logical materials like lipid bilayers that possess varying spontaneous curvature and bending.

c) Experiments on diffusion of collodial particle motion in microfluidic channels that are either cylindrical or sinusoidal curvatures would give more insight into the understanding of dynamics of complex fluids. The anomalous diffusion of colloidal particle when it is in hydrodynamic interaction with curvatures and with regular shapes can be verified.

d) Theoretical ways to describe the deformation of energy during the diffusion of colloidal particle in liquid crystals with tumbling nemato dynamics and how the presence of smectic clusters can be distinguished from the nematic phase also has to be addressed with theory.

e) Computer simulations is a better approach to verify the deformation of energy during the inplane and out of plane orientation of clusters of bent core liquid crystal molecules. Also, the same approach can be followed to address the spontaneous biaxiality.

f) Another consequence of field dependent motion in ferro fluids is negative magnetophoric effect (NMP). observing the consequence of NMP on microrheological properties can be considered as a future direction studies in ferrofluids.

BIBLIOGRAPHY

[1] Todd M. Squires and Thomas G. Mason, Annu. Rev. Fluid Mech. **42**, 413, (2010).

[2] J. C. Loudet, P. Hanusse, P. Poulin, Science, **306**, (2004).

[3] P.G.de Gennes, "The Physics of Liquid crystals", 2nd ed.(Oxford university Press,Oxford), (1993).

[4] S.Chandrasekhar, Liquid crystals, 2nd ed.(Cambridge University Press), (1992).

[5] Michael J. Stephen and Joseph P. Straley, Rev. of Mod. Phys, **46**, 4, (1974).

[6] T. Arun Kumar, "Study of perfluoro polymer as an alignment layer for nematic liquid crystals", University of Hyderabad, Ph.D. Thesis - Unpublished (2012).

[7] A. Rapini, M. Papoular, J. Phys. Colloq. France **30**, C4-54, (1969).

[8] P. Poulin and D. A. Weitz, Phys. Rev. E., **57**, 1, (1998).

[9] O. V. Kusenok, R. W. Ruhwandl, S. V. Shiyanovskiin, and E. M. Terentjev, Phys. Rev. E, **54**, 5198 (1996).

[10] S. Odenbach, J. Phys.: Condens. Matter, **16**, R1135, (2004).